Dissertation

submitted to the
Combined Faculty of Natural Sciences and Mathematics of the
Ruperto Carola University Heidelberg, Germany for the degree
of
Doctor of Natural Sciences

Presented by

M.Sc. Sherif Ismail

Born in: Giza, Egypt

Oral examination: 10.12.2021

Identification of the Primordial Pre-60S Subunit and How it Emerges from the 90S Pre-ribosome

Referees: Prof. Dr. Ed Hurt

Prof. Dr. Michael Brunner

Summary

Ribosomes are conserved in the three domains of life, Archaea, Bacteria and Eukarya. They are essential for protein synthesis in all living cells. Formation of ribosomes in eukaryotic cells occurs through an energy-consuming multi-step process, involving a myriad of ribosome assembly factors and snoRNAs. This complex process starts in the nucleolus by the synthesis of a large ribosomal RNA precursor, the 35S pre-rRNA in yeast, which is co-transcriptionally cleaved to separate the pre-40S and the pre-60S pathways. The first intermediate formed during the early phase of ribosome assembly is the 90S pre-ribosome, the precursor to the small subunit. While the 90S to pre-40S route proceeds with its own set of assembly factors and snoRNAs including U3 and U14, little is known about the formation of the earliest pre-60S intermediates and whether snoRNAs have a role in this process.

To gain insight into these early steps of large subunit synthesis, I isolated and studied a pre-60S assembly intermediate at the beginning of its construction, where specific snoRNAs also come into play. This analysis revealed a network of assembly factors and snoRNAs participating in the building of this primordial pre-60S particle. This particle is characterized by two large α-solenoid scaffold modules Rrp5 and Urb1, SPOUT methyltransferases Upa1 (YGR283C) and Upa2 (YMR310C), several RNA helicases including Mak5 and two prominent snoRNAs, C/D box snR190 and H/ACA box snR37. My findings suggest that snR190 and snR37 play a structural role in pre-60S assembly and their disruption caused changes in the primordial pre-60S composition. Moreover, I used the uncharacterized Upa1 and Upa2 as single baits to isolate the primordial pre-60S, which helped to unravel its overall shape by negative stain EM. By using a dominant *mak5* helicase mutant, I showed that this nascent pre-60S intermediate does not efficiently separate from the 90S pre-ribosome, which enabled for the first time the visualization of a 70 nm super 90S–pre-60S bipartite particle by electron microscopy. These findings are relevant for human ribosome biogenesis, which occurs predominantly via the post-transcriptional mechanism and, thus, is expected to also involve a pre-ribosomal intermediate carrying both 90S and pre-60S moieties before pre-rRNA cleavage. Altogether, this work sheds further light on the earliest steps of pre-60S assembly and its connection to the upstream 90S pathway.

Zusammenfassung

Ribosomen sind in den drei Domänen der Lebewesen Archaeen, Bakterien und Eukaryoten konserviert. Sie sind notwendig für die Proteinsynthese in allen lebenden Zellen. Die Bildung von Ribosomen in eukaryotischen Zellen erfolgt durch einen energieaufwändigen, mehrstufigen Prozess, an dem eine Vielzahl von Ribosom Biogenesefaktoren und snoRNAs beteiligt sind. Dieser komplexe Prozess beginnt im Nukleolus durch mit der Synthese eines großen ribosomalen RNA-Vorläufers, der 35S-prä-rRNA in Hefe, die co-transkriptionell gespalten wird um den Prä-40S- und den Prä-60S-Weg voneinander zu trennen. Die erste Zwischenstufe, die während der frühen Phase der Ribosomenbiogenese gebildet wird, ist das 90S-Prä-Ribosom, der Vorläufer der kleinen Untereinheit. Während die Route von 90S zu Prä-40S mit einer eigenen Menge von Biogenesefaktoren und snoRNAs einschließlich U3 und U14 verläuft, ist wenig über die Bildung der frühesten Prä-60S Zwischenstufen bekannt und ob snoRNAs in diesem Prozess eine Rolle spielen.

Um einen Einblick in diese frühen Schritte der Synthese großer Untereinheiten zu erhalten, habe ich zu Beginn ihre Konstruktion eine Prä-60S-Zwischenstufe, bei der auch spezifische snoRNAs ins Spiel kommen, isoliert und untersucht. Diese Analyse brachte ein Netzwerk von Biogenesefaktoren und snoRNAs zum Vorschein, das am Aufbau dieses primordial Prä-60S Partikel beteiligt ist. Dieses Partikel ist durch zwei große α-Solenoid-Gerüstmodule Rrp5 und Urb1, SPOUT-Methyltransferasen Upa1 (YGR283C) und Upa2 (YMR310C), mehrere RNA-Helikasen einschließlich Mak5 und zwei prominente snoRNAs, C/D-Box snR190 und H/ACA-Box snR37, gekennzeichnet. Meine Ergebnisse legen nahe, dass die snR190 und snR37 eine strukturelle Rolle bei der Prä-60S Biogenese spielen und ihre Beeinträchtigung zu Veränderungen in der primordialen Prä-60S-Zusammensetzung führte. Darüber hinaus habe ich die uncharakterisierten Upa1 und Upa2 als Einzelköder verwendet, um das primordiale Prä-60S Partikel zu isolieren, was dazu beitrug, seine Gesamtform durch negative stain EM zu lösen. Durch die Verwendung einer dominanten mak5-Helikase-Mutante zeigte ich, dass sich dieses entstehende Prä-60S Zwischenstufe nicht effizient vom 90S-Prä-Ribosom trennt, was zum ersten Mal die Visualisierung eines zweiteiligen 70-nm-Super-90S-Prä-60S Partikels durch Elektronen Mikroskopie ermöglichte. Diese Ergebnisse sind für die Ribosomenbiogenese in Menschen relevant, die hauptsächlich über den post-transkriptionellen Mechanismus abläuft und

daher voraussichtlich auch eine prä-ribosomales Zwischenstufe umfasst, die sowohl 90S als auch Prä-60S-Einheiten vor der prä-rRNA-Spaltung enthält. Insgesamt beleuchtet diese Arbeit die frühesten Schritte der Prä-60S-Biogenese und ihre Verbindung zum vorgelagerten 90S-Pfad.

Acknowledgements

I would like to thank Prof. Dr. Ed Hurt for supervising my PhD project, all fruitful discussions and advice to push the project forward. I learned from you that one should not quickly give up on his ideas.

I would like to acknowledge all the people I collaborated with, including Dr. Dirk Flemming, Dr. Jose Vincente Gomes-Filho (Randau lab) and Matthias Thoms (Beckmann lab). I am grateful to Prof. Dr. Michael Brunner, Dr. Mandy Jeske and Dr. Jika Pescheck for being in my PhD examination committee.

I would like to thank all my colleagues from the Hurt lab. I am very grateful to Martina and very happy to know her. Martina, you are the best. I would like to thank Jochen for his help, especially when I started in the lab. Ruth for being kind and for our discussions. Selene and Sabine for the technical support. I would like to acknowledge Andrea for helping with all the official paper work and making our life easier.

Thanks to my friends and colleagues Federica and Sven, I enjoy our coffee breaks and discussions more than you can imagine. I would like to thank my friends Omar, Ali, Mostafa and Shaymaa. I am happy because I know you. My friend Ahmed, who is always there since the start and will be at the end. I appreciate your friendship.

This work is dedicated to my mother and every member of my amazing family, who supports me at every step. Your support and encouragement kept me going.

Table of contents

1 Introduction

1.1 The eukaryotic ribosome

In all living cells, proteins are synthesized by the ribosomes, which are conserved in all domains of life. The ribosomes have a sophisticated structure made of ribonucleoproteins. These nanomachines translate the messenger RNAs (mRNAs) that carry genetic information from the genome. During the translation process, ribosomes decode the template mRNA molecules and catalyze peptide bond formation between amino acids in a sequential order specified by the codons of mRNA. This leads to formation of polypeptide chains.

In 1955, George Palade has observed “a small particulate component of the cytoplasm” in the tissues of rat and chicken using electron microscopy (Palade, 1955). He noticed that these particulates are preferentially bound to the membrane of the endoplasmic reticulum and they are also present in free form in the cytoplasm. Later, these microsomal ribonucleoprotein particulates were named ribosomes in a symposium in 1958. During these times, it was observed that ribosomes are responsible for protein synthesis in all organisms. It was found that multiple ribosomes can bind the same mRNA forming bigger structures (polysomes), which engage in protein synthesis (Warner et al., 1963). Extensive research and investigations of ribosomes were made to explore their origin, evolution, composition and role in protein synthesis.

The ribosome consists of two subunits made of ribosomal RNA (rRNA) and ribosomal proteins (r-proteins). In the eukaryotic 80S ribosome, the large subunit (60S) is made of 3 rRNAs 28S (25S in yeast), 5.8S and 5S combined with 47 r-proteins (46 in yeast), while the small subunit (40S) is made of 18S rRNA and 33 r-proteins. By contrast, in the prokaryotic 70S ribosome, the large subunit (50S) contains 23S and 5S rRNA with over 30 r-proteins, while the small subunit (30S) contains 16S rRNA with around 20 r-proteins. Crystal structures and cryogenic electron microscopy (cryo-EM) reconstructions of prokaryotic and eukaryotic ribosomes have revealed enormous details about the structure of mature ribosomes from different organisms and their conserved functional sites (Anger et al., 2013; Armache et al., 2010; Ben-Shem et al., 2011; Khatter et al., 2015; Yusupov et al., 2001). An example of these functional sites of the ribosome is the transfer RNA (tRNA) binding sites A, P and E: The A-site binds

aminoacyl-tRNA carrying substrate amino acid, the P-site binds peptidyl-tRNA which is a tRNA attached to the nascent polypeptide chain and the E-site binds a free tRNA after the acyl-amino acid is removed. The large subunit contains the peptidyl transferase center (PTC) that catalyzes peptide bond formation and the polypeptide exit tunnel (PET) where the nascent polypeptide exits the ribosome (Figure 1.1). Apparently, the small subunit contains the mRNA decoding center where the subunit matches the mRNA codons with the tRNAs anticodons. The small subunit also includes the mRNA entry and exit sites.

Notably, these functional sites (tRNA binding sites, PTC, PET and mRNA decoding center) are universally conserved between bacterial, archaeal and eukaryotic ribosomes and all of them are located in the core on the subunit interface (except the PET) (Konikkat and Woolford, 2017; Melnikov et al., 2012; Yusupova and Yusupov, 2014). However, eukaryotic ribosomes are larger than their prokaryotic counterparts because of features specific to ribosomes in eukaryotes including extra sequences within the rRNA (rRNA expansion segments), extensions of many r-proteins and extra eukaryotic r-proteins (Jenner et al., 2012; Klinge et al., 2011; Rabl et al., 2011). These eukaryotic specific features are mainly present on the solvent-exposed interface of the ribosome (Figure 1.1). Moreover, the three-dimensional shape of the large subunit has some recognizable features such as the central protuberance (including the 5S rRNA area), L1 stalk and P stalk (Figure 1.1). By contrast, different regions could be discerned in the small ribosomal subunit such as the head, beak, platform and body (Figure 1.1).

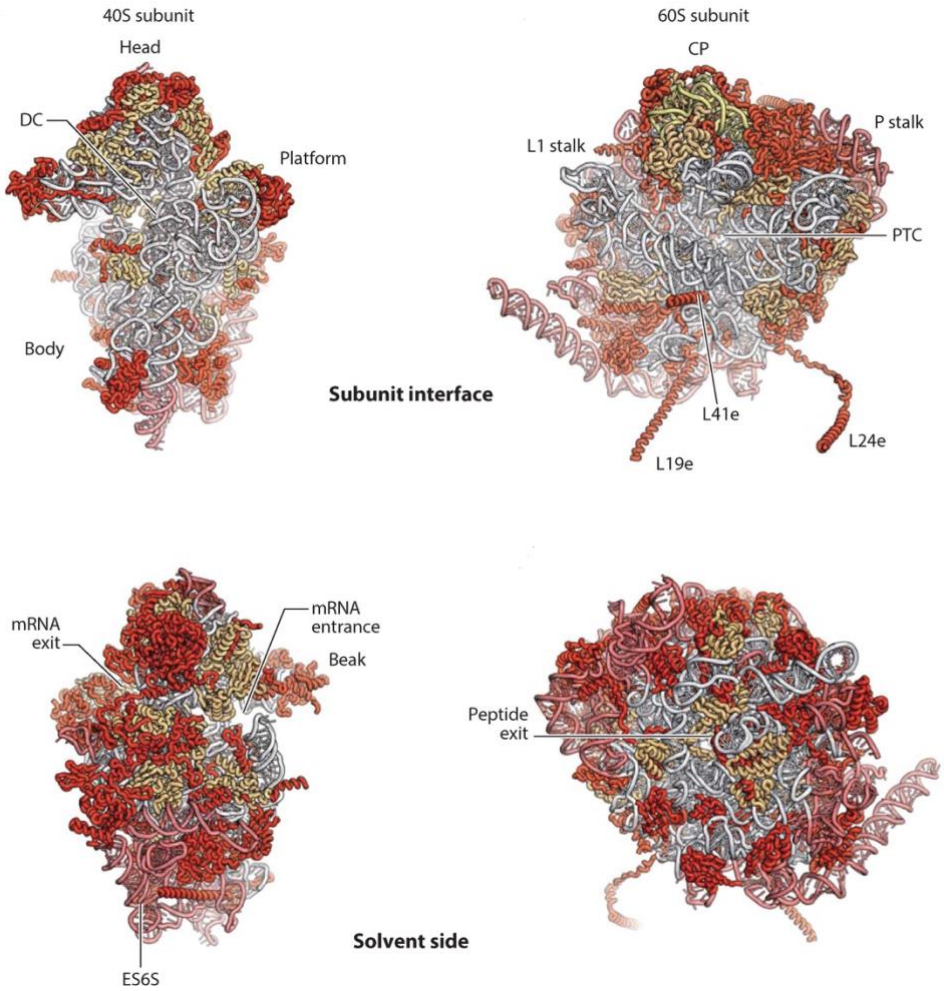

Figure 1.1 The large and small subunits of Yeast
The upper panel shows the subunit interface while the lower panel shows the solvent side of both subunits. The conserved core has rRNA (white) and r-proteins (light orange) while eukaryotic specific areas (red) are clustered mainly on the solvent side. DC: decoding center, CP: central protuberance, PTC: peptidyl transferase center. Figure adapted from (Yusupova and Yusupov, 2014).

1.2 Ribosome biogenesis in yeast *Saccharomyces cerevisiae*

Growing cells depend unequivocally on protein synthesis. Therefore, the cells need to generate ribosomes efficiently. Ribosome biogenesis or ribosome assembly is an immensely energy-consuming multi-step process that is conserved in eukaryotes and essential for living cells. Rapidly growing yeast cells generate about 2000 ribosomes per minute and a typical yeast cell can make nearly 200 000 ribosomes in its cell cycle (Warner, 1999). To maintain cell growth and support this high demand for ribosomes production, yeast cells allocate remarkable number of resources exploiting all three RNA polymerases. Strikingly, the transcription of rRNA by RNA polymerase I

represents 60% of total RNA transcription in fast growing yeast cells. Meanwhile, 50% of RNA polymerase II transcription is dedicated to the genes of r-proteins (Warner, 1999). From the most highly expressed genes in yeast, r-proteins genes are the source for 20 out of the 30 most abundant expressed mRNAs (Velculescu et al., 1997). Splicing of r-proteins mRNAs represents 90% of all mRNA splicing events in yeast (Warner, 1999).

Early research on ribosome assembly has shown that bacterial ribosomal subunits can be reconstituted *in vitro* from their purified components rRNA and r-proteins (Held et al., 1973; Nierhaus and Dohme, 1974; Traub and Nomura, 1968). It was believed back then that the complete information for ribosomal subunits assembly is contained within its components and no need for other external non-ribosomal factors. However, eukaryotic ribosomes could not be reconstituted with the same approach indicating a more complex ribosome assembly for eukaryotes, which involves more factors. In early 1960s, research studies have used radioactive labelling of RNA in HeLa cells (pulse labelling) and identified a large precursors of rRNA (45S pre-rRNA), which is later processed to give rise to the different mature rRNAs (Scherrer and Darnell, 1962; Scherrer et al., 1963). Further work on this large precursor rRNA in HeLa cells revealed that it associates with proteins forming ribonucleoprotein precursor particles (pre-ribosomes) that precede formation of the cytoplasmic ribosomes (Tamaoki, 1966; Warner and Soeiro, 1967). In yeast, these precursor particles or pre-ribosomes had a sedimentation on sucrose gradient at approximately 90S, 66S (precursor for 60S subunit) and 43S (precursor for 40S subunit) (Trapman et al., 1975). The pre-ribosomes, especially the 90S and 66S, had higher protein to RNA ratio than the mature ribosomal subunits, indicating that these pre-ribosomes carry non-ribosomal proteins that are absent from the mature ribosomes (Trapman et al., 1975). The non-ribosomal proteins were also detected in the pre-ribosomes of HeLa cells (Kumar and Warner, 1972). Apparently, these non-ribosomal proteins were believed to play a role in processing of the pre-ribosomal particles to mature ribosomes then they get discarded and re-used for subsequent assembly of ribosomes (Kumar and Warner, 1972). The non-ribosomal proteins were later named ribosome biogenesis factors or ribosome assembly factors (AFs).

1.2.1 Ribosomal RNA synthesis in the nucleolus

The initial steps of ribosome assembly occur in the cell nucleolus with rRNA transcription from the ribosomal DNA (rDNA) genes located inside the nucleolus (reviewed in Mélèse and Xue, 1995; Thiry and Lafontaine, 2005). Notably, transcription of rDNA was visualized by Miller and Beatty using the Miller spreads technique in 1969 revealing a first look at the nascent pre-rRNA precursors being transcribed from rDNA in the nucleolus of amphibian oocytes (Miller and Beatty, 1969). The nucleolus is a well-defined membrane-free subnuclear compartment as seen by electron microscopy (Hernandez-Verdun et al., 2010; Léger-Silvestre et al., 1999; Warner, 1990). It is organized into three distinct components as defined by electron microscopy: the fibrillar centers which are surrounded by the dense fibrillar component and together they are embedded in a granule-rich compartment called the granular component. The rDNA genes are mainly present in the fibrillar centers, while the transcription of pre-rRNA occur at the interface between the fibrillar centers and the dense fibrillar component. Early steps of pre-rRNA processing appear to be in the dense fibrillar component and subsequent steps of maturation occur in the granular component (Thiry and Lafontaine, 2005; Thiry et al., 2000).

In yeast, the crescent-shaped nucleolar compartment is formed around more than 150 rDNA repeats present on chromosome XII (Figure 1.2). Only one half of these rDNA repeats is transcriptionally active while the other half is transcriptionally repressed (Toussaint et al., 2011; Woolford and Baserga, 2013). However, each rDNA repeat is not always active or inactive in transcription but the repeats cycle between both states so that the ratio is maintained and most repeats get active in transcription at some point in a single yeast cell (Tan and Van Oudenaarden, 2010). Typically, rDNA genes are transcribed by RNA polymerase I at a rate of 40-60 nucleotides per second (Koš and Tollervey, 2010), producing a polycistronic transcript called 35S pre-rRNA. This 35S pre-rRNA includes the rRNAs that will later form the small 40S subunit (18S rRNA) and the large 60S subunit (5.8S and 25S rRNAs). The 35S pre-rRNA contains internal (ITS1 and ITS2) and external (5`-ETS and 3`-ETS) transcribed spacer sequences (Figure 1.2). By contrast, 5S rRNA is transcribed separately by RNA polymerase IIII in the opposite direction and it forms a complex with the r-proteins Rpl5 (uL18) and Rpl11 (uL5) before the formed 5S RNP gets incorporated into pre-60S particles at an early step of the maturation pathway.

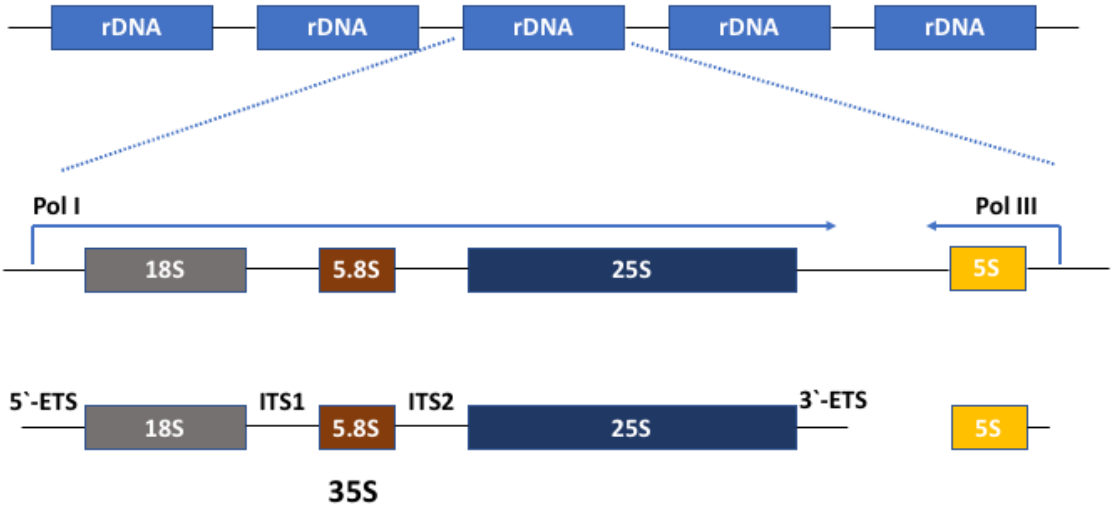

Figure 1.2 Transcription of rDNA repeats in Yeast
rDNA genes are arranged in tandem repeats in the nucleolus. RNA polymerase I (Pol I) produce a precursor 35S pre-rRNA which is later processed to produce the mature 18S, 5.8S and 25S. 5S is independently transcribed by polymerase III (Pol III) then it joins 5.8S and 25S for 60S ribosomal subunit synthesis.

Ribosome biogenesis pathway proceeds by several 35S pre-rRNA cleavage to finally generate the mature rRNAs, accompanied by rRNA modification, folding of the pre-rRNA and recruitment of ribosomal proteins. Remarkably, these processes are facilitated by many ribosome assembly factors that sequentially associate with the continuously maturing pre-ribosomes and drive the progression of the pathway from the nucleolus to the nucleoplasm passing through the nuclear pore complex (NPC) to the cytoplasm, where both subunits acquire final maturation and become competent for protein synthesis (reviewed in Baßler and Hurt, 2019; Henras et al., 2015; Klinge and Woolford, 2019; Peña et al., 2017; Woolford and Baserga, 2013).

In 2001, the development of the tandem affinity purification (TAP) approach has allowed the biochemical isolation of discrete pre-ribosomal particles, which opened the doors to study the assembly factors and pre-rRNAs associated with these particles by mass spectrometry and RNA analyses techniques (Baßler et al., 2001; Fatica et al., 2002; Harnpicharnchai et al., 2001; Saveanu et al., 2001). Therefore, these methods have enabled the categorization of the pre-ribosomes into early (nucleolar), intermediate (nuclear) and late (cytoplasmic) particles (Nissan et al., 2002; Schäfer et al., 2003; Tschochner and Hurt, 2003).

There are more than 200 ribosome assembly factors identified so far, which fall into different categories. Some of these factors have enzymatic function e.g.

endonucleases, exonucleases, GTPases, ATPases, RNA helicases, methyltransferases and protein kinases. By contrast, other assembly factors have no enzymatic activity but rather they have other domains that allow them to bind rRNA and/or provide protein-protein interaction platform, which eventually enable these assembly factors to chaperone and drive ribosome biogenesis. Many of these ribosome assembly factors are essential for cell growth and conserved in eukaryotes. However, they only function in ribosome biogenesis, not in protein synthesis, and they are not present in mature ribosomes.

1.2.2 Co-transcriptional versus post-transcriptional pre-rRNA processing

The nascent 35S pre-rRNA needs to be processed and cleaved through a series of enzymatic reactions to generate the mature rRNAs. Endonucleases and exonucleases process this nascent pre-rRNA to sequentially remove the externally and internally transcribed spacer sequences (Figure 1.3). One of the earliest steps of the nascent pre-rRNA processing is an endonucleolytic cleavage in the ITS1 sequence to split the assembly pathway of the large and small ribosomal subunits, which follow independent maturation (Udem and Warner, 1972). Cleavage and processing of pre-rRNA can occur co-transcriptionally and/or post-transcriptionally. Under optimal growth conditions, the nascent pre-rRNA in yeast is mainly co-transcriptionally processed as the cells require fast ribosome assembly to support cell growth (Koš and Tollervey, 2010; Osheim et al., 2004). This has been studied using electron microscopy on chromatin spreads of yeast rDNA genes, which revealed that the majority of yeast nascent pre-rRNA is co-transcriptionally processed (Osheim et al., 2004). Biochemical experiments combined with mathematical modelling to study pre-rRNA processing in yeast have estimated that around 70% of the nascent transcripts go through co-transcriptional processing (Koš and Tollervey, 2010). Yeast cells can still process their pre-rRNA post-transcriptionally and a shift between these two modes of processing is possible. Interestingly, the co-transcriptional cleavage at site A_2 of yeast pre-rRNA can be strongly diminished under various stress conditions including nutrient limitation, oxidative stress or heat shock (Kos-Braun et al., 2017; Osheim et al., 2004). Moreover, disruption of some yeast ribosome assembly factors can also inhibit the co-transcriptional cleavage of nascent pre-rRNA and shift the pathway to a post-transcriptional processing (Axt et al., 2014; Lebaron et al., 2013; Talkish et al., 2016). It was shown that depletion of the essential pre-60S assembly factor Drs1 has

blocked pre-rRNA co-transcriptional processing, which led to accumulation of 35S pre-rRNA in yeast cells and pre-ribosomal particles to carry both pre-60S and 90S assembly factors simultaneously (Talkish et al., 2016).

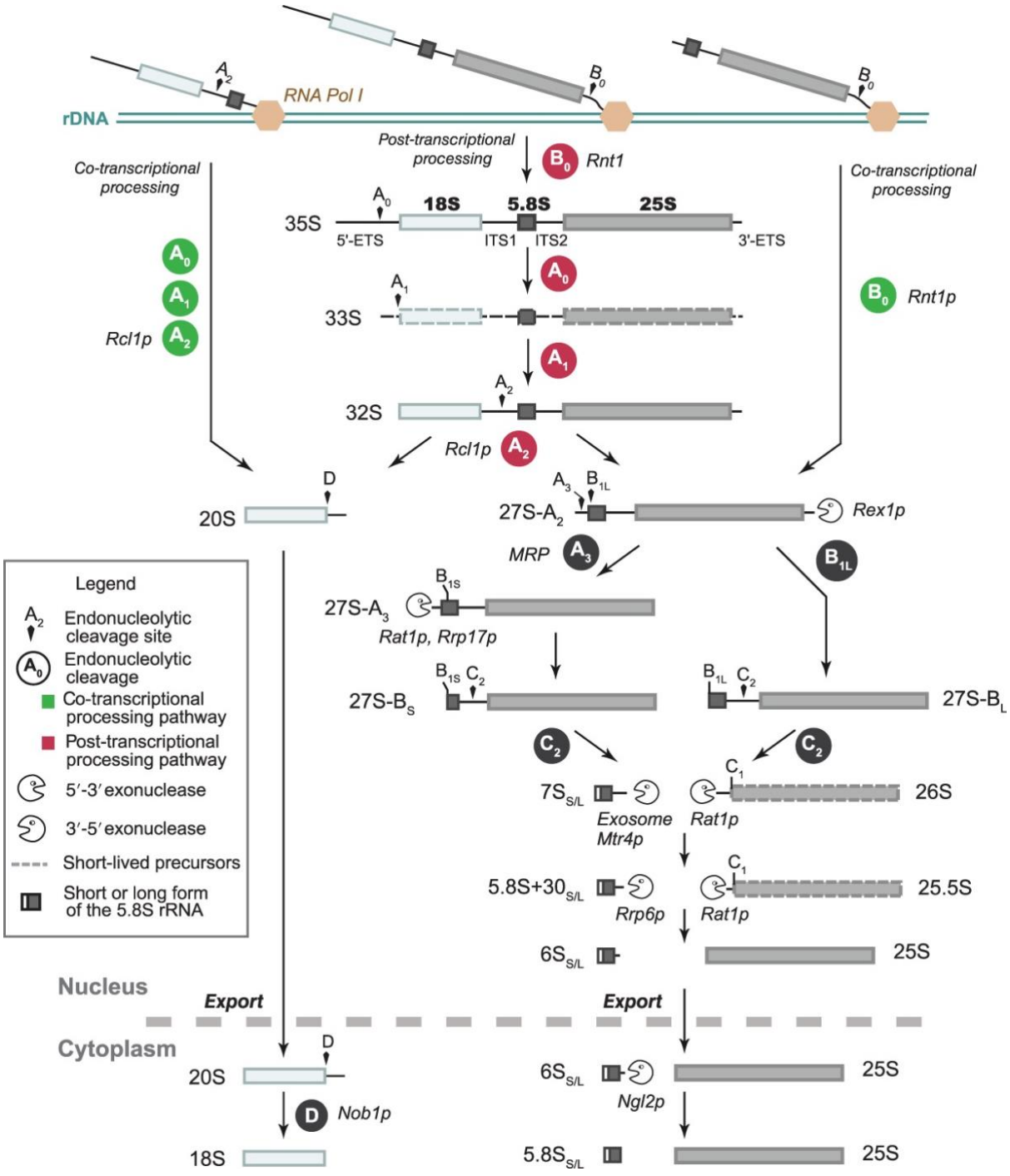

Figure 1.3 Overview of pre-rRNA processing in yeast
Endo and exonucleolytic cleavage steps of the nascent pre-rRNA are summarized with the enzymes responsible for some steps indicated. Figure adapted from (Henras et al., 2015).

Apparently, ITS1 co-transcriptional cleavage at site A_2, separating 40S and 60S subunit maturation pathways, does not occur immediately after ITS1 transcription but is delayed until the transcription of 5.8S rRNA, ITS2 and beginning of 25S rRNA (approximately 1.5 kb downstream of A_2) has occurred (Axt et al., 2014; Koš and Tollervey, 2010; Osheim et al., 2004). On the other hand, processing of pre-rRNA in higher eukaryotes, including humans, occur exclusively post-transcriptionally (Gamalinda et al., 2014). In fact, chromatin spreads of *Xenopus* oocytes rDNA genes showed no co-transcriptional cleavage of nascent pre-rRNA (Osheim et al., 2004).

1.2.3 Modifications of rRNA in yeast

Another major process in ribosome biogenesis is the covalent modifications of rRNA bases and ribose. These modifications occur mainly during early steps of rRNA folding co-transcriptionally (Koš and Tollervey, 2010) and also post-transcriptionally. The rRNA modifications are introduced at early steps of ribosome biogenesis so that the rRNA is still not compactly folded and the target rRNA sites are accessible to the modification machineries. RNA modifications exist in all three kingdoms and around 2% of rRNA nucleotides are modified corresponding to 112 sites identified in yeast and 201 sites identified in human (Sharma and Lafontaine, 2015; Sloan et al., 2017). There are two major types of rRNA modifications: 2`-O-ribose methylation, which can be introduced at any nucleotide and isomerization of uridine to pseudouridine. So far, 55 methylated nucleotides, 45 pseudouridines and 2 acetylated cytosines were identified in yeast rRNA. Few of these modifications are introduced by stand-alone enzymes that can directly identify their target site e.g. Emg1, Spb1, Rcm1 and Nop2 (Lapeyre and Purushothaman, 2004; Meyer et al., 2011; Sharma et al., 2013). On the other hand, the majority of rRNA modifications are introduced by snoRNA-guided enzymes that form snoRNA ribonucleoprotein complexes (snoRNPs), which are classified into two classes, the C/D box and H/ACA box snoRNPs. Each of these snoRNP classes use a snoRNA that can base-pair with the pre-rRNA at a specific location and guide the enzymatic component to modify a specific nucleotide (Ganot et al., 1997; Kiss-László et al., 1996).

The C/D box snoRNPs use C/D box snoRNAs that are characterized by two conserved motifs, C box and D box, in addition to two degenerate C` and D` boxes (Figure 1.4 A). The C box with sequence (RUGAUGA) is located near the 5`-end of the snoRNA, while the D box with sequence (CUGA) is located near the 3`-end. The

C/D box snoRNPs carry out the 2'-O-ribose methylation using Nop1 (Fibrillarin in human) as the principal methyltransferase and co-factors Nop58, Nop56 and Snu13 which help to structurally stabilize the complex. On the other hand, the H/ACA snoRNPs use H/ACA snoRNAs that form a double hairpin structure and contain two conserved sequences: H box (ANANNA) and ACA sequence (Figure 1.4 B). The H/ACA snoRNPs are responsible for isomerization of uridine to pseudouridine (pseudouridylation) using the pseudouridine synthase Cbf5 (Dyskerin in human) besides the co-factors Gar1, Nhp2 and Nop10 (Reviewed in Reichow et al., 2007; Sloan et al., 2017; Watkins and Bohnsack, 2012).

.

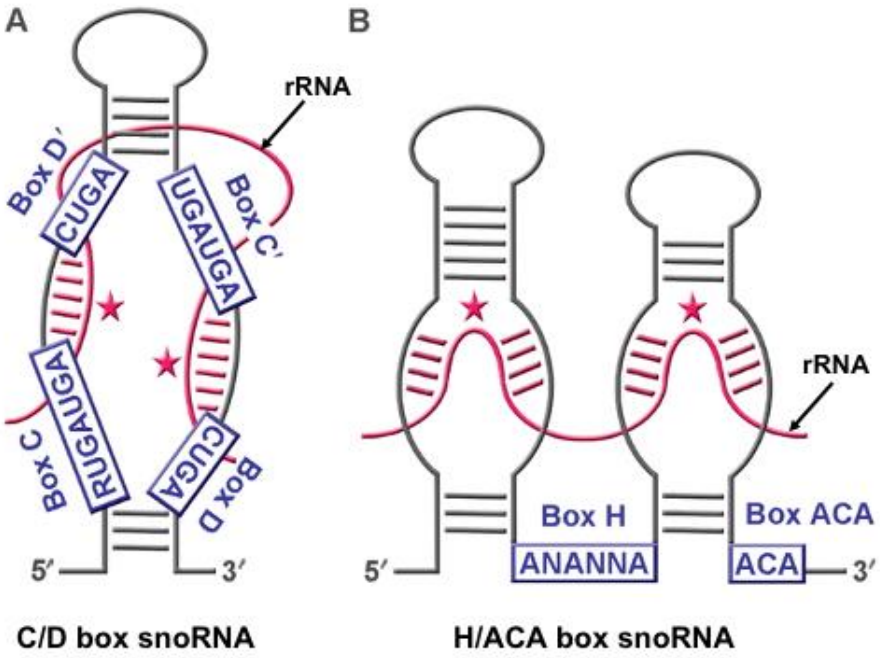

Figure 1.4 Schematic representation of snoRNAs structure
The figure shows the C/D box (A) and H/ACA Box (B) snoRNAs structures with their conserved motifs and their interactions with the target rRNA. Figure modified from (Reichow et al., 2007).

It is believed that RNA modifications can stabilize secondary and tertiary structure of RNA by enhancing base-stacking, increasing the hydrogen bonding potential and supporting structural rigidity (Decatur and Fournier, 2002; Helm, 2006). Thus, rRNA modifications stabilize the structure of mature ribosomes to ensure efficient translation. Indeed, a number of the highly conserved modifications are clustered around functionally important sites of ribosome, located at the ribosomal subunits interface where translation takes place, such as the peptidyl transferase center (PTC), the

decoding center and the intersubunit interface (Figure 1.5) (Baudin-baillieu et al., 2009; Decatur and Fournier, 2002; Sloan et al., 2017).

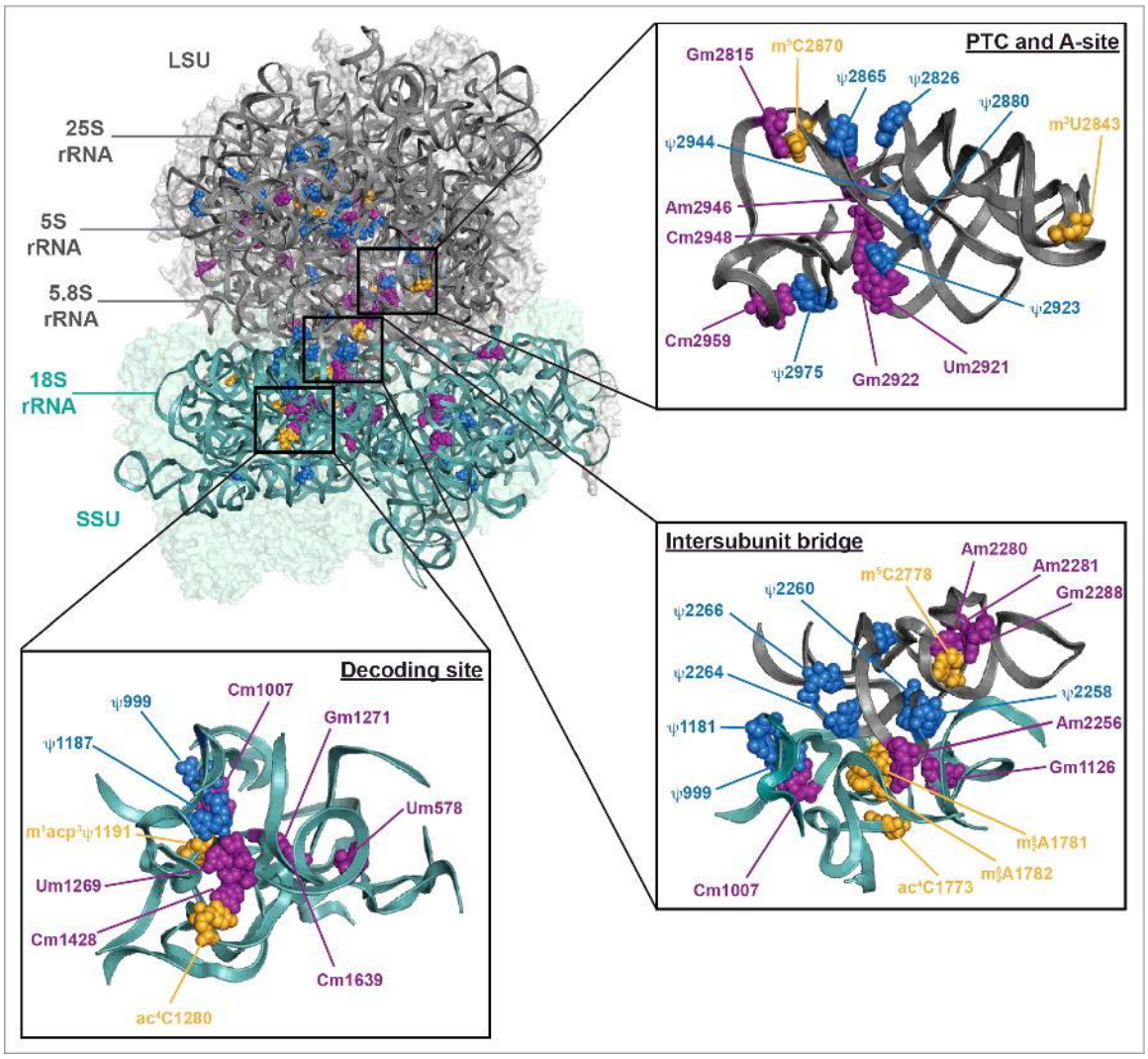

Figure 1.5 rRNA modifications on the yeast ribosome
The figure shows the distribution of modification sites on the yeast mature ribosome and highlights the cluster of modifications on three functional regions. Ribose methylation is colored in purple, pseudouridines are colored in blue and modifications by stand-alone enzymes are colored in orange. Figure adapted from (Sloan et al., 2017).

Notably, it was found that yeast cells with ribosomes lacking single or a cluster of rRNA modifications, caused by deletion of their respective snoRNAs, are outcompeted by wild-type cell as the absence of certain modifications can have an effect on protein translation activity and/or accuracy including increased sensitivity to antibiotics (Baudin-baillieu et al., 2009; King et al., 2003; Liang et al., 2007, 2009). Additionally, there is a link between rRNA modifications machinery and diseases in vertebrate. For

example, impairing rRNA modifications in zebrafish through disrupting the expression of three snoRNAs has caused sever developmental defects (Higa-Nakamine et al., 2012). In humans, several reports have identified mutations in snoRNAs and proteins from the rRNA modifications machinery that are involved in development of human diseases or syndromes (Armistead et al., 2009; Dong et al., 2008, 2009; Heiss et al., 1998; Liao et al., 2010; Sahoo et al., 2008; Schosserer et al., 2015; Tanaka et al., 2000).

1.2.4 Small ribosomal subunit maturation

The biogenesis of the small subunit biogenesis starts with the transcription of rDNA genes as ribosome assembly factors co-transcriptionally associate with the emerging nascent pre-rRNA transcript in a hierarchical order, forming the first pre-ribosomal intermediate, the 90 pre-ribosome, which can be biochemically isolated and further characterized (Dragon et al., 2002; Grandi et al., 2002; Pérez-Fernández et al., 2007). Notably, the 90 particles contain assembly factors and r-proteins required for assembly of the small subunit but lack assembly factors and r-proteins of the large subunit assembly pathway (Dragon et al., 2002; Grandi et al., 2002; Kornprobst et al., 2016; Pérez-Fernández et al., 2007). This indicates that the 90S pre-ribosome forms the precursor for the small subunit assembly pathway.

Inside the nucleolus, many assembly factors get incorporated into the 90S particles in the form of sub-complexes or modules (Krogan et al., 2004; Pérez-Fernández et al., 2007) (Figure 1.6). The UTP-A module attaches to the nascent 5`-ETS co-transcriptionally and it includes the factors Utp4, Utp5, Utp8, Utp9, Utp10, Utp15 and Nan1 (Gallagher et al., 2004; Pérez-Fernández et al., 2007; Pöll et al., 2014). Another module which also associates with 5`-ETS, is the UTP-B Module with its components: Utp1 (Pwp2), Utp6, Utp12 (Dip2), Utp13, Utp18 and Utp21 (Kornprobst et al., 2016; Pérez-Fernández et al., 2007; Pöll et al., 2014). The U3-snoRNP (U3 snoRNA, Nop1, Nop56, Nop58, Snu13 and Rrp9) is another interesting module within the 90S particles which does not install any rRNA modification, but supports the 90S structure (Chaker-Margot et al., 2017; Kornprobst et al., 2016; Sun et al., 2017). The UTP-A, UTP-B, U3-snoRNP together with the Mpp10 module (Mpp10, Imp3, Imp4 and Sas10) form a 5`-ETS particle, which provides a structural support for subsequent assembly of the 18S rRNA subdomains (Chaker-Margot et al., 2015; Zhang et al., 2016). Electron microscopy of chromatin spreads (Miller spreads) revealed the formation of terminal

balls or knobs near the 5`-end of nascent pre-rRNA transcripts, which were later attributed to the 5`-ETS particle within the evolving 90S pre-ribosomes (Miller and Beatty, 1969; Mougey et al., 1993; Osheim et al., 2004). Further assembly of the 18S rRNA subdomains proceeds with incorporation of other modules (UTP-C, Kre33 and Noc4-Nop14) and assembly factors (e.g. Efg1, Cms1, Bms1-Rcl1, Dhr1, Utp20, Rrp5…etc) (Figure 1.6) (reviewed in Barandun et al., 2018; Klinge and Woolford, 2019).

The nascent pre-rRNA is cleaved co-transcriptionally at sites A_0 and A_1 to remove the 5`-ETS, with its associated modules, and begin with the 90S particle disassembly. The other endo-nucleolytic cleavage at site A_2 releases the 20S pre-rRNA (precursor of 18S rRNA) and the $27SA_2$ pre-rRNA (precursor of 5.8S and 25S rRNAs), thus separating the pre-40S and pre-60S assembly pathways (Udem and Warner, 1972). After dismantling the 5`-ETS particle and A_2 cleavage, few 90S assembly factors (Enp1, Pno1, Rrp12) remain associated with the evolving pre-40S in the nucleus, where some additional pre-40S assembly factors (Ltv1, Tsr1, Rio2, Dim1 and Nob1) and r-proteins get incorporated (reviewed in Henras et al., 2008; Klinge and Woolford, 2019). At this point, the pre-40S particles have already acquired some regions of the mature 40S such as the head, platform and body but not the beak. Afterwards, the pre-40S particles get exported to the cytoplasm for further maturation.

In the cytoplasm, formation of the 40S beak region is facilitated by the release of Enp1 and Ltv1, which occur after their phosphorylation via the kinase Hrr25 (Ghalei et al., 2015; Schäfer et al., 2006). Their release allows the r-protein Rps3 (uS3) to adopt its mature position, which promotes the beak region formation (Mitterer et al., 2016; Schäfer et al., 2006). Interestingly, a quality control step involves the interaction of the pre-40S particle with the mature 60S subunit forming an 80S-like particle to test the pre-40S particle in a translation-like cycle (Strunk et al., 2012). This test drive cycle triggers the final cleavage of the 20S pre-rRNA at the D site, by the endonuclease Nob1, to generate the mature 18S rRNA and subsequently the removal of the remaining assembly factors (Lamanna and Karbstein, 2009; Pertschy et al., 2009; Strunk et al., 2012). At this stage, all the r-proteins have already been incorporated with the small subunit which is mature and competent for translation.

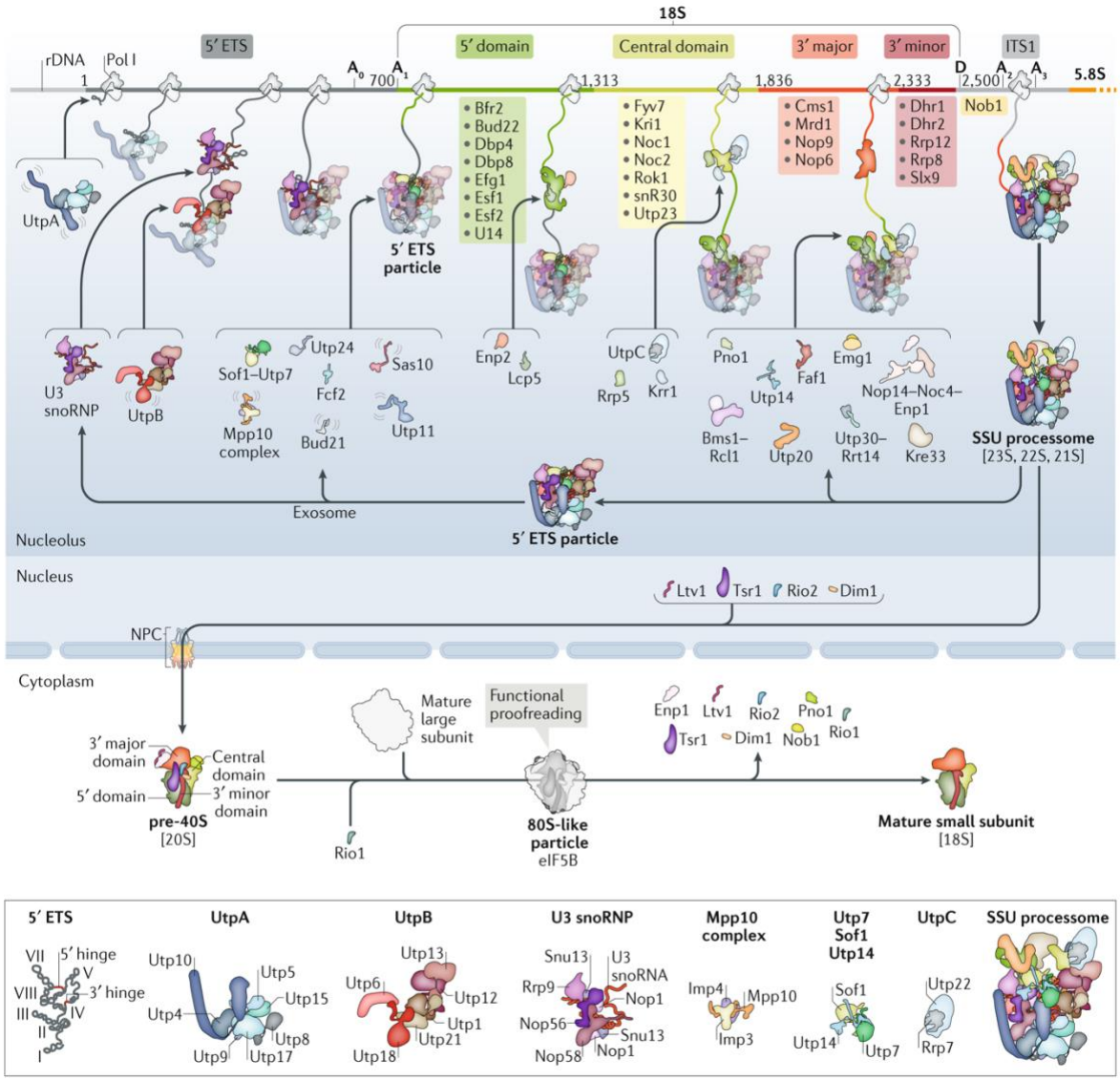

Figure 1.6 Small ribosomal subunit maturation

Schematic representation of major steps in assembly of the small ribosomal subunit from formation of 90S pre-ribosomes (SSU processome) in the nucleolus until the complete maturation of the small subunit in the cytoplasm. Figure adapted from (Klinge and Woolford, 2019).

1.2.5 Large ribosomal subunit maturation

The structure of mature 60S subunit is more intricate than the mature 40S subunit, hence its biogenesis follows extensive pre-rRNA processing (see Figure 1.3) and structural rearrangement events. The 25S rRNA consists of six domains, domains I-VI from 5` to 3`, intertwined with each other in the mature large subunit which requires complex biogenesis, involving many energy-consuming enzymes, to drive and chaperone the correct folding of these domains (Reviewd in Baßler and Hurt, 2019; Greber, 2016; Klinge and Woolford, 2019; Konikkat and Woolford, 2017; Kressler et al., 2010).

Initial assembly of the large subunit occurs during the co-transcriptional cleavage at site A_2, which generates the $27SA_2$ pre-rRNA, the earliest pre-rRNA precursor for 60S assembly. Interestingly, the assembly factor Rrp5 has a dual role in the assembly of both the small and the large subunits (Venema and Tollervey, 1996). It binds to the ITS1 region near the A_2 site, bridging between the 90S pre-ribosome and the emerging pre-60 pre-ribosome, and co-ordinates the co-transcriptional processing (Khoshnevis et al., 2019; Lebaron et al., 2013). After A_2 cleavage, Rrp5 detaches from the 90S pre-ribosome, but stays associated with the nascent pre-60 and forms a complex with the assembly factors Noc1 and Noc2 (Rrp5 module) (Hierlmeier et al., 2013). Following the end of pre-rRNA transcription, the earliest precursor for 60S assembly is formed, which carries the $27SA_2$ pre-rRNA and the Rrp5 module. This primordial 60S is poorly characterized and no structural information of this particle is available so far. Obtaining a structure for this primordial 60S is challenging because most of the rRNA domains, at this early stage, are not folded yet. However, biochemical studies show that this $27SA_2$ pre-rRNA-containing particle interact with another module of unknown function, consisting of Urb1 (Npa1), Urb2 (Npa2), Nop8, Dbp6 and Rsa3, called Urb1 module (Dez et al., 2004; Joret et al., 2018; Mnaimneh et al., 2004; Rosado and De La Cruz, 2004; Rosado et al., 2007). At this stage, modifications of rRNA nucleotides are expected to occur as the pre-rRNA is not compacted yet and the modification machineries could access their target nucleotides.

Most of the $27SA_2$ pre-rRNA is then cleaved at site A_3 by the MRP RNase (Chu et al., 1994; Lindahl et al., 1992; Lygerou et al., 1996; Schmitt and Clayton, 1993) and the remaining sequence of ITS1 is processed by the exonucleases Rat1, Xrn1 and Rrp17 to yield the $27SB_S$ pre-rRNA (see Figure 1.3) (Henry et al., 1994; Oeffinger et al., 2009). Cryo-EM structures of the nucleolar pre-60S intermediates carrying the

27SB pre-rRNA, have provided interesting insights into the folding events of its rRNA domains and the organization of the associated assembly factors and r-proteins (Kater et al., 2017; Sanghai et al., 2018; Zhou et al., 2018). These cryo-EM structures revealed that initial assembly of this intermediate begins with the formation of the solvent-exposed interface by folding of 5.8S rRNA, ITS2 and the 25S rRNA domains I and II to form a stable core for further assembly. Afterwards, the 25S domain VI is integrated with domains I and II leading to formation of a tightly packed ring-like structure, while domains III, IV and V remain initially flexible and not stably assembled. Notably, the 5S RNP, 5S rRNA together with the r-proteins Rpl5 (uL18) and Rpl11 (uL5), is already recruited to these pre-60S intermediates but is not yet resolved in these cryo-EM structures, indicating that it is flexibly attached and not yet stably incorporated (Figure 1.7) (Kater et al., 2017; Sanghai et al., 2018; Zhou et al., 2018). Ribosome assembly factors and r-proteins stabilize the RNA domains in these nucleolar intermediates. For example, ITS2 is organized and stabilized by CIC1 (Nsa3), Rlp7 and Nop15, Has1, Nop7, Ytm1 and Erb1 to create the foot structure. Also, the Brix domain-containing assembly factors (Brx1, Rpf1 and Ssf1) together with their protein partners stabilize, chaperone and bridge various rRNA domains to each other (Baßler et al., 2017; Bogengruber et al., 2003; Kaser et al., 2001). Brx1 and its partner bind and stabilize domains I and II. Rpf1-Mak16-Nsa1-Rrp1 module sits on a location near to where later the PET will be formed and are in contact with 5.8S, domains I and II (Kater et al., 2017). Ssf1 and its partners Rrp15 and Rrp14 are located at the interface of domains I and VI (Sanghai et al., 2018). The assembly factors Noc3, Nop2 and Spb1 appear from the subunit side and bind to domains VI and V in a location, which later the PTC will be formed (Kater et al., 2017). Thus, release of these assembly factors in the following steps of assembly is important to drive and complete the maturation of the rRNA domains, subsequent association of other assembly factors/r-proteins and further construction of the functional sites.

Cryo-EM structures combined with biochemical studies of late nucleolar and nuclear pre-60S intermediates have clarified further maturation steps including ITS2 processing to remove the foot structure, docking and rotation of the 5S RNP as well as further maturation of the functional regions PET and PTC (Barrio-Garcia et al., 2016; Bradatsch et al., 2012; Gasse et al., 2015; Leidig et al., 2014; Thoms et al., 2015; Wu et al., 2016).

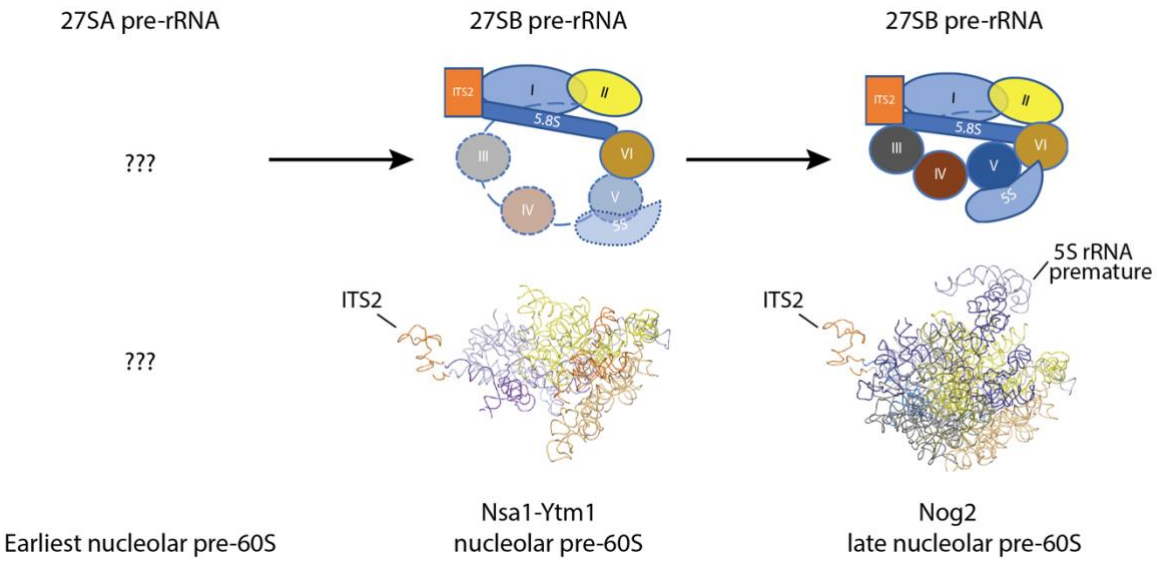

Figure 1.7 Organization of rRNA domains in nucleolar pre-60S particles
The figure shows schematic representation and 3D structure of rRNA domains organization discovered in the nucleolar pre-60S particles Nsa1-Ytm1 (PDB: 6EM1) and Nog2 (PDB: 3JCT). Dashed circles represent flexible domains.

The prominent foot structure, including ITS2 as well as the associated assembly factors Nsa3 (Cic1), Rlp7, Nop15 and Nop7, is removed in the nucleoplasm through ITS2 processing. Processing of ITS2 proceeds with the cleavage of the 27SB pre-rRNA at site C2 by the endonuclease Las1 (Gasse et al., 2015), which generates a 7S and 26S pre-rRNAs (See Figure 1.3). Subsequently, the 5`-3` exonuclease Rat1-Rai1 trims some nucleotides of the 26S pre-rRNA to yield the 25 rRNA (Gasse et al., 2015). Meanwhile, the nuclear exosome is recruited to the 7S pre-rRNA via Nop53 (Thoms et al., 2015) and trims the extra nucleotides in the 3`-5`directions, yielding 6S pre-rRNA (Mitchell et al., 1997; Schuller et al., 2018). In the cytoplasm, 3`-end of the 6S pre-rRNA is finally processed by the exonuclease Ngl2 to produce mature 5.8S rRNA (Thomson and Tollervey, 2010).

At an early step, the Brix domain-containing Rpf2 and its partner Rrs1 interact with the 5S RNP and facilitate its incorporation into the nucleolar pre-60 pre-ribosome at the CP (Asano et al., 2015; Kharde et al., 2015; Madru et al., 2015; Zhang et al., 2007). Interestingly, the 5S RNP is initially associated with the pre-60 particles in a twisted conformation around 180° rotated compared to its position in mature 60S subunit (Leidig et al., 2014; Wu et al., 2016). At a later nuclear step, the maturation of the CP region involves the rotation of the 5S RNP by around 180° to adopt its mature

conformation. This conformational rearrangement seems to be coupled with action of the ATPase Rea1 (Mdn1) on pre-60 particles inducing structural changes (Barrio-Garcia et al., 2016). The maturation of the large subunit at this stage involves successive action of Rea1. Upon ATP hydrolysis, the ATPase Rea1 can create a pulling force to release many assembly factors and stimulate remodeling of the pre-60S particles. At an earlier step, Rea1 binds to its substrate Ytm1 and utilize its ATPase activity to trigger the release of Ytm1-Erb1-Nop7 subcomplex (Baßler et al., 2010). The long N-terminus of Erb1 meanders over the pre-60 particle, extending through ITS2 to 25S domain I and II areas, contacting a couple of assembly factors. Thus, release of Erb1 seems to also cause the exit of these factors from the pathway (Kater et al., 2017). A second round of binding of Rea1 to pre-60S particles, together with Rix1-Ipi1-Ipi3, triggers the removal of Rsa4 (Ulbrich et al., 2009). Recruitment of the Rea1-Rix1 machinery to pre-60S particles coincides with the dissociation of Rpf2-Rrs1 which allows rotation of the 5S RNP (Barrio-Garcia et al., 2016). This second round of Rea1 binding and Rsa4 removal, activates the GTPase Nog2 and cause its release from the particle (Matsuo et al., 2014). The nascent PTC is covered by the GTPases Nog1 and Nog2 and release of these factors allows the rearrangement of the RNA neighborhood around the PTC leading to formation of an almost-mature PTC and recruitment of the export factor Nmd3 (Ma et al., 2017; Matsuo et al., 2014). Therefore, the remodeling events of Rea1, Nog2 and maturation of the CP as well as the PTC establish a checkpoint, which gives export competence to 60S pre-ribosomal particles.

The export competent pre-60S particles are exported from the nucleus to the cytoplasm through the nuclear pore complex (NPC). The pre-60S particles utilize a couple of export factors such as Nmd3, Arx1 and Mex67-Mtr2 to facilitate their passage through the NPC channel which is filled with Phenylalanine-Glycine (FG)-rich repeats nucleoporins. These export factors shield the hydrophilic surface of the pre-60S particles from the hydrophobic surroundings inside the NPC meshwork. Some of these export factors such as Arx1 and Mex67-Mtr2 interact directly with FG-rich nucleoporins (Bradatsch et al., 2007; Yao et al., 2007). On the other hand, Nmd3 does not directly bind to nucleoporins, but contains a nuclear export sequence that is recognized by the exportin Crm1, which interacts with nucleoporins and mediates the export (Gadal et al., 2001; Ho et al., 2000).

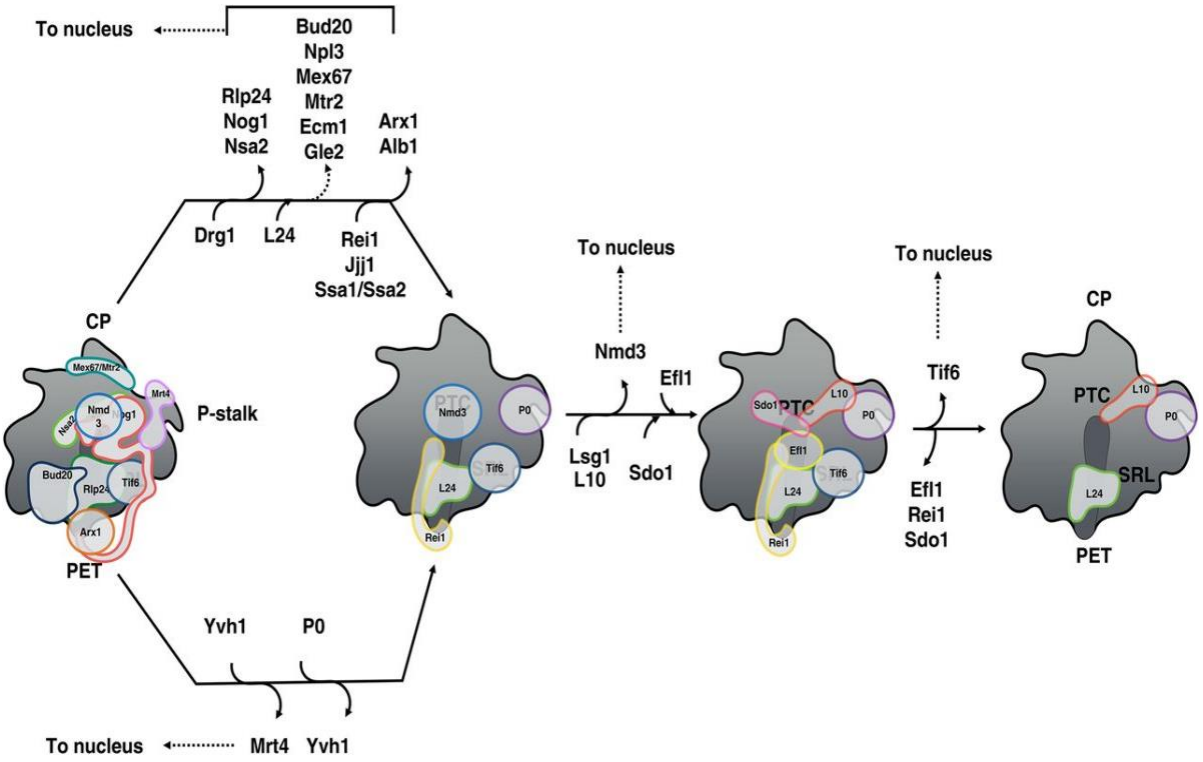

Figure 1.8 Cytoplasmic maturation of pre-60S particles
The figure shows a summary of final steps of maturation of 60S pre-ribosomal particles in the cytoplasm. Figure adapted from (Konikkat and Woolford, 2017).

After export to the cytoplasm, the pre-60S particles go through the final maturation steps where the remaining assembly factors are released and the last r-proteins get incorporated (Figure 1.8) (reviewed in Greber, 2016; Karbstein, 2013; Panse and Johnson, 2010). The ATPase Drg1 catalyze the release of Rlp24 and Nog1 from the particles, and subsequently Rlp24 is replaced by its homologous r-protein L24 (eL24) (Kappel et al., 2012; Pertschy et al., 2007). This step initiates further downstream maturation steps as it enables the assembly factors Rei1, Jjj1 and Ssa1/2 to dissociate Arx1-Alb1 from the rim of the PET (Demoinet et al., 2007; Hung and Johnson, 2006; Lebreton et al., 2006; Meyer et al., 2007). Meanwhile, the phosphatase Yvh1 facilitates the removal of Mrt4, a structural homolog of the r-protein P0 (uL10), and the concomitant association of P0, leading to the P-stalk formation (Kemmler et al., 2009; Lo et al., 2009; Sarkar et al., 2016). Apparently, the final steps include incorporation of the r-protein L10 (uL16) as well as release of Tif6 and Nmd3 (Figure 1.8). The anti-association factor Tif6 (eIF6), prevents the association of pre-60S particles with mature 40S, is released by Ria1 (Efl1) and Sdo1 (SBDS) (Bécam et al., 2001; Menne et al., 2007; Senger et al., 2001). Meanwhile, Nmd3 release is facilitated by the

GTPase Lsg1 and coupled with the stable integration of the r-protein L10 (uL16) (Hedges et al., 2005; West et al., 2005). At this point, the PTC as well as other functional sites have matured and the 60S subunit is ready to associate with the 40S subunit and engage in protein synthesis.

1.3 Ribosome biogenesis and human diseases

In humans, mutations in ribosome assembly factors or ribosomal proteins can lead to a range of human diseases, termed ribosomopathies (reviewed in Armistead and Triggs-Raine, 2014; Farley and Baserga, 2016; Kampen et al., 2020; Narla and Ebert, 2010; Yelick and Trainor, 2015). Such mutations result in reduced ribosome biogenesis and affect overall protein translation. At an early phase, most of ribosomopathies cause bone marrow failure and anemia leading to cellular hypo-proliferation. However, there is an intriguing paradox after ribosomopathy patients survive this lethal phase with supportive treatments (De Keersmaecker et al., 2015). Surprisingly, the patients have higher risk of developing cancer, cellular hyper-proliferation, later in life. There are several interesting theories to explain the relation between ribosomopathies and cancer discussed in (Kampen et al., 2020; Sulima et al., 2019).

Diamond-Blackfan anemia (DBA) is an autosomal dominant disorder and one of the most studied ribosomopathies. Many r-proteins mutations leading to haploinsufficiency have been identified in patients with DBA, including mutations in Rps19 (eS19), Rps10 (eS10), Rps17 (eS17), Rpl5 (uL18), Rpl11 (uL5), RpL26 (uL24), Rpl35A (eL33) and Rpl36A (eL42) (Armistead and Triggs-Raine, 2014; Choesmel et al., 2007; Draptchinskaia et al., 1999; Farrar et al., 2008; Gazda et al., 2012; Horos et al., 2012). This disease is characterized by anemia, craniofacial abnormalities, short stature, thumb abnormalities and sometimes bone marrow failure.

Schwachman-Diamond syndrome is an autosomal recessive ribosomopathy with most patients having inactivating mutations in SBDS gene (Sdo1 in yeast) (Boocock et al., 2003; Woloszynek et al., 2004). As I mentioned in last section (1.2.5 Large ribosomal subunit maturation), yeast Sdo1 is involved in the release of the anti-association factor Tif6 (eIF6 in human) from pre-60S particles in the cytoplasm. Therefore, inefficient release of eIF6 from the pre-60S particles delays the maturation of the large ribosomal subunit in patients with Schwachman-Diamond syndrome

(Finch et al., 2011). Patients with this disorder display exocrine pancreatic insufficiency, skeletal abnormalities, ineffective hematopoiesis and predisposition to cancer.

Examples for other ribosomopathies include X-linked dyskeratosis congenita, Treacher Collins syndrome, Cartilage hair hypoplasia, Bowen-Conradi syndrome, ANE syndrome, North American Indian childhood cirrhosis and chromosome 5q syndrome (Armistead et al., 2009; Chagnon et al., 2002; Ebert et al., 2008; Heiss et al., 1998; Nousbeck et al., 2008; Ridanpää et al., 2001; Trainor et al., 2009). Ribosome biogenesis is highly conserved from yeast to human. Therefore, studying ribosome biogenesis in yeast could expand our understanding of the related diseases in humans, including ribosomopathies and cancer, as well as facilitate treatments development.

2 Aim of work

Biogenesis of ribosomes has been extensively studied in eukaryotes over the last two decades, with each study revealing a drop in the ocean of this intricate and essential pathway, but also raising new questions. The 90S pre-ribosome is the first stable intermediate formed after the co-transcriptional cleavage of the pre-rRNA at ITS1, which was structurally well studied over the last years. However, many aspects of the earliest steps of pre-60S assembly are still unclear and little is known about their link to the upstream 90S pathway.

Prompted by this lack of knowledge, the project started with revisiting an old observation that a *nop1-4* mutant allele has caused a defect in pre-60S particles, indicating that snoRNPs could trigger the pre-60S assembly pathway. Thus, I aimed to find and isolate the earliest pre-60S particle in order to characterize it and study the role of snoRNPs in pre-60S assembly as well as delineate this particle from the succeeding nucleolar pre-60S particles. In this context, I sought to further investigate some of the uncharacterized components, assembly factors and snoRNAs, in this particle to shed further light into the earliest stage of pre-60S assembly. Moreover, structural analysis of the earliest pre-60S was lacking. Therefore, I tried to gain structural information on the overall architecture of the earliest pre-60S. Using a dominant negative Mak5 mutant, I aimed to finally isolate and visualize a large pre-ribosomal intermediate containing both 90S and pre-60S moieties unseparated.

3 Results

3.1 Mutant *nop1-4* cells show abnormal pre-60S particles

It was found in the case of the U3 snoRNP that it does not introduce pre-rRNA modification, but it rather has a structural role essential for pre-rRNA processing and maturation (Beltrame and Tollervey, 1995; Hughes, 1996; Hughes and Ares, 1991; Sharma and Tollervey, 1999). Subsequently, this has been biochemically and structurally proven for the U3 snoRNP, which forms a structural module integrated within the 90S pre-ribosome (Chaker-Margot et al., 2017; Cheng et al., 2020; Kornprobst et al., 2016; Sun et al., 2017). However, it is still unclear whether snoRNPs could be integrated within the early pre-60S particles to play a role in their assembly similar to the U3 snoRNP in the 90S pre-ribosome.

This open question prompted me to follow an old observation that a mutation in the yeast methyltransferase Nop1 (*nop1-4* allele; Ala245>Val), a well characterized 90S and core C/D box snoRNA factor, has induced formation of abnormal pre-60S particles (Tollervey et al., 1993). To check this defect, I isolated pre-60S particles from wild-type and *nop1-4* mutant yeast cells using tandem affinity purification (TAP) of the pre-60S assembly factor Nsa3 (Cic1) (Figure 3.1). In wild-type cells, affinity purification of Nsa3, an ITS2 foot factor, yields a broad range of early nucleolar to intermediate nuclear stages pre-60S particles. Surprisingly, purification of Nsa3 from *nop1-4* mutant cells shows abnormal 60S pre-ribosomes with accumulation of 90S assembly factors beside the typical pre-60S assembly factors (Figure 3.1A). To analyze the protein composition difference between these wild-type and mutant particles, I performed semi quantitative mass spectrometry analysis (Figure 3.1B). The analysis shows an accumulation of many 90S modules and factors (e.g. UTP-A, UTP-B, UTP-C, Rrp12, Kre33, UTP20, Emg1 and Mpp10) on these Nsa3 particles purified from *nop1-4* mutant background, as if a fraction of the particles purified by Nsa3 is still connected to the 90S pre-ribosome (Figure 3.1B). Notably, some assembly factors existing in later large subunit intermediates such as Rea1 and Rix1 complex or Sda1 were significantly reduced in the Nsa3 eluate of the *nop1-4* mutant (Figure 3.1A and 3.1B). On the other hand, other core pre-60S assembly factors such as the ITS2-associated factors, Erb1, Ytm1, Nsa1, Nog1 and Spb1 did not show significant change (Figure 3.1B).

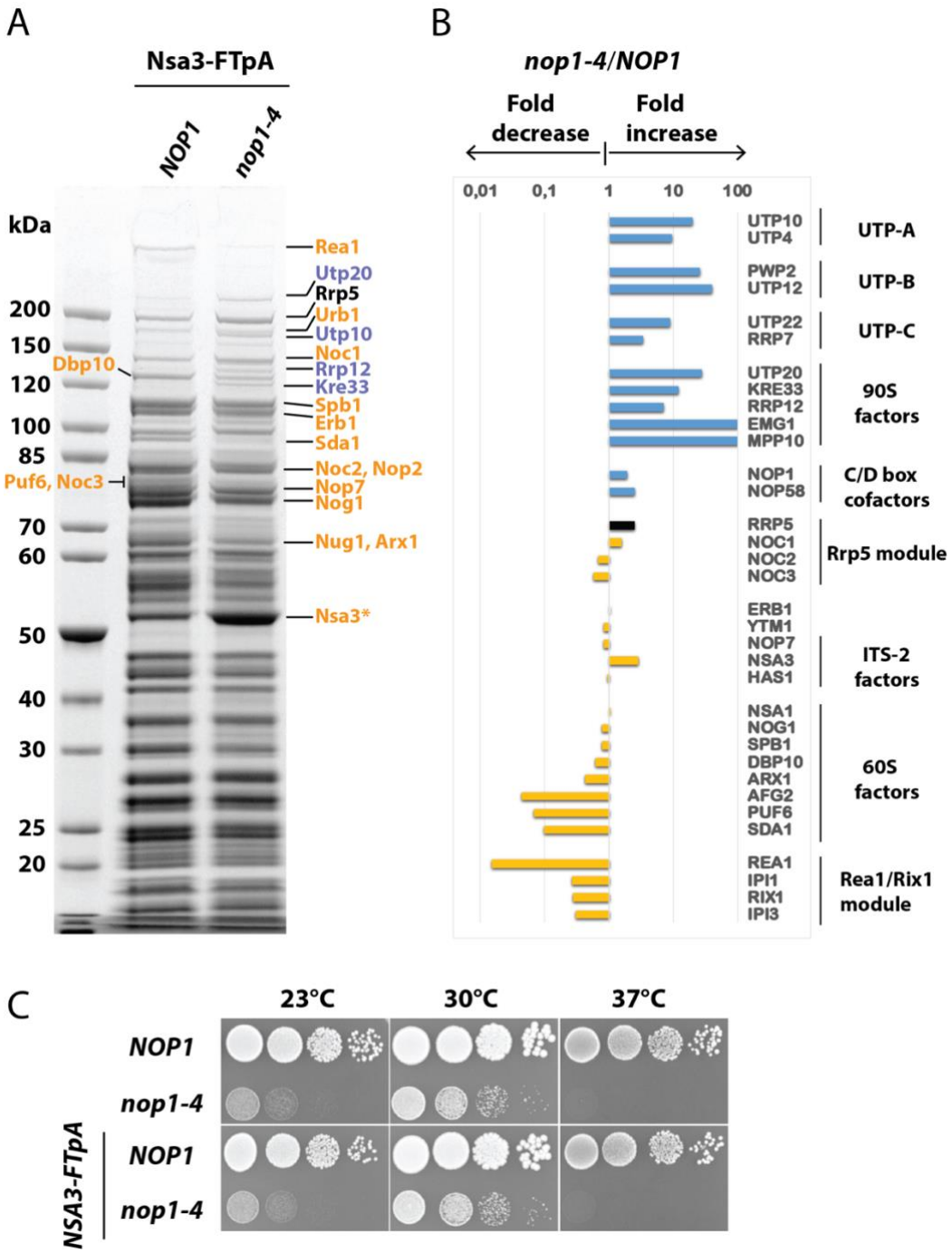

Figure 3.1 Affinity purification of Nsa3 particles from wild-type *NOP1* and *nop1-4* mutant cells

(A) Nsa3 tagged with Flag-TEV-ProtA (Nsa3-FTpA) was affinity purified from wild-type and *nop1-4* cells. The final eluates were separated on a 4-12% gradient SDS-polyacrylamide gel followed by Coomassie staining. Major bands were identified by mass spectrometry. Pre-60S assembly factors are colored in orange and 90S assembly factors are colored in blue. The bait Nsa3 (Cic1) is indicated by an asterisk.

(B) Semiquantitative mass spectrometry analysis was performed on the Nsa3-FTpA eluates depicted in (A). The LFQ values (normalized to Erb1) derived from the nop1-4 mutant particles were divided by the values derived from the wild-type particles (*NOP1*) to show the fold change of the assembly factors. The values for 90S assembly factors are colored in blue and the

values for the pre-60S assembly factors are colored in orange. Rrp5 is labeled in black due to its dual role in 90S and pre-60S assembly.
(C) Dot spot growth analysis of *nop1-4* and isogenic *NOP1* cells not containing (top) or carrying (bottom) chromosomally integrated *Nsa3*-FTpA. The strains were spotted in tenfold serial dilutions on YPD plates, which were incubated at 23°C, 30°C and 37°C for 3 days.

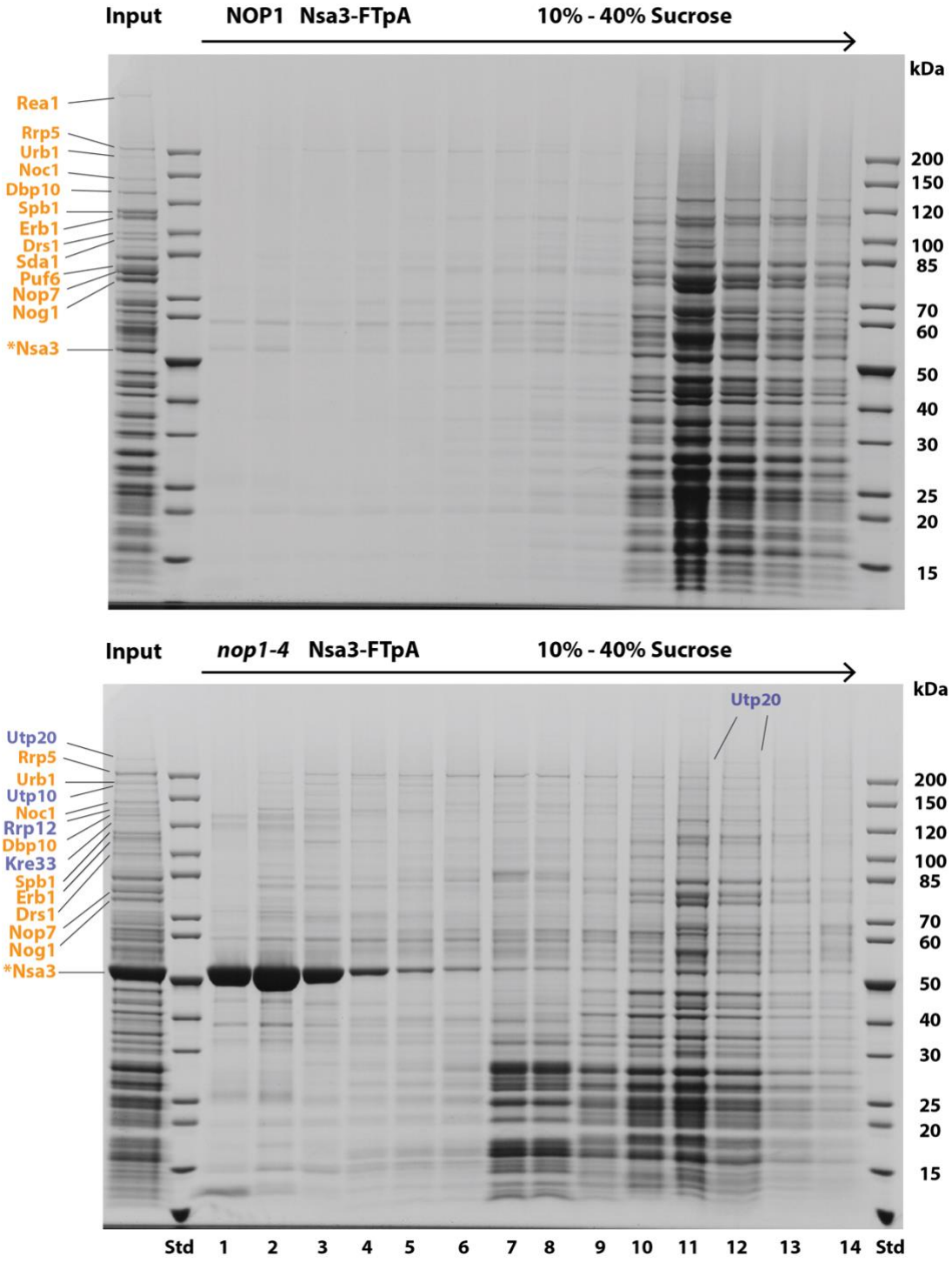

Figure 3.2 Sucrose gradient centrifugation of Nsa3 particles from *nop1-4* cells
Flag eluates of Nsa3-FTpA particles from wild-type *NOP1* and *nop1-4* cells were fractionated by sucrose gradient centrifugation (10%-40%) (w/v). From each gradient, 14 fractions were collected and precipitated by TCA. The samples were analyzed by 4-12% SDS-PAGE and

stained with Coomassie. Pre-60S assembly factors (orange) and 90S assembly factors (blue) are labeled. The bait Nsa3 (Cic1) is indicated by an asterisk.

Mutant *nop1-4* cells show a slow growth phenotype at 30°C, which is the temperature used to grow the cultures. To exclude the possibility that tagging Nsa3 with FTpA (**F**lag-**T**EV-**p**rot**A**) is exaggerating the phenotype of *nop1-4* mutant cells, I checked the cells in a growth test (Figure 3.1C). This showed that the tag did not exaggerate the phenotype of *nop1-4* mutant cells.

To test whether the Nsa3 particles from the mutant *nop1-4* cells could form a stable pre-ribosome containing both the pre-60S and 90S factors simultaneously, the final eluates of Nsa3 particles from *NOP1* wild-type and *nop1-4* cells were fractionated by sucrose gradient centrifugation followed by SDS-PAGE and Coomassie staining of the collected fractions (Figure 3.2). The *nop1-4* mutant Nsa3 particles showed extra 90S factors co-migrating with pre-60S factors in fraction 11 such as Utp20 and Rrp5, compared to *NOP1* wild-type. The mutant also showed small subunit r-proteins in fractions 7 and 8 as if they fell off the particle, fraction 11. Another possibility is that the free pool of Nsa3 in the mutant cells had non-specific binding to small subunit r-proteins.

Overall, these results suggest that the mutant *nop1-4* has caused a shift in the pre-60S particles purified by Nsa3 to an earlier stage, explaining the initial discovery of an impaired large subunit biogenesis in *nop1-4* mutant cells (Tollervey et al., 1993).

3.2 Isolation and characterization of snoRNPs-containing early pre-60S particles

There is the possibility that the mutant *nop1-4* has impaired 90S biogenesis first before a pleiotropic feedback effect on pre-60S biogenesis. The other scenario is that *nop1-4* mutation has directly affected pre-60S biogenesis at an early stage through one or a couple of pre-60S specific C/D box snoRNPs, carrying the mutant Nop1. To further investigate the role of Nop1 and the snoRNPs in 60S ribosomal assembly, I sought to isolate very early pre-60S particles that might contain these unknown snoRNPs. However, all the structurally characterized nucleolar pre-60S particles, so far, are devoid of snoRNPs (Kater et al., 2017; Sanghai et al., 2018; Zhou et al., 2018). The early pre-60S assembly factors Urb1 (Npa1) and Urb2 (Npa2) are good candidates to isolate such early pre-60S ribosomes. Urb1 and Urb2 are part of a chaperone module

Urb1-Urb2-Dbp6-Nop8-Rsa3 (Urb1 module) that was found in association with early pre-60S particles and mainly interacts with the $27SA_2$ pre-rRNA (Dez et al., 2004; Joret et al., 2018; Rosado et al., 2007), which is the earliest pre-rRNA precursor for 60S assembly.

Therefore, I tried to isolate snoRNP-containing early pre-60S by affinity purification of FTpA-tagged Urb1 or Urb2 (Figure 3.3). Both Urb1 and Urb2 purifications yielded particles that have free pool of Urb1 and Urb2 and distinct subcomplexes, while many bands appeared sub-stoichiometric. Mass spectrometry of the co-purified bands revealed the presence of other factors from the Urb1 module (Urb1-Urb2-Dbp6-Nop8-Rsa3), the Rrp5 module (Rrp5-Noc1-Noc2) and, interestingly, C/D box snoRNP factors such as Nop1, Nop56 and Nop58 (Figure 3.3). However, the other assembly factors were sub-stoichiometric.

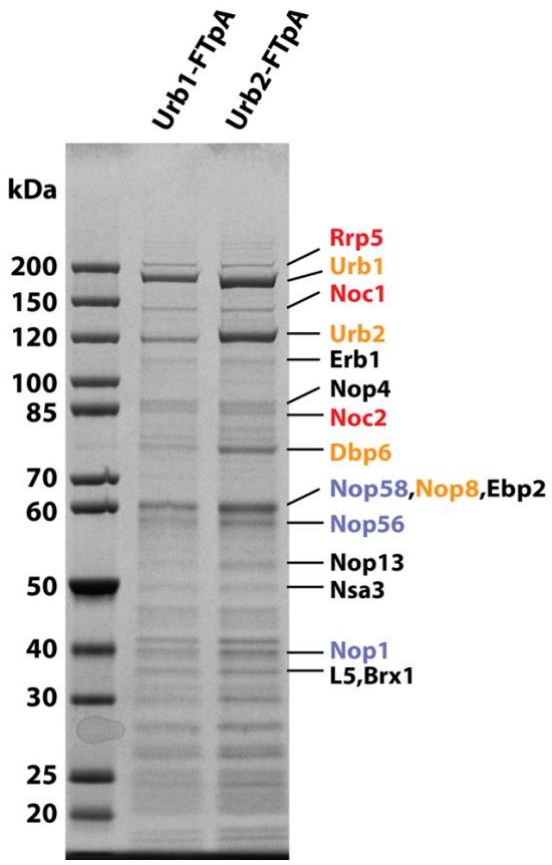

Figure 3.3 Affinity purification of Urb1 and Urb2 particles
Tagged Urb1-FTpA and Urb2-FTpA were affinity purified to isolate their associated pre-ribosomal particles. Final eluates were analyzed on 4-12% gradient SDS-PAGE gel and stained with Coomassie. The indicated bands have been identified by Mass spectrometry. Rrp5 module factors are colored in red, Urb1 module factors in orange and C/D box snoRNA cofactors in blue.

In order to enrich for only pre-60S particles without the dominance of Urb1 and Urb2, a split-tag affinity purification method was considered, using Urb2 as the first bait (with TAP tag calmodulin-TEV-protA) and Noc1 as second bait (with Flag tag). Noc1 was chosen, because it is an early pre-60S assembly factor with an essential role in the Rrp5 module, with Rrp5 potentially bridging to the 90S pre-ribosome (Hierlmeier et al., 2013). Isolation of pre-ribosomes using Urb2-Noc1 revealed pre-60S particles with better stoichiometry of assembly factors than the particles purified by Urb1 or Urb2 alone (Figure 3.4). I have also tried different split-tag combinations with Urb2 as first bait and Nop58 (C/D box snoRNPs factor) or Nsa3 as second baits. In both cases, Urb2- Nop58 and Urb2-Nsa3, the particles purified with these split combinations were highly similar to the pattern obtained with Urb2-Noc1 particle (Figure 3.4).

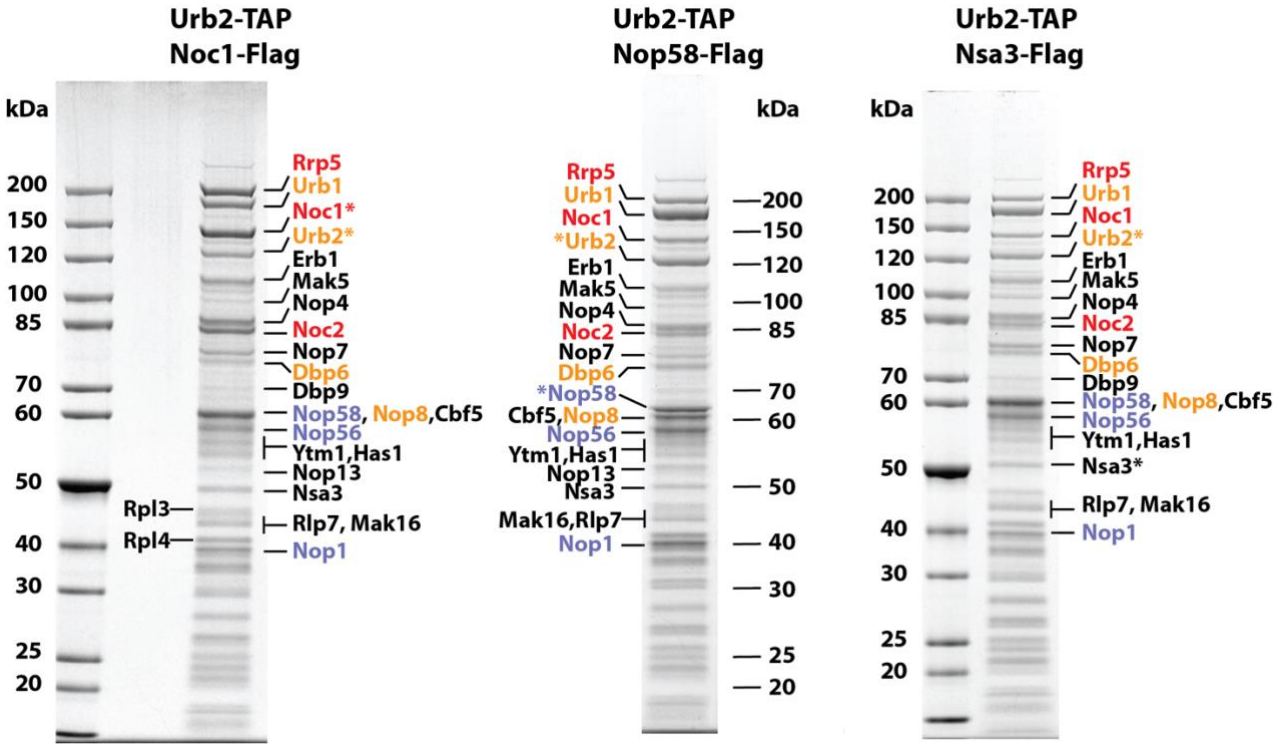

Figure 3.4 Isolation of primordial pre-60S particles with unique pattern of assembly factors and snoRNPs

Split-tag affinity purification of Urb2-TAP Noc1-Flag, Urb2-TAP Nop58-Flag and Urb2-TAP Nsa3-Flag. Final eluates were analyzed on a 4-12% gradient SDS-PAGE gel followed by Coomassie staining. Major bands were excised from the gel and identified by MALDI-TOF mass spectrometry. Different factors are colored according to their module: Rrp5 module is red, Urb1 module is orange and C/D box snoRNA cofactors are blue. The bait proteins are indicated by asterisks.

Mass spectrometry of the co-purified bands with Urb2-Noc1 baits revealed a unique pattern of early pre-60S assembly factors including the Urb1 module, Rrp5 module and some core 60S factors (e.g. Erb1, Ytm1, Nop7, Nsa3, Has1). Additionally, the Urb2-Noc1preparation shows strong enrichment of the C/D box snoRNPs factors Nop1, Nop56 and Nop58, which are all visible as stoichiometric bands by Coomassie staining (Figure 3.4). This unique pattern of Urb2-Noc1 particle with its associated snoRNPs indicates that it could be an extremely early pre-60S particle, the primordial pre-60S.

To distinguish the characteristic assembly factors of this primordial pre-60S from the succeeding well-characterized pre-60S particles, I compared the fold increase or decrease of assembly factors from Urb2-Noc1 particle with those purified with Nsa1-Ytm1, using semiquantitative mass spectrometry (Figure 3.5). Nsa1-Ytm1 split combination were chosen because they purify nucleolar pre-60S particles, which are structurally characterized (Kater et al., 2017). In addition to the Urb1 and Rrp5 modules, both C/D box (Nop1-Nop56-Nop58-Snu13) and H/ACA (Cbf5-Gar1-Nhp2-Nop10) snoRNPs are strongly and specifically enriched in Urb2-Noc1 particle compared to Nsa1-Ytm1 nucleolar pre-60S particles (Figure 3.5 B). The Coomassie-stained gel (Figure 3.5A) and semiquantitative mass spectrometry (Figure 3.5B) show clear enrichment of Noc1 with Noc2 in the Urb2-Noc1 particle, then Noc1 gets exchanged for Noc3 in the succeeding Nsa1-Ytm1 particle. Apparently, the Urb2-Noc1 particle is packed with several RNA helicases. Some of these RNA helicases are poorly characterized such as Dbp6, Dbp7, Dbp9 and Mak5, yet Dbp9 is retained in the succeeding Nsa1-Ytm1 particle. These helicases are not purified in stoichiometric amounts within the particles, indicating that they only associate transiently with the pre-ribosomes. It seems that at such early stage of 60S biogenesis, the RNA helicases could assist with pre-rRNA folding or removal of snoRNAs and assembly factors from the developing 60S pre-ribosome. In addition to these helicases, some other assembly factors stand out in the Urb2-Noc1 particle such as Nop4, Nop12, Nop13. The essential RNA-binding assembly factor Nop4 (Nop77) (Sun and Woolford, 1994) is strongly enriched in the Urb2-Noc1 primordial pre-60S (Figures 3.4 and 3.5). Nop4 was identified in a synthetic lethality screen with another *nop1* mutant allele, *nop1-5* (Bergès et al., 1994). Notably, a mutation in RBM28, the human ortholog of Nop4, is involved in the human ribosomopathy ANE syndrome (Nousbeck et al., 2008). On the other hand, not much is known about the non-essential RNA-binding assembly factors

Nop12 and Nop13, although Nop12 together with Pwp1 were shown to be involved in early 5.8S rRNA folding (Talkish et al., 2014). Additionally, YCR016W is a an uncharacterized, but conserved, protein that associates specifically with the Urb2-Noc1 pre-60S particle (Figure 3.5B), which has a unique RNA-binding domain (see Discussion). Further unique and components discovered in the Urb2-Noc1 particle include the putative methyl-transferases YGR283C (which we termed Upa1, for **U**rb2 **p**article **a**ssociated methyl-transferase **1**) and its paralog YMR310C (termed Upa2 accordingly), both are specifically enriched in the primordial pre-60S (Figure 3.5B) (for further characterization see chapter 3.7).

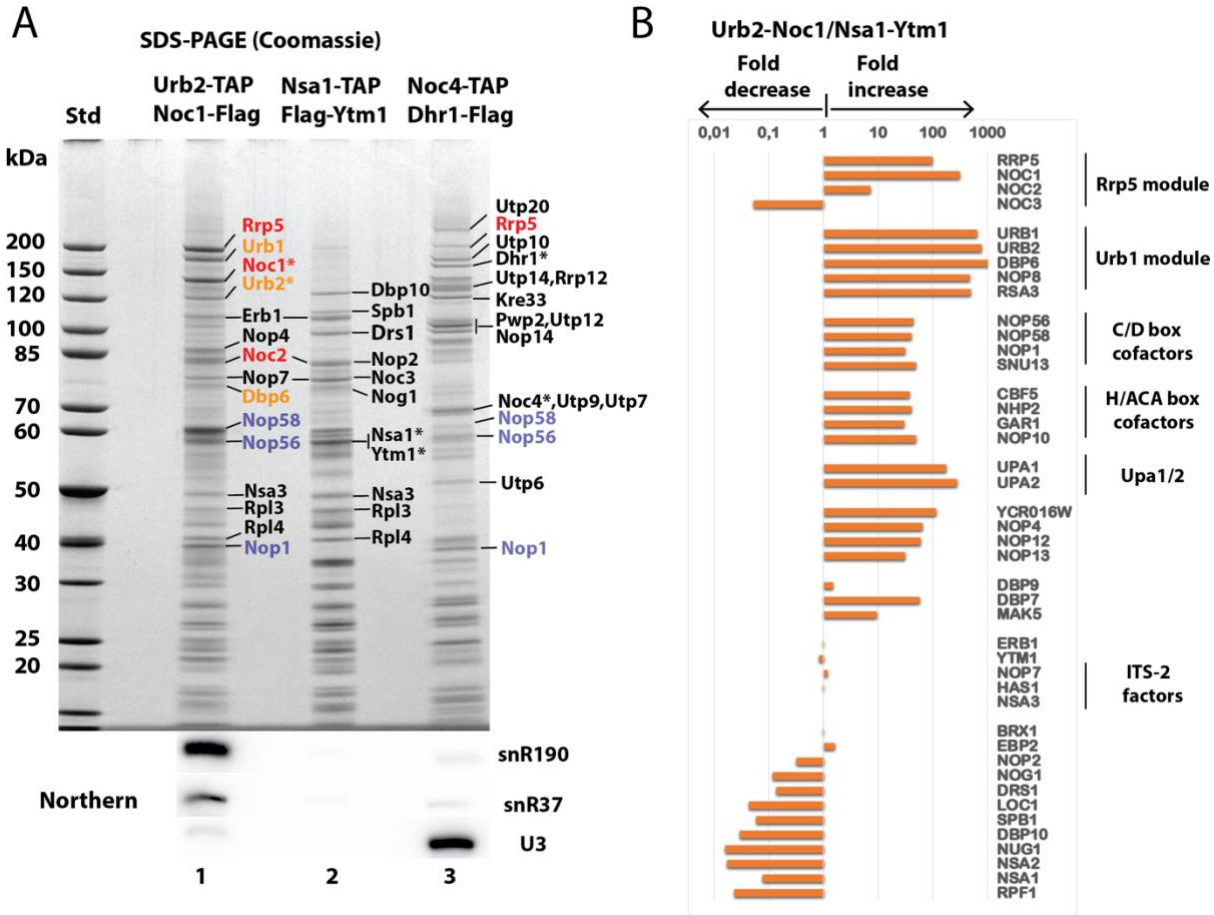

Figure 3.5 Comparison of the primordial pre-60S with the succeeding nucleolar pre-60S particles

(A) Split-tag affinity purification of Urb2-Noc1, Nsa1-Ytm1 and Noc4-Dhr1 particles. Flag eluates were divided: one half was separated by 4-12% gradient SDS-PAGE and stained with Coomassie blue (upper part) to reveal the protein composition; the other half was used for RNA extraction, which was analyzed by northern blotting using specific probes for the different snoRNAs snR190, snR37 and U3 (lower part).

(B) Semiquantitative mass spectrometry analysis of the final Urb2-Noc1 and Nsa1-Ytm1 eluates were compared. The LFQ values (normalized to Nsa3) of the co-enriched assembly

factors from the Urb2-Noc1 were divided by the values from Nsa1-Ytm1 preparation, which indicated the fold increase or decrease.

In contrast, a group of other pre-60S assembly factors, which are enriched in Nsa1-Ytm1 nucleolar pre-60S particles (e.g. Nog1, Drs1, Dbp10, Spb1, Loc1, Nug1, Nsa2, Nsa1 and Rpf1), were strongly diminished in the Urb2-Noc1 particles. Interestingly, the Urb2-Noc1 particle has less of the r-protein Rpl3 compared to Rpl4, since Rpl3 band appears sub-stoichiometric to Rpl4 band in the SDS-polyacrylamide gel, while both bands have similar intensity in the later classical pre-60S particles (Figure 3.4 and 3.5A). Although Rpl4 is already associated with the primordial pre-60S, the later observation indicates that Rpl3 is still not incorporated into the particle. Notably, the Urb2-Noc1 preparation contains few but sub-stoichiometric 90S factors, probably from a small pool before the separating cleavage at ITS1.

In summary, the Urb2-Noc1 particle, which precedes the previously characterized nucleolar pre-60S particles, is distinguished by the presence of large α-solenoid scaffold complexes (the Urb1 and Rrp5 modules), C/D box and H/ACA snoRNPs, the methyltransferases Upa1-Upa2 and a group of poorly studied RNA helicases. As indicated in next chapters, I investigated and characterized some of these factors.

3.3 Affinity purification of early assembly factors

The primordial pre-60S particle purified via Urb2-Noc1 contains many poorly characterized assembly factors. Therefore, I individually tagged some of these assembly factors, affinity-purified them and identified the pattern of their co-purified factors with by SDS-PAGE and mass spectrometry (Figure 3.6). I performed these purifications searching for a suitable single bait that could isolate the primordial pre-60S, similar to what I obtained with the split tag affinity-purified Urb2-Noc1. Although all these assembly factors are mainly associated with the primordial pre-60S particle, none of their purifications showed the stoichiometric pattern of assembly factors obtained with Urb2-Noc1 particle. For example, isolation of pre-60S particles via Nop4 revealed a pattern of early pre-60S assembly factors, but the C/D box snoRNA cofactors Nop1-Nop56-Nop58 were not enriched in the particle and the Urb1 module was sub-stoichiometric (Figure 3.6A). Although Nop4 purified a pre-60S particle, I could detect the 90S factor Rrp12 band in the gel (Figure 3.6A; Rrp12 colored in red).

To confirm that Rrp12 is an intrinsic part of this particle, the Nop4-FTpA particle was fractionated by sucrose gradient centrifugation (Figure 3.6B). Rrp12 co-migrated on the sucrose gradient with the particle (Figure 3.6B; fraction 10) as confirmed by mass spectrometry. Notably, a yeast two-hybrid screen showed an interaction between yeast Nop4 and Rrp12 (McCann et al., 2015). However, the authenticity of this interaction should be further clarified in future research.

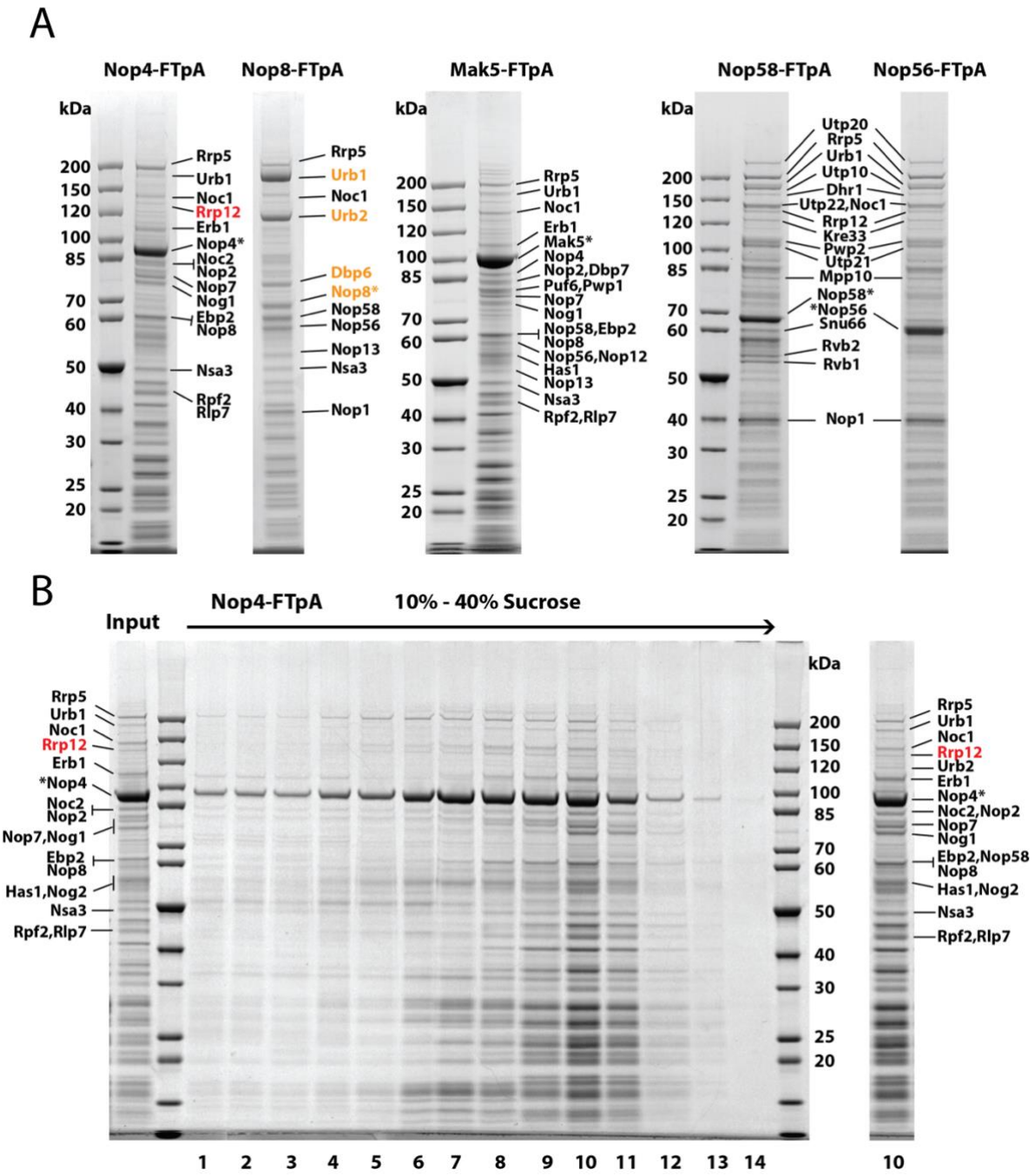

Figure 3.6 Affinity purification of early assembly factors

(A) Affinity purification of the early pre-60S assembly factors Nop4-FTpA, Nop8-FTpA, Mak5-FTpA as well as the C/D box cofactors Nop58-FTpA and Nop56-FTpA. Flag eluates were

analyzed on a 4-12% gradient SDS-PAGE gel and stained with Coomassie. Major bands were identified by mass spectrometry. The bait proteins are indicated by asterisks.
(B) Flag eluate of Nop4-FTpA (Input) was fractionated by sucrose gradient centrifugation (10%-40%) (w/v). Fourteen fractions were collected, precipitated by TCA and resuspended in SDS protein sample buffer. The samples were analyzed by 4-12% SDS-PAGE and stained with Coomassie blue.

Affinity purification of Nop8, a member of the Urb1 module, showed mainly the Urb1 module and the C/D box cofactors Nop1-Nop56-Nop58, but not a stoichiometric pre-ribosome. Early pre-60S factors have been co-purified with the RNA helicase Mak5, in addition to other proteins that are not involved in ribosome biogenesis. On the other hand, the particles purified via the C/D box snoRNA cofactors Nop56 and Nop58 showed mainly a pattern of 90S factors and few pre-60S factors. Notably, the Nop58 particle enriched two prominent proteins Rvb1 and Rvb2 (Figure 3.6A). Rvb1 and Rvb2 are part of the R2TP complex (Rvb1-Rvb2-Tah1-Pih1), which is involved in multiple processes including C/D box snoRNP biogenesis (Kakihara and Houry, 2012; Zhao et al., 2008).

3.4 The primordial pre-60S specifically carries two major snoRNAs

The strong enrichment of the C/D box and H/ACA snoRNPs core factors in the primordial pre-60S particles prompted me to investigate and identify the associated snoRNAs. Hence, I extracted the RNA from Urb2-Noc1 and Urb2-Nop58 final eluates, in addition to other controls, then separated the RNA on polyacrylamide/urea gel and stained with SYBR Green (Figure 3.7A). This revealed two major RNA bands that were strongly enriched in the Urb2-Noc1 and Urb2-Nop58 particles, but not detected in the nuclear pre-60S (Arx1) and 90S (Noc4-Dhr1) particles. Judging by their sizes, the two bands were assigned to the C/D box snR190 and the H/ACA box snR37 (Figure 3.7A). For confirmation, northern blot analysis showed that these two snoRNAs are specifically enriched in Urb2-Noc1, but completely absent from the Nsa1-Ytm1 nucleolar pre-60S and the Noc4-Dhr1 90S particles (Figure 3.5A). Another evidence came from the isolation of Urb2-Noc1 particle from a *snR190Δ snR37Δ* double knockout strain, which is devoid of these two snoRNA bands (Figure 3.7B). To confirm whether snR190 and snR37 are stably associated with the earliest pre-60 particles, the Urb2-Nop58 eluate was fractionated by sucrose gradient centrifugation followed

by Northern blotting of the collected fractions (Figure 3.7C). Indeed, both snR190 and snR37 co-migrated with the pre-60S particles in the lower part of the sucrose gradient.

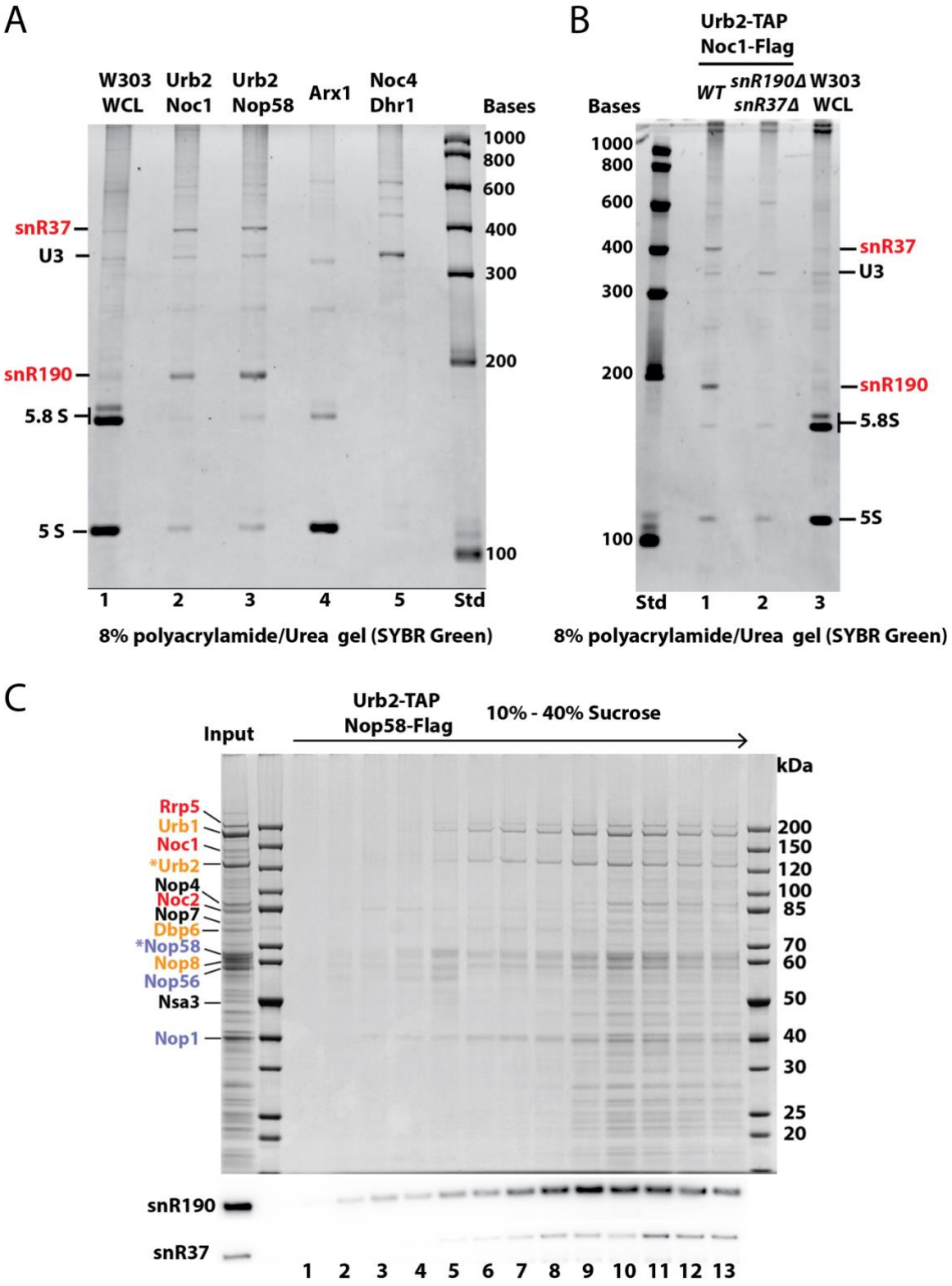

Figure 3.7 Specific enrichment of snR190 and snR37 with the primordial pre-60S particles

(A) 8% polyacrylamide/urea gel electrophoresis showing the analysis of low-molecular-weight RNA extracted from the split-tag affinity-purified Urb2-Noc1, Urb2-Nop58, Arx1 and Noc4-

Dhr1 pre-ribosomes. Total RNA from a wild-type strain W303 whole cell lysate (WCL) and the final eluates from the purifications were separated on the gel and stained by SYBR Green RNA gel stain.
(B) RNA was extracted from the final eluates of affinity-purified Urb2-TAP Noc1-Flag, derived from the wild-type or *snR190Δ snR37Δ* double deletion strain, then separated on 8% polyacrylamide/urea gel and SYBR Green staining. RNA of a whole cell lysate (WCL) from wild-type strain W303 was also included. The gel was stained with SYBR Green RNA gel stain to detect the snR37 and snR190 bands, which are indicated in red.
(C) Final eluate of affinity purified Urb2-TAP Nop58-Flag pre-ribosomal particle was separated by sucrose gradient centrifugation (10-40% sucrose gradient). Part of each fraction was used for RNA extraction and northern blotting using probes for snR190 and snR37, and the rest was analyzed by 4-12% gradient SDS-PAGE gel and stained with Coomassie. Rrp5 module factors are colored in red, Urb1 module factors in orange and C/D box snoRNA cofactors in blue. The bait proteins are indicated by asterisks.

Another trial was done using the co-precipitated RNA from the affinity purification of the C/D box cofactor Nop58, to show the complete pool of C/D box snoRNAs, in comparison to Urb2-Nop58 split-tag affinity purification, which shows the snoRNAs associated with the primordial pre-60S (Figure 3.8A). Various snoRNAs species were co-purified with Nop58 including strongly enriched U3, a C/D box snoRNA associated with 90S particles, and snR190. On the other hand, the Urb2-Nop58 particles purified the C/D box snR190 and the H/ACA box snR37, the latter was not enriched with the C/D box snoRNA cofactor Nop58.

In order to further identify additional snoRNAs of lower abundance in the nascent pre-60S particles, RNA Illumina sequencing was performed. The sequencing was done in collaboration with Dr. Jose Vincente Gomes-Filho from the Randau lab at Max Planck Institute for Terrestrial Microbiology, Marburg. For this purpose, I performed affinity purification of the following particles: Urb2-Noc1 / Urb2-Nop58 (primordial pre-60S particles), Nop58 to obtain the entire C/D box snoRNAs pool, Kre33 as a bait for the 90S pre-ribosome and Arx1 as a bait for late nuclear pre-60S particles. Then, I forwarded the final eluates to the Randau lab, where Dr. JV Gomes-Filho performed the Illumina sequencing and analysis of the small RNAs co-precipitated with the different preparations (Figure 3.8B). Analysis of the sequencing data revealed that Urb2-Noc1 and Urb2-Nop58 particles, in comparison to other preparations, contained a similar set of snoRNAs, with the highest enrichment for the C/D box snR190, snR73, snR38, snR39, snR48 and snR52 as well as the H/ACA box snR37 and snR42 (Figure 3.8B). As expected, snR190 appeared in the sequencing data as a major snoRNA associated with the Urb2-derived particles, but snR37 did not stand out as much. This

resulted from a technical limitation of the Illumina sequencing method, which was optimized for RNAs that are smaller than 200 nucleotides, but snR37 is an extraordinary long snoRNA with 386 nucleotides.

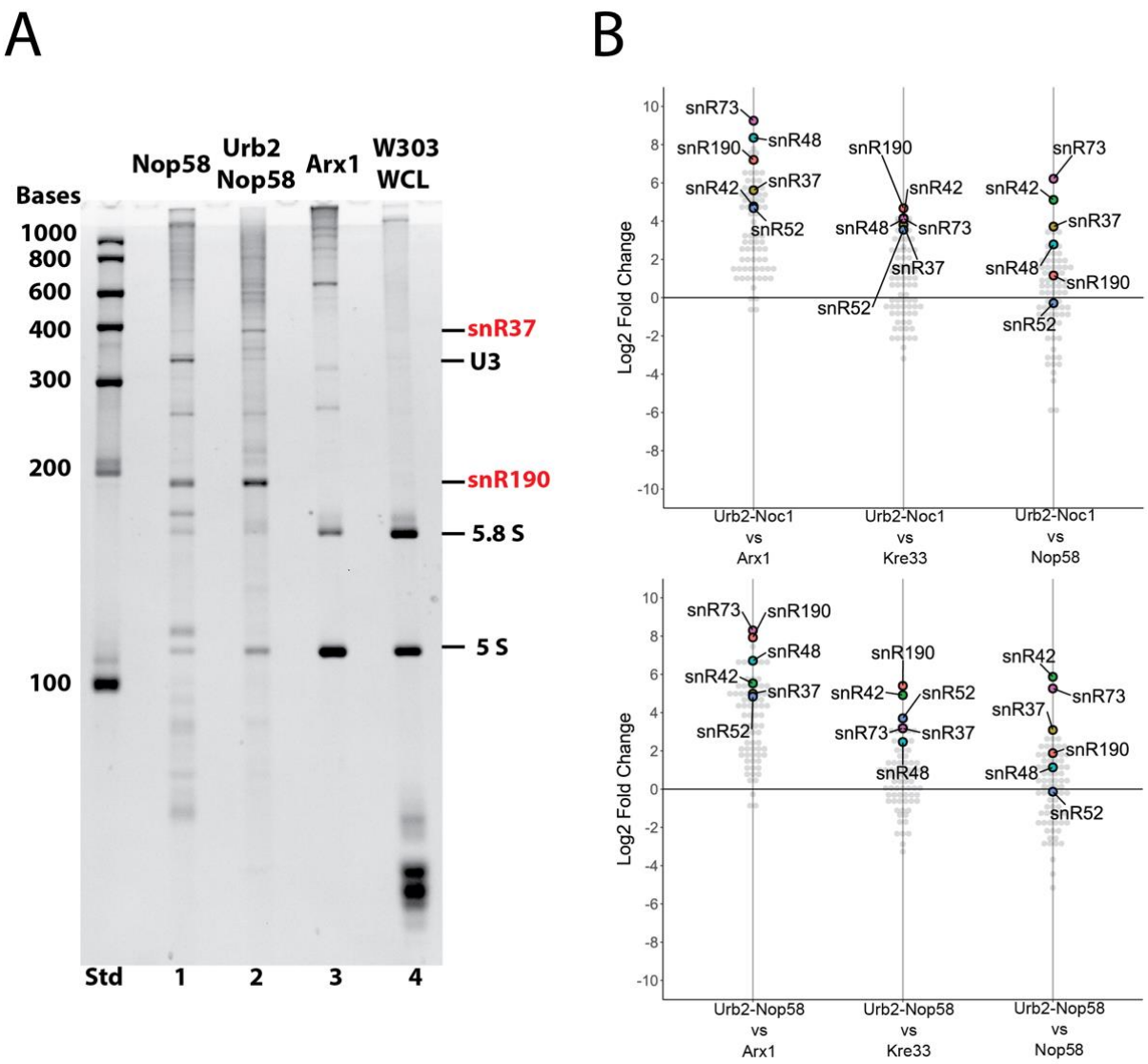

Figure 3.8 Identification of the snoRNAs co-enriched in the primordial pre-60S particles
(A) SYBR Green staining of the 8% polyacrylamide/urea gel, which exhibits the separated RNA extracted from Nop58-FTpA, Urb2-TAP/Nop58-Flag and Arx1-FTpA affinity-purified particles, in comparison to total RNA from the whole cell lysate (WCL) of the wild-type W303 strain. The snoRNAs snr190 and snR37 are labeled in red to highlight their specific enrichment with the primordial pre-60S particle purified by Urb2-Nop58.
(B) Illumina RNA sequencing of RNA extracted from the eluates of Urb2-TAP/Noc1-Flag, Urb2-TAP/Nop58-Flag, Nop58-FTpA, Kre33-FTpA and Arx1-FTpA preparations. Log2 Fold change of Illumina read counts was calculated for Urb2-Noc1 and Urb2-Nop58 samples in comparison to Arx1, Kre33 and Nop58. (B) was done by Dr. JV Gomes-Filho.

3.5 C/D box snR190 and H/ACA box snR37 play a role in the primordial pre-60 particles

Since snR190 and snR37 were prominent and specifically enriched in the primordial pre-60S particles, I was encouraged to study their role in these early steps of the large subunit biogenesis. To better understand their role, I performed both genetic and biochemical experiments. Apparently, the C/D box snR190 does not guide any known ribose methylation of rRNA (Kiss-László et al., 1996; Taoka et al., 2016; Yang et al., 2016). Thus, it might be involved in rRNA folding or having a structural role within the earliest pre-60S particles, similar to the U3 snoRNA in the 90S pre-ribosome. On the contrary, computational prediction suggested that the H/ACA box snR37 guides the pseudouridylation of yeast 25S rRNA at position U2944 (Piekna-Przybylska et al., 2007; Schattner et al., 2004). However, it is not experimentally proven that snR37 functions as a guide snoRNA for the pseudouridylation at the predicted position yet.

The genes for both snoRNAs were disrupted individually to assess their essentiality for cell growth. As previously shown and confirmed here, neither snR190 nor snR37 are essential for cell growth in yeast (Figure 3.9A) (Balakin et al., 1996; Zagorski et al., 1988). Subsequently, the genes of both snR190 and snR37 were disrupted from the yeast genome, *snR190Δ snR37Δ* double disruption, to determine the combined effect of absence of both snoRNAs on cell growth. This revealed a synergistic growth defect at 37°C upon the double disruption of both snR190 and snR37 (Figure 3.9A). In order to examine whether this was the result of an assembly defect in the primordial pre-60S particles, Urb2-Noc1 was affinity purified from the single deletion strains (*snR190Δ* or *snR37Δ*) as well as from the double deletion strain (*snR190Δ snR37Δ*), which was already confirmed to be devoid of these two snoRNAs by RNA polyacrylamide gel electrophoresis and SYBR Green staining (Figure 3.7B).

To identify the change in protein composition, I separated the final eluates by SDS-PAGE followed by Coomassie staining and used semiquantitative mass spectrometry to analyze the change of assembly factors between these preparations (Figures 3.9B and 3.9C). Single disruption of snR190 has already caused a specific and significant reduction of the RNA helicases Dbp7, Dbp9 and Mak5, concomitant with a slight accumulation of some 90S factors such as Utp10, Utp20, Kre33 and Rrp12. Additionally, the Ssf1/Ssf2-Rrp15-Mak11 subcomplex was diminished, which however

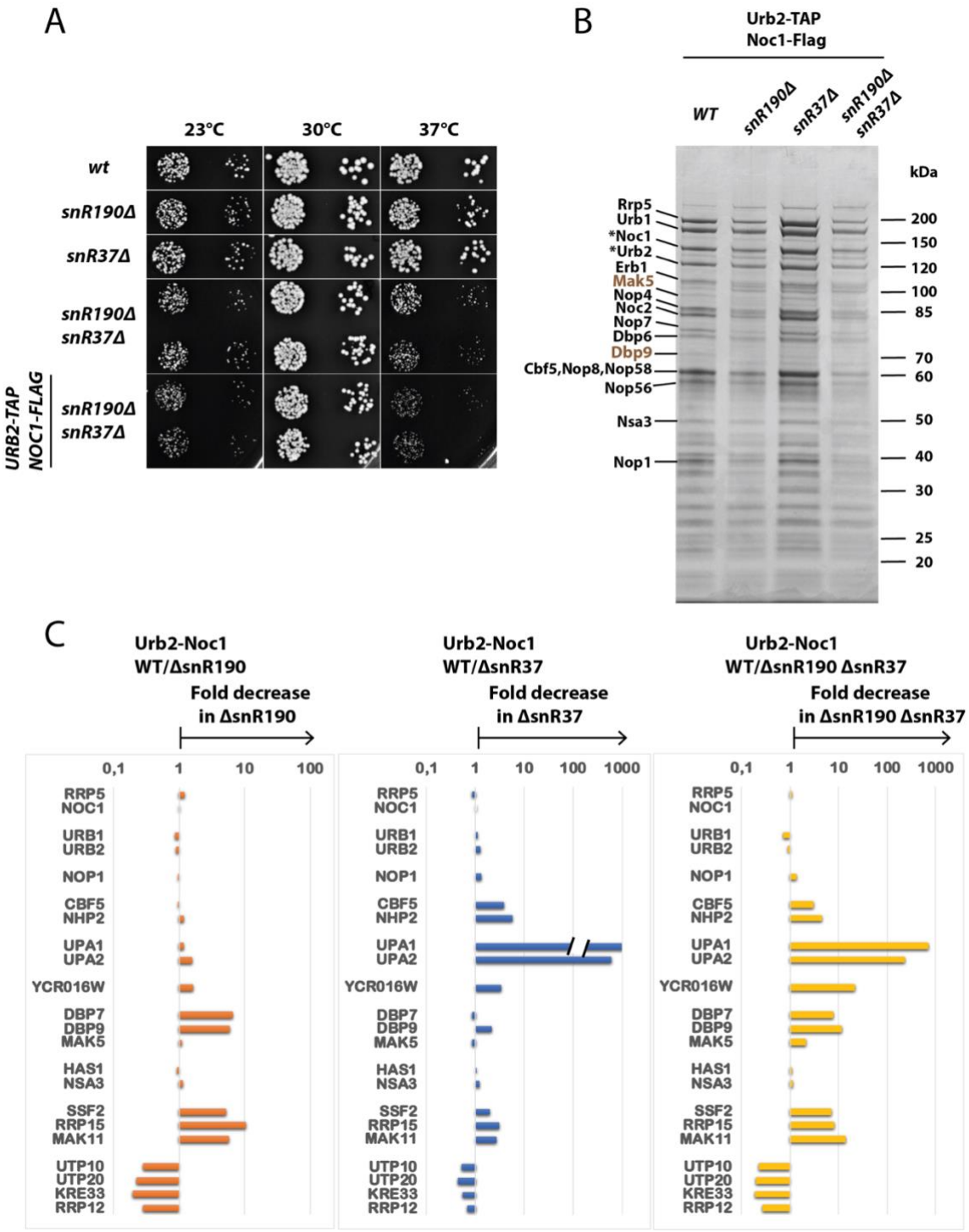

Figure 3.9 Disruption of snR190 and snR37 promotes specific changes in Urb2-Noc1 particle

(A) For growth comparison, the indicated strains wild-type W303, *snR190Δ*, *snR37Δ* and *snR190Δ snR37Δ* double deletion were spotted in tenfold serial dilutions on YPD plates. The plates were incubated at 23°C, 30°C and 37°C for 2 days.

(B) Affinity-purification of Urb2-TAP Noc1-Flag from the indicated strains wild-type, *snR190Δ*, *snR37Δ* and *snR190Δ snR37Δ* double deletion. Flag eluates were analyzed on a 4-12% gradient SDS-PAGE gel and stained with Coomassie. Mak5 and Dbp9 are colored in bold green to highlight their reduction in the *snR190Δ* carrying strains.

(C) Semiquantitative mass spectrometry analysis of the final Flag eluates from the strains described in (B). The LFQ values were normalized to Noc1 in each sample. Bar graph representation was done for representative co-enriched assembly factors to show their fold reduction in the mutant by dividing the normalized LFQ values from the wild-type by the individual snoRNA deletion strains (*WT* / *snR190Δ*, *WT* / *snR37Δ* and *WT* / *snR190Δ snR37Δ*). Note that Upa1 was no longer detected in the *ΔsnR37* strain (LFQ value of 0). In this case, I arbitrarily set a low LQF value of 1 for the calculation.

was only moderately present in the wild-type Urb2-Noc1 particles. To my surprise, the putative methyl-transferases Upa1 (YGR283C) and Upa2 (YMR310C) were completely absent from Urb2-Noc1 particle when isolated from the *snR37Δ* strain (Figure 3.9C) (see Discussion). Also, the H/ACA snoRNA cofactors such as Cbf5 and Nhp2 were reduced in the Urb2-Noc1 particles when isolated from the *snR37Δ* strain. All these described alterations observed in the single disruption strains were also sustained in the *snR190Δ snR37Δ* double disruption mutant, except for YCR016W. Interestingly, the uncharacterized YCR016W did not significantly change by disrupting snR190 (1.6-fold) or snR37 (3-fold), however it was significantly reduced by disrupting both snoRNAs (21-fold), which is clearly a synergistic effect (Figure 3.9C). Hence, this uncharacterized protein could play a role in the synthetically enhanced phenotype observed between snR190 and snR37.

3.6 Genetic interaction between snR190 and the assembly factor Rsa3

Most of the described genetic interaction experiments and screens regarding the ribosome assembly pathway, were based on the test of the functional relationship between ribosome assembly factors (proteins) and/or r-proteins (Bergès et al., 1994; Daugeron and Linder, 1998; Dichtl and Tollervey, 1997; De La Cruz et al., 2004). Since snR190 was always highly enriched and robust in my analysis of the primordial pre-60S particles, I checked if there is a genetic interaction between snR190 and other early assembly of the primordial pre-60S particles. The first choice was to check for genetic interaction between snR190 and Nop4 because Nop4 was discovered in a synthetic lethality screen with Nop1 (C/D box snoRNAs cofactor) (Bergès et al., 1994), suggesting that its function might be related to C/D box snoRNPs. Therefore, I created strains carrying temperature sensitive (ts) alleles of Nop4 (*nop4-19* and *nop4-3*), which

were described by (Sun and Woolford, 1997). Testing these ts alleles in *snR190Δ* strain did not yield a synergistic effect at 30°C, but there was an enhancement of the ts phenotype at 37°C (Figure 3.10A). Another test candidate was Dbp7, which was reduced from Urb2-Noc1 particles purified from *snR190Δ* cells. Dbp7 is a RNA helicase required for the biogenesis of the large ribosomal subunit (Daugeron and Linder, 1998). Dbp7 is also involved in genetic interactions with some members of the Urb1 module such as Urb1, Urb2 and Dbp6 (Daugeron and Linder, 1998; Rosado et al., 2007). Although Dbp7 is not essential for cell growth, disruption of its gene *dbp7Δ* causes severe growth defect (Figure 3.10B) (Daugeron and Linder, 1998). However, double disruption of snR190 and Dbp7 (*snR190Δ dbp7Δ*) has actually induced a better cell growth than the *dbp7Δ* strain alone (partial rescue of the *dbp7Δ* phenotype) (Figure 3.10B). This result was unexpected and is potentially interesting, which will be followed in future studies.

Apparently, snR190 associates with Urb1 as revealed by a UV cross-linking and analysis of cDNAs (CRAC) (Joret et al., 2018). Notably, Rsa3 is the only non-essential assembly factor in the Urb1 module Urb1-Urb2-Dbp6-Nop8-Rsa3. This prompted me to examine whether there is a functional relationship between Rsa3 and snR190. Combined gene disruption of *snR190Δ rsa3Δ* caused a synthetically enhanced (SE) growth defect at all temperatures tested, 23°C, 30°C and 37°C (Figure 3.11A). Next, I was curious to examine the pre-60S ribosomal particles from the slowly growing *snR190Δ rsa3Δ* double disruption strain. Hence, pre-60 particles were isolated via affinity purification of Nsa3 from wild-type, *snR190Δ*, *rsa3Δ* or *snR190Δ rsa3Δ* double mutant cells in order to check for change in the associated assembly factors. SDS-PAGE combined with Coomassie staining (Figure 3.11B) and semiquantitative mass spectrometry analysis (Figure 3.11C) of final eluates revealed some changes. Nsa3-derived pre-60S particles from the *snR190Δ rsa3Δ* double mutant showed an altered pattern of co-purifying assembly factors, with accumulation of many 90S factors (e.g. Utp20, Utp22, Pwp2, Utp10, Rrp12, Kre33), reminiscent of what has been found for Nsa3 particles isolated from *nop1-4* strain. In contrast, a group of pre-60 assembly factors (e.g. Dbp10, Sda1, Spb1, Nug1and Arx1) were reduced from the Nsa3 pre-60 particles when isolated from the *snR190Δ rsa3Δ* double mutant (Figure 3.11B and 3.11C). Altogether, these results suggest that snR190 could play a role, functionally related to the Urb1 module, in the early steps of 60S ribosomal subunit biogenesis.

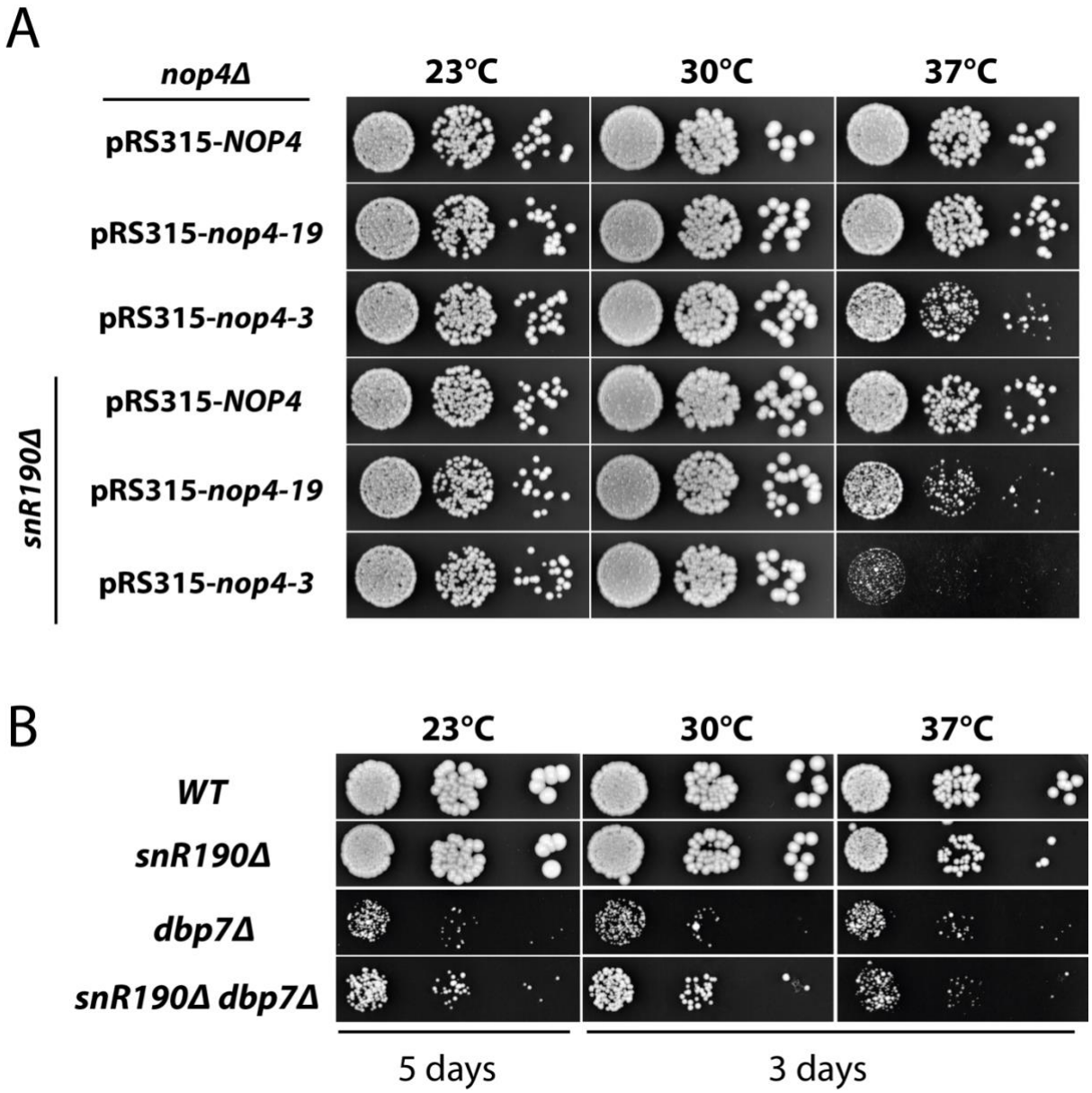

Figure 3.10 Disruption of snR190 cause partial rescue of *Dbp7Δ* phenotype
(A) Growth test analysis of strains carrying *NOP4*, *nop4-19* ts allele or *nop4-3* ts allele in wild-type background compared to *snR190Δ* background. Tenfold serial dilutions were spotted on YPD plates. The plates were incubated at 23°C, 30°C and 37°C for 3 days.
(B) Growth test analysis of the indicated strains: wild-type W303, *snR190Δ*, *dbp7Δ* and *snR190Δ dbp7Δ* double disruption. Tenfold serial dilutions were spotted on YPD plates, which were incubated at 23°C for 5 days or at 30°C and 37°C for 3 days.

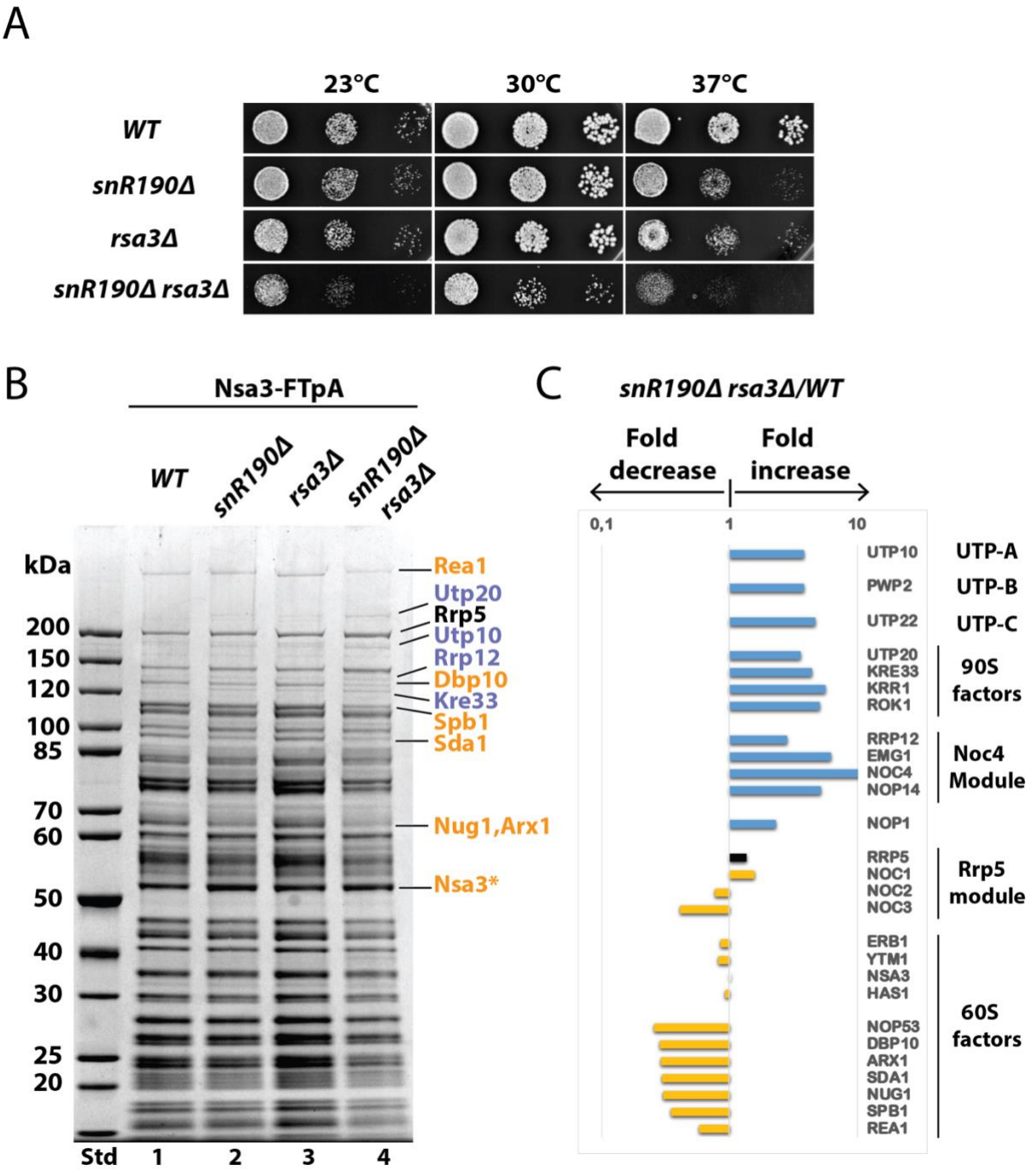

Figure 3.11 Synthetic enhancement between snR190 and the Urb1 module factor Rsa3
(A) Dot-spot growth analysis of wild-type W303, *snR190Δ*, *rsa3Δ* and *snR190Δ rsa3Δ* strains. Tenfold serial dilutions were spotted on YPD plates. The plates were incubated at 23°C, 30°C and 37°C for 2 days.
(B) Isolation of Nsa3-FTpA particles from wild-type W303, *snR190Δ*, *rsa3Δ* and *snR190 Δ rsa3Δ* strains. Final eluates were analyzed on 4-12% gradient SDS-PAGE gel and Coomassie staining. Major bands have been excised from the gel and identified by MALDI-TOF mass spectrometry. The 90S factors are indicated in blue, while pre-60S factors are indicated in orange. The bait Nsa3 is indicated by an asterisk.
(C) Semiquantitative mass spectrometry analysis of the Nsa3-FTpA eluates depicted in (B). The LFQ values (normalized to Nsa3) derived from the *snR190Δ rsa3Δ* were divided by the

values obtained for the wild-type particles (*WT*) to represent the fold change of assembly factors. The values for 90S factors are colored in blue, while the values for the pre-60S factors are colored in orange. The bridging factor Rrp5 is labeled in black.

3.7 Isolation of the primordial pre-60S particles using the methyl-transferases Upa1 and Upa2

The fact that Upa1 and Upa2 were specifically co-enriched on Urb2-Noc1 particles and were absent from these particles upon deletion of the H/ACA box snR37, prompted me to further investigate these two uncharacterized proteins. Both Upa1 and Upa2 are putative methyl-transferases that have a SPOUT domain. The SPOUT class of methyl-transferases are present in all three domains of life. The SPOUT class proteins can bind S-adenosyl-L-methionine (SAM) and facilitate the transfer of SAM methyl group to the substrate which is usually RNA or protein (Anantharam et al., 2002; Tkaczuk et al., 2007). Actually, yeast Upa1 and Upa2 are paralogs that resulted from yest genome duplication. They are both non-essential for cell growth (Giaever et al., 2002) and predicted to methylate RNA not proteins (Szczepińska et al., 2014), however they are not associated with any known RNA modification yet. The human homologue of Upa1/Upa2, called SPOUT1 or C9orf114, forms a homodimer (PDB: 4RG1), which is characteristic for SPOUT domain-containing proteins (See Discussion).

Since I showed that Upa1 and Upa2 are associated with the Urb2-Noc1 pre-ribosomal particles (Figure 3.5B), I wanted to affinity-purify these assembly factors to check the pattern of their co-purified proteins. Thus, I created C-terminally tagged Upa1 and Upa2 yeast strains, namely Upa1-FTpA and Upa2-FTpA. For both baits Upa1 and Upa2, affinity purification showed an almost identical pattern of co-associated proteins (Figure 3.12A). Notably, this pattern was highly similar to Urb2-Noc1 primordial pre-60S particles. Although I have tried many affinity purifications with different early assembly factors as single bait such as Nsa3, Nop4, Mak5, Nop8, Nop58 and Nop56 (see Figures 3.1 and 3.6), I never got the stoichiometric pattern of Urb2-Noc1 primordial pre-60S particles except when I used Upa1 and Upa2. Semiquantitative mass spectrometry analysis was performed using the final eluates of affinity- purified Upa1 and Upa2 (Figure 3.12B). Similar to Urb2-Noc1 primordial pre-60S, Upa1 and Upa2 particles contain the Rrp5 and Urb1 modules, H/ACA box and C/D box core factors, Nop4, Nop12, Nop13, YCR016W and the RNA helicases Dbp7,

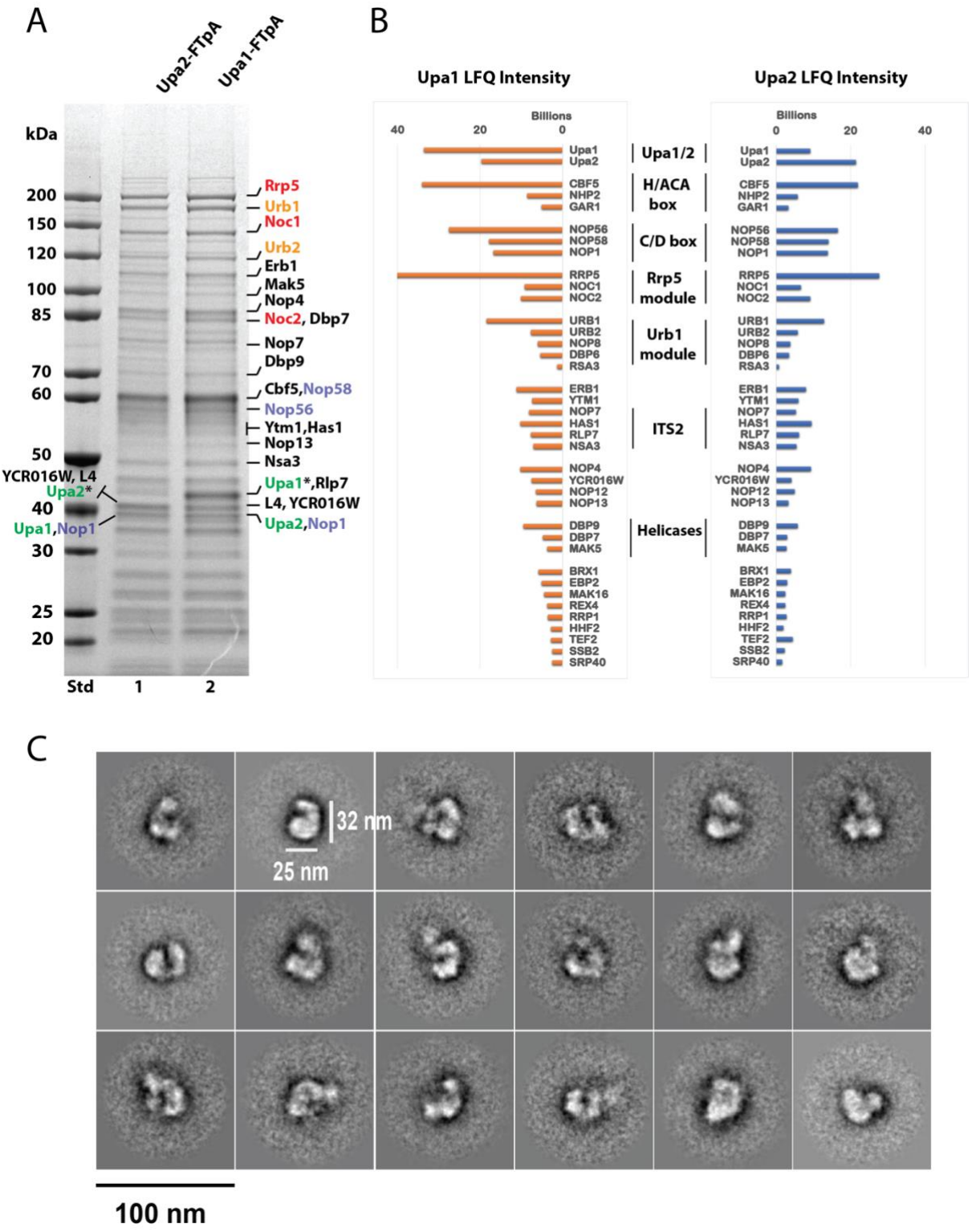

Figure 3.12 Affinity purification of the methyltransferases Upa1 and Upa2 enriches early pre-60S particles similar to the pattern of Urb2-Noc1 particles

(A) Final eluates from the affinity purification of Upa1-FTpA and Upa2-FTpA were analyzed on a 4-12% gradient SDS-PAGE gel and stained with Coomassie. Major bands, including Upa1 and Upa2, were excised from the gel and identified by MALDI-TOF mass spectrometry. The Rrp5 module is labeled in red, Urb1 module in orange, C/D box snoRNA cofactors in blue and Upa1/Upa2 in green. The bait proteins are indicated by asterisks.

(B) Semiquantitative mass spectrometry of the eluates from Upa1 and Upa2 purifications. The absolute LFQ intensities are depicted in the bar graph and the assembly factors are categorized into groups.
(C) Negative stain electron microscopy of Upa1-FTpA preparation. Shown are typical 2D classes of these early pre-60S particles. The scale bar indicates 100 nm. This negative stain electron microscopy was done by Dr. Dirk Flemming.

Dbp9 and Mak5 as well as other early assembly factors. Surprisingly, the H/ACA box core factor Cbf5, a pseudouridine synthase, is one of the most strongly enriched factors associated with Upa1 and Upa2 particles (Figure 3.12A and 3.12B). Interestingly, the Upa1 particle contained Upa2, and *vice versa* the Upa2 particle contained Upa1, verified by either MALDI-TOF of the corresponding gel-excised bands (Figure 3.12A) or semiquantitative mass spectrometry analysis (Figure 3.12B). This indicates that Upa1 and Upa2 might form a dimer, similar to their human ortholog C9orf114 (SPOUT1) and other SPOUT-domain containing proteins, which form and function as homodimers (see Discussion).

In order to get more information about the structure of the early pre-60S particles affinity-purified by Upa1, the particles were analyzed by negative stain electron microscopy and 2D classification (Figure 3.12C). I conducted the affinity purification of Upa1, which was subsequently analyzed by Dr. Dirk Flemming (head of the electron microscopy facility at the Biochemistry Center, Heidelberg), who performed negative stain electron microscopy and 2D classification of the sample. This revealed that Upa1 pre-60S particles are ca. 32 nm long and 25 nm wide, and often show a U-shaped appearance (Figure 3.12C). In a number of 2D classes, a blurry extra density at one tip of the U-arms was observed. This blurry extra density might correspond to a flexibly attached substructure such as Rrp5, Urb1 or snoRNP modules.

Altogether, the uncharacterized SPOUT methyl-transferases Upa1 and Upa2 are exclusively associated with the earliest pre-60S ribosomal particles and can ideally be used as single bait to affinity-purify this primordial pre-60S, which often shows a U-shaped appearance by negative stain electron microscopy.

3.8 Dominant Mak5 helicase mutant facilitates the isolation and structural analysis of a 90S-pre-60S super particle

The RNA helicase Mak5 is known to be involved in early 60S biogenesis (Bernstein et al., 2006; Brüning et al., 2018; Pratte et al., 2013). It binds specifically to early pre-60S particles but appears under-stoichiometric (see Figure 3.4) and its binding to Urb2-Noc1 particle is reduced in *snR190Δ* cells (see Figure 3.9B). Therefore, we wanted to further analyze this essential RNA helicase, for which a dominant negative mutant mapping in the Walker B motif (Mak5 D333A, defective in ATP hydrolysis) has been described (Bernstein et al., 2006). I cloned the *mak5* D333A mutation in a plasmid under *GAL* promoter and introduced the plasmid into yeast strains with different tagged baits for isolation of various pre-60S particles and studying them under the effect of the dominant negative Mak5.

First, I checked the growth of cells with overexpressed *mak5* D333A to confirm the dominant negative phenotype in our yeast background with tagged Urb2-TAP/Noc1-Flag (Figure 3.13A). Second, the Nsa3 and Nsa1-Ytm1 pre-60 particles were affinity-purified and prominent bands were identified by mass spectrometry. Notably, overexpression of Mak5 mutant caused the mutant protein to be massively stuck on Nsa3 and Nsa1-Ytm1 pre-60S particles, whereas the methyltransferase Spb1, the GTPase Nug1 and the export factor Arx1 were strongly reduced (Figure 3.13B). I checked the reason of this specific change with Spb1 and Nug1 reduction upon Mak5 D333A overexpression. Interestingly, the Nug1 N-terminus and Spb1 C-terminus, which are seen in the cryo-EM structure of state D Nsa1-Ytm1 pre-60S particles (Kater et al., 2017), are close to the 25S rRNA CRAC crosslinking sites of Mak5 (Brüning et al., 2018) (Figure 3.13C). This suggests that the overexpressed Mak5 D333A, unable to hydrolyze ATP, is not efficiently dissociated from its binding site, and accordingly it could have blocked Spb1 and Nug1 from stable association with the pre-60S particles.

On the other hand, the earlier Urb2-Noc1 primordial pre-60S showed a different phenotype upon overexpression of Mak5 D333A. The dominant Mak5 D333A has caused accumulation of many 90S factors on the Urb2-Noc1 particles (e.g. Utp20, Utp10, Utp22, Bms1, Rrp12, Utp21, Pwp2, Utp12 and Nop14), which caused the particle to co-enrich both pre-60S and 90S factors (Figure 3.14A). At the same time, the r-protein Rpl3 was markedly absent from Urb2-Noc1 particle in this mutant.

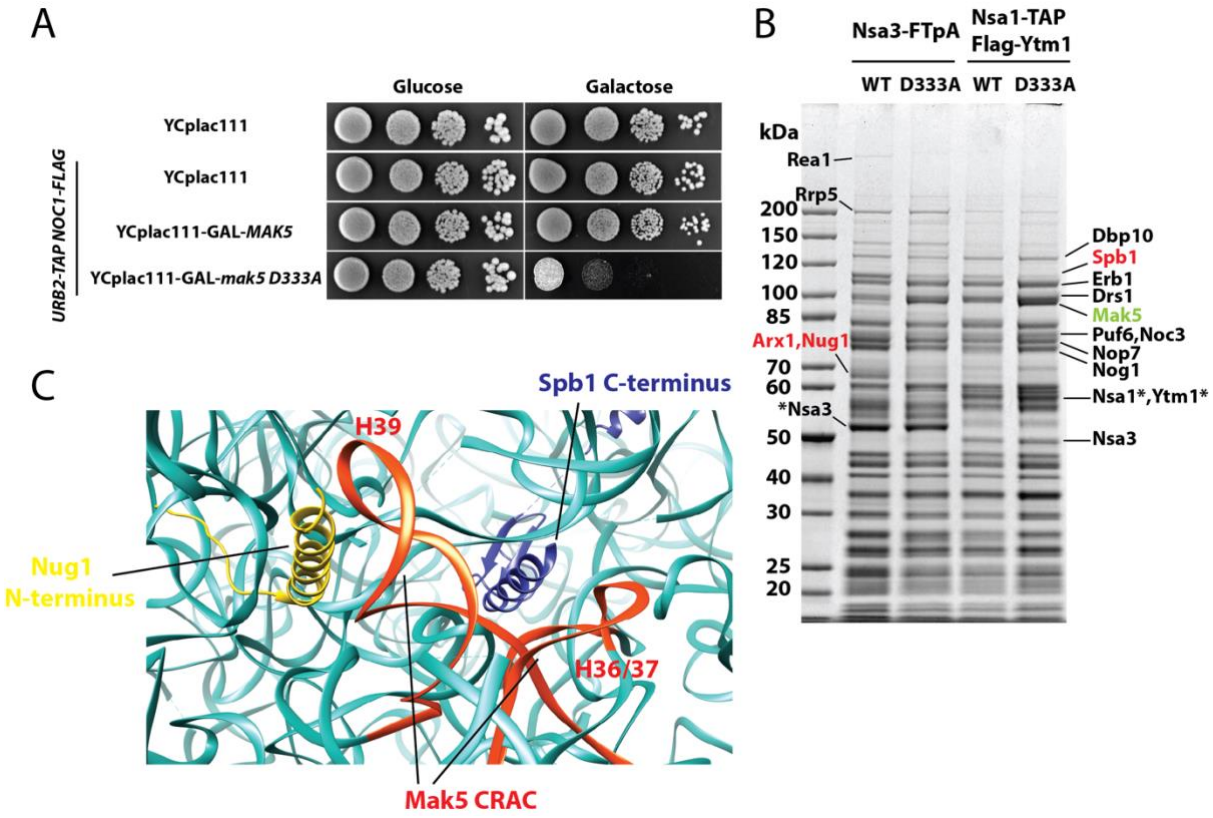

Figure 3.13 Overexpression of *mak5* D333A mutant

(A) Dot spots to show the dominant negative phenotype of Mak5 D333A overexpression in the Urb2-TAP Noc1-Flag background. Tenfold serial dilutions of the indicated strains were spotted on SDC-Leu (glucose) and SGC-leu (galactose) plates, which were incubated at 30°C for 3 days.

(B) Affinity purification of Nsa3-FTpA and Nsa1-TAP Flag-Ytm1 particles with overexpressed wild-type Mak5 and Mak5 D333A mutant. The Nsa3-FTpA and Nsa1-TAP Flag-Ytm1 strains were transformed with YCplac111-GAL-*MAK5* or *mak5* D333A. The cells were grown in glucose media (SDC-Leu) then shifted to galactose media (YPG) and grown for 8 hours. Final eluates were analyzed on a 4-12% gradient SDS-PAGE gel and Coomassie staining. Major bands have been identified by mass spectrometry. The assembly factors Spb1, Nug1 and Arx1 are colored in red to highlight their reduction in the case of mak5 D333A overexpression. The overexpressed Mak5 is indicated in light Green. The bait proteins are indicated by asterisks

(C) Nsa1-Ytm1 cryo-EM structure state D (PDB:6EM5) with indicated CRAC crosslink sites of Mak5 (Brüning et al., 2018) at helices H36/37 and H39 (red). The nearby Nug1 N-terminus (yellow) and Spb1 C-terminus (blue) are highlighted. I used UCSF Chimera for preparing (C).

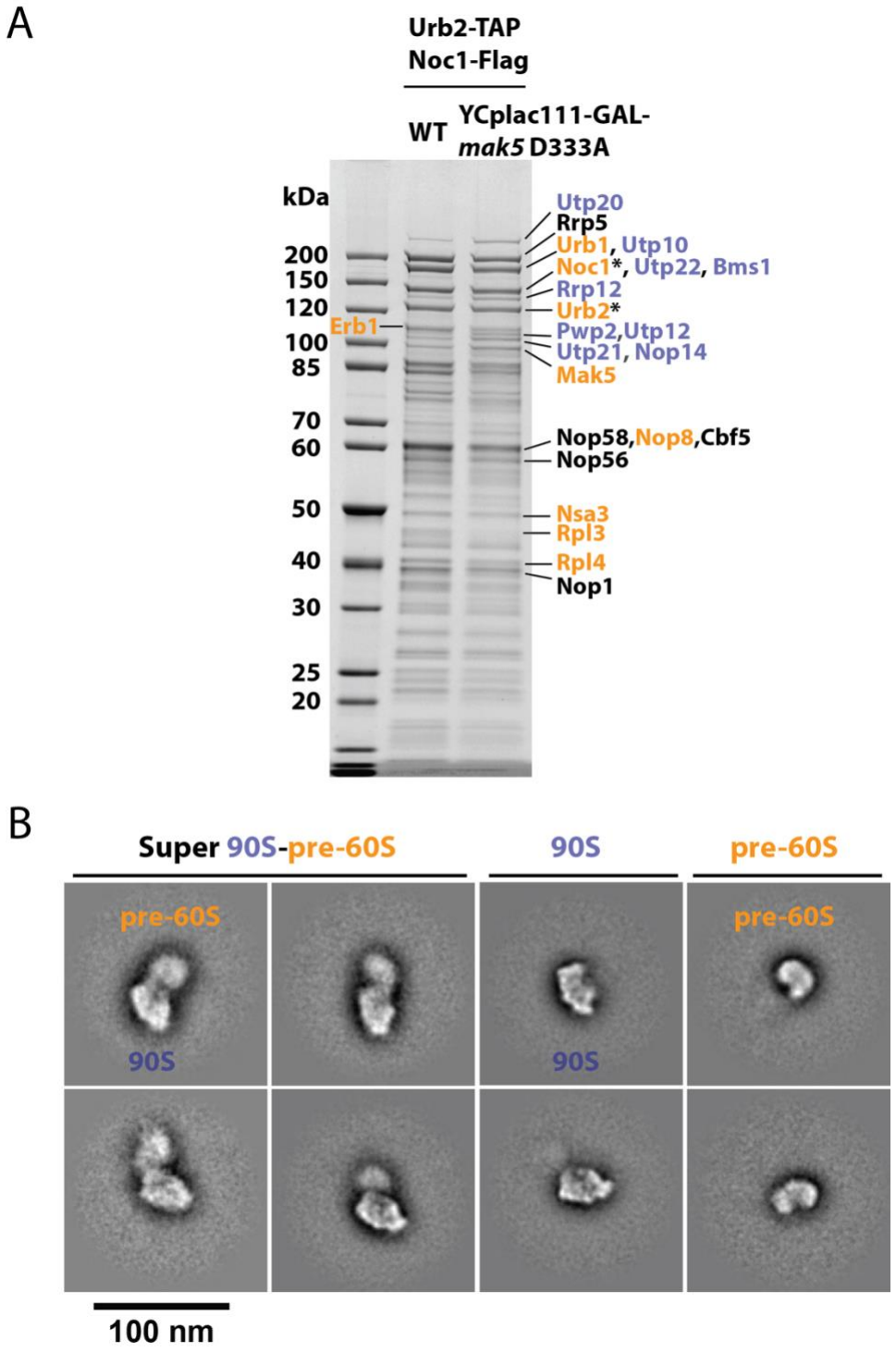

Figure 3.14 Dominant Mak5 D333A Mutant of Super 90S-pre-60S Particles
(A) Affinity purification of Urb2-TAP Noc1-Flag particle (WT) and after overexpression of Mak5 D333A. Urb2-TAP Noc1-Flag strain was transformed with YCplac111-GAL-*mak5* D333A. The cells were grown in SDC-Leu glucose media then shifted to YPG galactose media and grown for 8 hours. Final eluates were analyzed on a 4-12% gradient SDS-PAGE gel and stained with Coomassie blue. Major bands have been identified by mass spectrometry. 90S assembly factors are colored in blue, while pre-60S factors are colored in orange. The bait proteins are indicated by asterisks.

(B) Negative stain electron microscopy of the Urb2-TAP Noc1-Flag particles isolated from dominant *mak5* D333A mutant background. 2D classes showing 90-pre-60S super particles with 90S attached to a flexible fuzzy pre-60S moiety. Individual 90S and pre-60S particles from the same sample are also shown. The scale bar indicates 100 nm. This negative stain electron microscopy was done by Dr. Dirk Flemming.

These biochemical data encouraged me to further use the Urb2-Noc1 particles isolated from the Mak5 D33A dominant mutant for structural analysis. Thus, I isolated these particles and sent them to Dr. Dirk Flemming, who analyzed them by negative stain electron microscopy. This revealed small size particles in the range of (~32 nm in diameter) and medium-sized particles (around 40 nm in diameter). Moreover, we found very large-sized bipartite particles (around 70 nm long, 40 nm wide), which exceeds by far the size of either pre-60S or 90S particles (Figure 3.14B). Thus, the small particles could be the primordial pre-60S, while the medium particles highly resemble the classical 90S particles. On the other hand, the large-sized particles could be a super-assembly between 90S and pre-60S particles, consistent with the biochemical data. Indeed, the bigger half of the large-sized super particles appears distinct and highly similar to the typical 90S structure as seen by negative stain EM, while the smaller half appear less distinct and more flexible, resembling in its overall shape the primordial pre-60S found for the Upa1 particles (Figure 3.14B).

It was very intriguing to gain deeper insights into the structure of this super 90S-pre-60S particle using cryo-EM. Therefore, I isolated the Urb2-Noc1 particles from the dominant Mak5 D333A mutant again and Dr. Dirk Flemming prepared the cryo-EM grids as well as collected data using the Glacios cryo-transmission electron microscope. Matthias Thoms, from Beckmann lab at LMU Munich, has processed and analyzed this data. This has revealed three major intermediates with a low resolution, but good enough for assignment of some assembly factors. The smaller pre-ribosomes looked like pre-60S particles exhibiting the ITS2-foot structure, 25S rRNA domains I and II, the 5.8S and the Erb1-Ytm1 complex, similar to the early the Nsa1-Nop2 pre-60S particles state 3 (Sanghai et al., 2018), while Nsa1 was absent supporting the biochemical data (Figure 3.15A). Domains IV, V and VI of the 25S rRNA as well as the Rrp5 and Urb1 modules were not visible because of their flexible attachment. The medium-sized particles had typical 90S features and resembled the Noc4-Dhr1 90S particle (pre-A_1; EMD-11359; Cheng et al., 2020), which allowed us to assign classical factors on these medium-sized 90S particles like Kre33, Utp22-Rrp7,

Utp13, Utp12 and Helix 44 of 18S rRNA (h44) (Figure 13.5B). Using a larger box size for re-extraction of the 90S particles, has resulted in the appearance of an extra density near the head of the 90S, which resembled in dimension the early pre-60S particles. Due to high degree of expected flexibility, this extra density could not be further resolved. Based on its overall dimension, my biochemical data and the negative stain results, we can assign this blurry additional density to the pre-60S moiety.

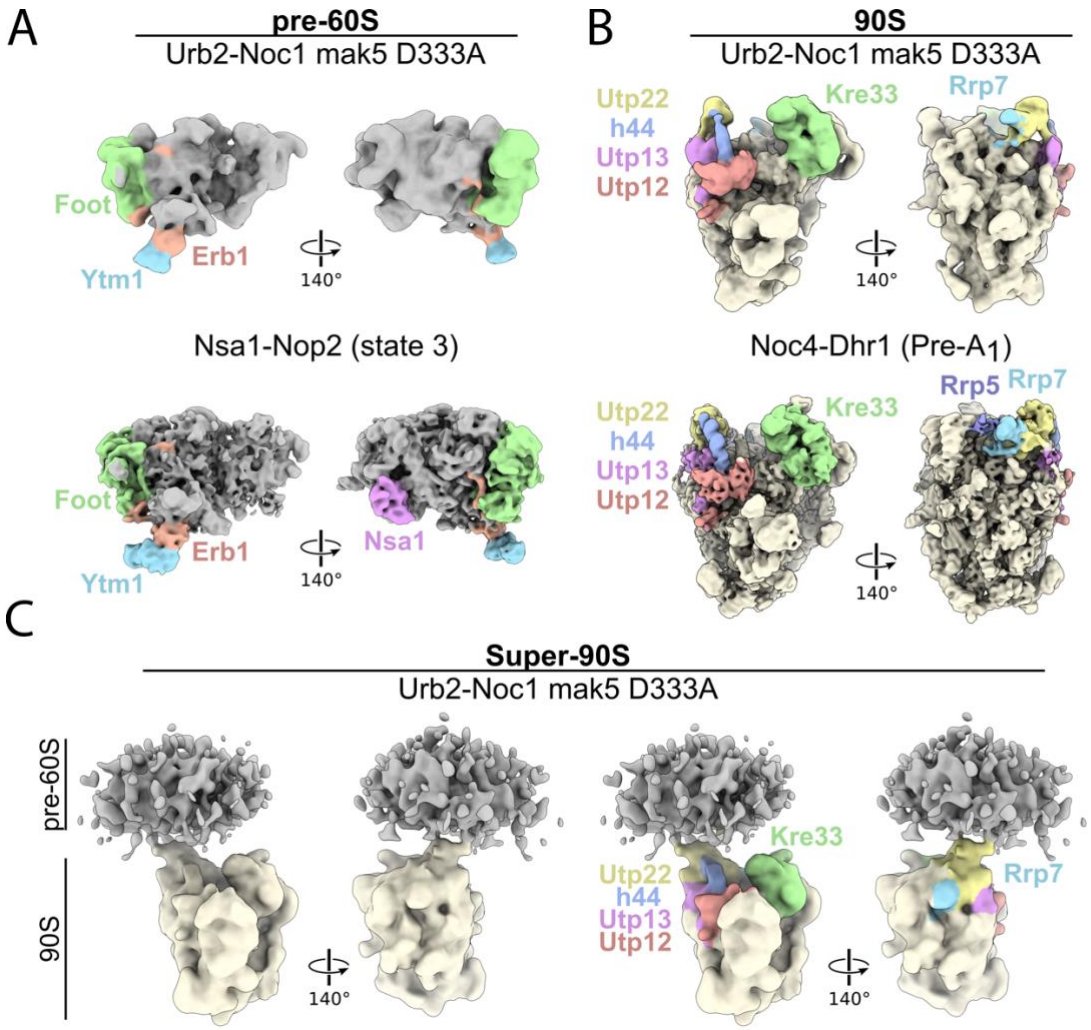

Figure 3.15 Cryo-EM structure of the 90S-pre-60S super particle
(A) Comparison of the Urb2-Noc1 mak5 D333A pre-60S cryo-EM reconstitution (upper panel) with the Nsa1-Nop2 map (state 3, EMDB: 7445, PDB: 6CB1) lowpass filtered to 10 Å. The Foot structure consisting of Nsa3, Nop7, Rlp7, Nop15 as well as Erb1, Ytm1 and Nsa1 are labeled.
(B) The obtained Urb2-Noc1 mak5 D333A 90S cryo-EM map (upper panel) compared to the Noc4-Dhr1 pre-A_1 particle filtered to 10 Å (EMDB: 11359, PDB-ID: 6ZQC). Utp12, Utp13, Utp22, Kre33, Rrp7 and Rrp5 are highlighted and labeled.

(C) Gaussian filtered cryo-EM map of the 90S particle connected to a flexible extra density. The 90S and the extra density are colored in yellow and gray, respectively and Utp12, Utp13, Utp22, Kre33, Rrp7 are highlighted.
This figure and its legend are provided by Matthias Thoms. See also Figure 3.16 for the sorting scheme of the particles.

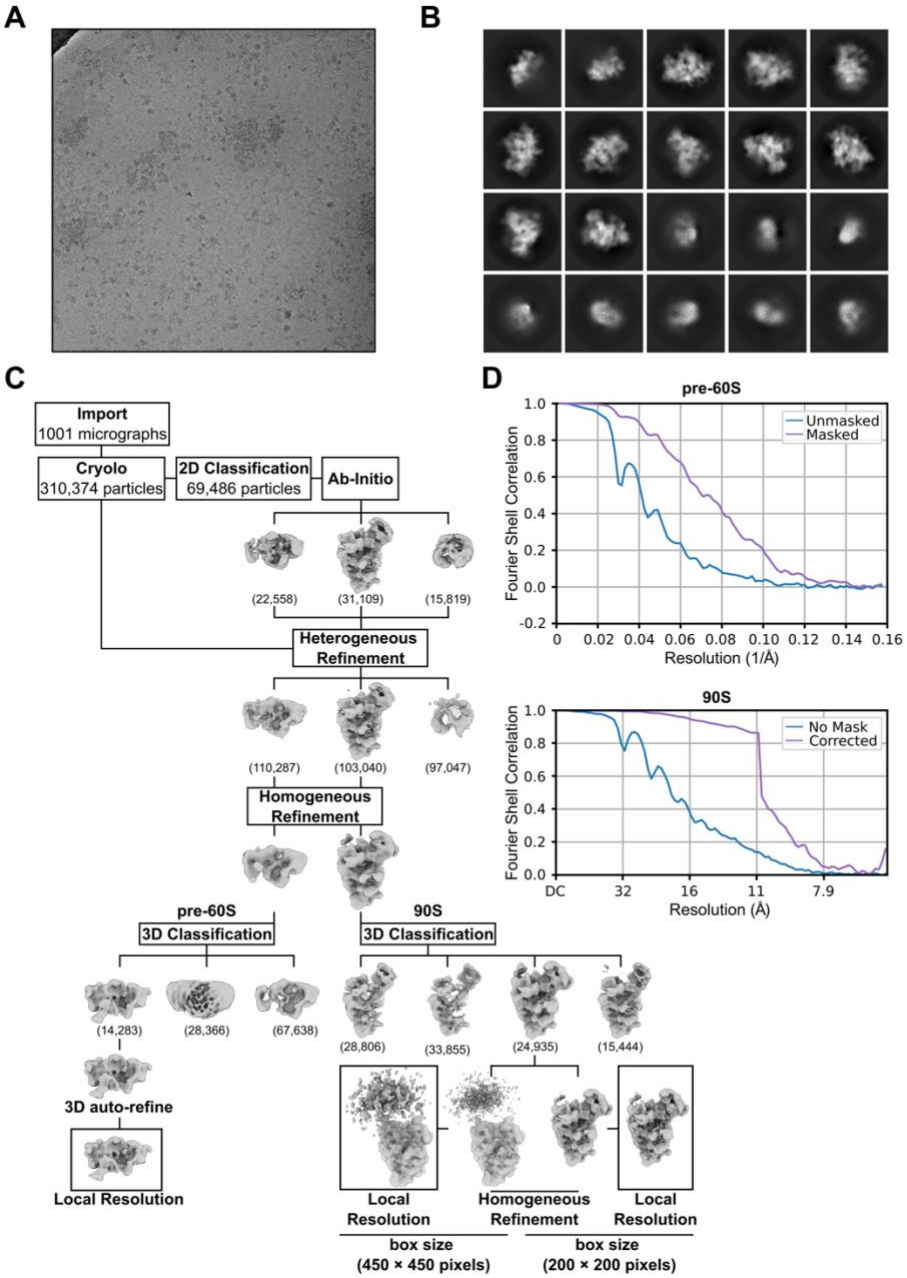

Figure 3.16 Sorting scheme of the Urb2-Noc1-Mak5-333 particles
(A-B) Representative electron micrograph (A) and selected 2D classification averages (B).
(C) Cryo-EM processing scheme. Particle numbers are provided in brackets.
(D) Fourier shell correlation curves of the final pre-60S and 90S reconstructions.
This figure and its legend are provided by Matthias Thoms.

In this super 90S-pre-60S particle, the pre-60S moiety is connected to the 90 particle, where it emerges from the area of the Utp22-Rrp7 (UTP-C) of the 90S, at the site where Rrp5 is typically located (Figure 13.5C). This finding is consistent with Rrp5 binding to ITS1 area and bridging between the 90S pre-ribosome and the emerging pre-60S (Khoshnevis et al., 2019; Lebaron et al., 2013; Venema and Tollervey, 1996). In general, Rrp5 is still not well resolved within 90S structures. However, a part of it (C-terminal residues 1457-1721) is well seen in Noc4-Dhr1 90S particle, which is in close contact with Utp22. We do not see Rrp5, not resolved, in the 90S moiety of our super particle. Thus, it is possible that Rrp5 is more towards the 60S moiety of our super 90S-pre-60S particle, but still bridging between both the pre-60S and 90S moieties.

In summary, these data provide for the first time a visual understanding of the nascent small and large ribosomal subunits while they are still connected at an early stage of eukaryotic ribosome biogenesis.

4 Discussion

The earliest steps in 60S ribosomal subunit assembly are the least understood and characterized of the large subunit biogenesis pathway. Using a combination of biochemical, genetic and structural analyses, this work provides molecular insights into the earliest stage of 60S biogenesis, which revealed a primordial pre-60S particle. This primordial pre-60S is distinguished by two large scaffold protein modules, the Rrp5 module (Rrp5-Noc1-Noc2) and the Urb1 module (Urb1-Urb2-Dbp6-Nop8-Rsa3), and further discerned by enrichment of two specific snoRNPs, snR190 and snR37. Additionally, this very early pre-60S particle contains some poorly characterized RNA helicases including Mak5 and the uncharacterized proteins YCR016W as well as the SPOUT-domain-containing methyl-transferases Upa1 and Upa2. The use of negative stain electron microscopy further enabled the identification of how the early pre-60S isolated via Upa1 looks like. Moreover, disrupting ribosome assembly using a dominant negative *mak5* helicase mutant has delayed the early detachment of the primordial pre-60S from the 90S pre-ribosome. For the first time, this has allowed the visualization, using electron microscopy, of the largest pre-ribosomal intermediate containing both the 90S and pre-60S moieties, the 90S-pre-60S super particle.

4.1 The primordial pre-60S is associated with two large α-solenoid modules

The mammalian ortholog of Nop1, Fibrillarin, has been linked to and studied in different diseases as it is found to be regulated by p53 and overexpressed in different cancer cells (Marcel et al., 2013; Su et al., 2014). Due to Nop1 importance and essential function in ribosome maturation, I have further investigated an old *nop1-4* mutant (Tollervey et al., 1993), and here I showed that the mutant *nop1-4* affected the pre-60S particles protein composition significantly with accumulation of 90S factors on the Nsa3-derived pre-60S particles. This has initially directed the project towards studying the role of snoRNPs in 60S subunit biogenesis. Nop1 was seen on the cryo-EM structure of different 90S particles as part of the U3-snoRNP, which is not modifying rRNA but rather having a structural role (Chaker-Margot et al., 2017; Cheng et al., 2020; Kornprobst et al., 2016; Sun et al., 2017). On the other hand, the absence of snoRNPs from all the nucleolar pre-60S cryo-EM structures analyzed so far (Kater et al., 2017; Sanghai et al., 2018; Zhou et al., 2018) indicated that they could only be

involved in earlier steps of 60S assembly. Some studies have reported that Urb1 and Urb2 associates with the $27SA_2$ pre-rRNA and the particles isolated via Urb1 and Urb2 contained snoRNPs (Dez et al., 2004; Joret et al., 2018; Mnaimneh et al., 2004; Rosado and De La Cruz, 2004; Rosado et al., 2007). However, these reports did not provide information on the stoichiometry or relative abundance of these snoRNPs or the assembly factors associated with Urb1 and Urb2. Indeed, when I isolated Urb1 and Urb2 particles, the bait proteins Urb1 and Urb2 were over-stoichiometric compared to other pre-60S assembly factors. However, when a split affinity purification approach using either Urb2-Noc1, Urb2-Nop58 or Urb2-Nsa3 was employed, I could successfully isolate the primordial pre-60S, which definitely has a unique pattern of assembly factors with stoichiometric enrichment of different components, including the C/D box snoRNA cofactors Nop1, Nop56 and Nop58.

Electron microscopy of nascent rRNA transcripts has revealed formation of distinct 5`-terminal knobs for the evolving 90S pre-ribosome (Miller and Beatty, 1969; Mougey et al., 1993). The terminal knobs for the 90S were ascribed to the large complexes at the 5`-ETS such as the U3-snoRNP and the UTP modules (Mougey et al., 1993). Interestingly, new 5`-terminal knobs, for the emerging pre-60S particle, also appeared after the co-transcriptional cleavage at ITS1 (Osheim et al., 2004). The similarity here is intriguing because the primordial pre-60S also contains two large complexes: the Rrp5 and the Urb1 modules, as described in my PhD thesis. Most of the proteins of the Rrp5 and Urb1 modules are predicted to have α-helical repeats forming α-solenoid structures (Figure 4.1A), similar to some UTP proteins from the 90S pre-ribosome (Figure 4.1B). α-solenoid proteins are usually elongated and known to work as scaffold proteins for the 90S pre-ribosome, NPC and vesicle coating complexes (Devos et al., 2004; Fournier et al., 2013; Kornprobst et al., 2016). For example, the large α-solenoid proteins Utp20 and Utp10 scaffold the 90S pre-ribosome and cover wide areas of the structure, including contact to the pre-rRNA (Figure 4.1B). Accordingly, the α-solenoid proteins from the Rrp5 and Urb1 modules are expected to behave similarly, chaperoning the primordial pre-60S particles and allowing the snoRNPs to dock and have access to the immature pre-rRNA.

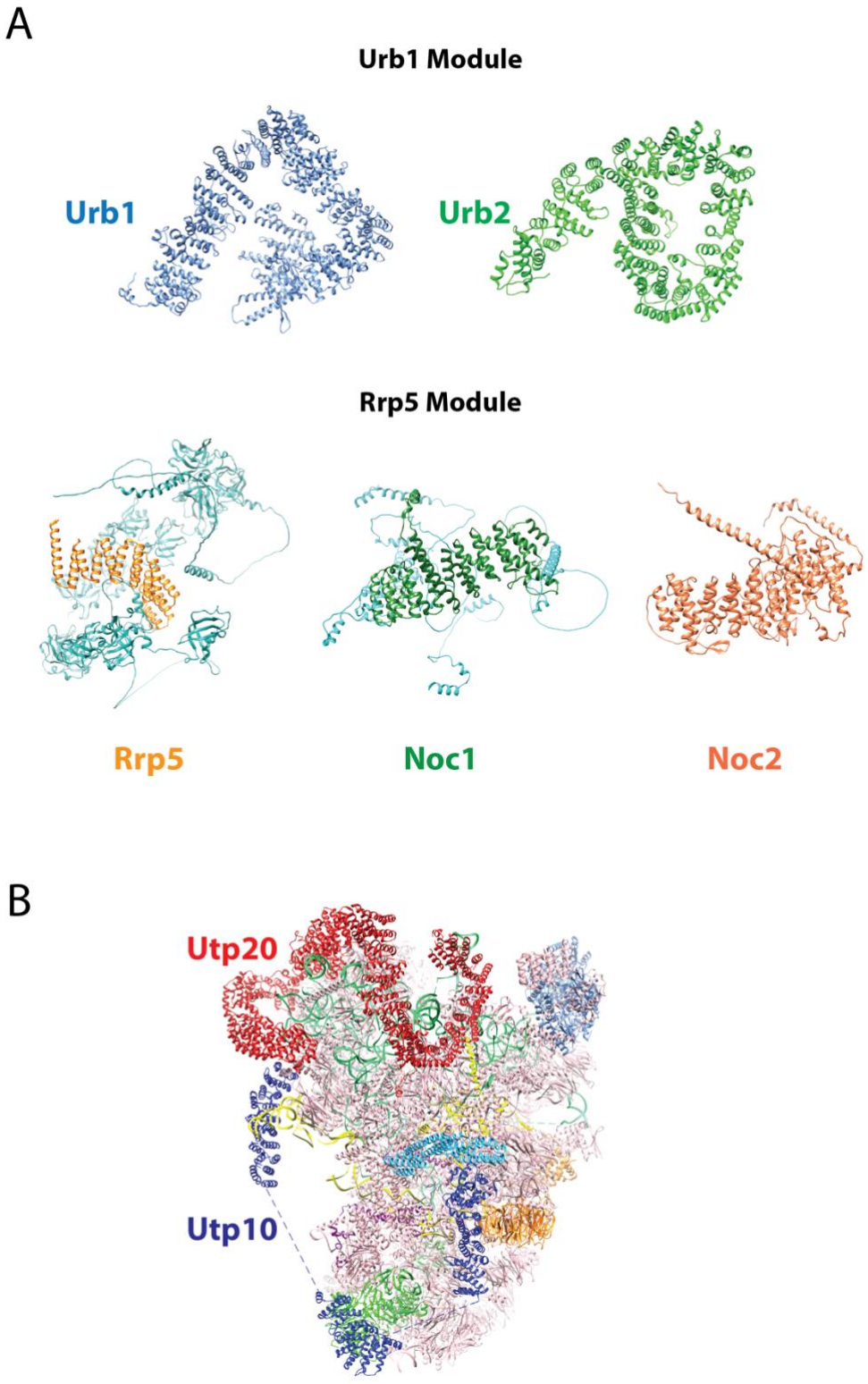

Figure 4.1 Members of Urb1 and Rrp5 modules form α-solenoid structures similar to some 90S UTP factors

(A) Structure prediction of assembly factors from the Urb1 and Rrp5 modules using AlphaFold (Jumper et al., 2021). The α-helical repeats of Urb1 (light blue; Identifier: P34241), Urb2 (light green; Identifier: P47108), Rrp5 (orange; Identifier: Q05022), Noc1 (dark green; Identifier: Q12176) and Noc2 (coral; Identifier: P39744) form α-solenoid structures.

(B) Cryo-EM structure of the 90S pre-ribosome Noc4-Dhr1 (pre-A_1; PDB: 6ZQC) is shown with the α-solenoid proteins Utp20 (red) and Utp10 (dark blue) highlighted.

4.2 C/D box snR190 and H/ACA snR37 dominate the primordial pre-60S

Several snoRNAs associated with the primordial pre-60S particle have been identified by Illumina sequencing through our collaboration with the Randau lab in Marburg. However, we were surprised by the specific and robust enrichment of snR190 and snR37 in the primordial pre-60S particle, seen by SYBR Green staining, suggesting a role of these C/D box and H/ACA snoRNAs at the earliest stage of pre-60S pathway. Although single deletion of either snrR190 or snR37 showed they are not essential for cell growth, their double deletion caused a synergistic growth defect at higher temperatures. Normally, snoRNPs associate transiently with the pre-rRNA in a short time frame to introduce rRNA modifications as suggested by (Osheim et al., 2004). However, the strong enrichment of snR190 and snR37 suggests their stable association with the primordial pre-60S, thereby playing a structural role similar to the U3 snoRNA in the 90S pre-ribosome, which does not guide rRNA modification but supports and/or chaperones the 90S particle.

Particularly, snR190 is closely linked to the Urb1 module as shown by CRAC analysis (Joret et al., 2018) and the genetic interaction I found between snR190 and Rsa3 showing a synthetic enhancement between snR190 and the Urb1 module member Rsa3, which further indicates that snR190 is a part of the Urb1 module network. Therefore, snR190 snoRNP could occupy a region on the 27S pre-rRNA and keep it from pre-mature folding and/or prevent this region from associating with assembly factors that only bind at later steps. For example, the Ssf1 module and the r-protein Rpl3 are not yet incorporated into the primordial pre-60S particle as the Urb1 module was found to bind to the site (Joret et al., 2018), where later the Ssf1 module together with Rpl3 are recruited (Sanghai et al., 2018). Together with the Urb1 module, snR190 could organize such step. Initially, Rpl3 is incorporated in an immature position when recruited with Ssf1 module (Sanghai et al., 2018). After dissociation of Ssf1 module, Rpl3 can reach its final position and bind to the root helices in the pre-60S particle (Gamalinda et al., 2014). For clarification, the root helices are the helices

at the beginning and end of each of the six 25S rRNA domains. These root helices cluster together in the 3D structure of the mature 60S subunit (Gamalinda et al., 2014).

Another interesting finding was the reduction of the RNA helicase Dbp7 from the Urb2-Noc1 primordial pre-60S particle when isolated from *snR190Δ* strain. Moreover, the extremely sick phenotype of *dbp7Δ* cells, which was partially rescued by disrupting snR190 (see Figure 3.10). One possible scenario is that the RNA helicase Dbp7 is involved in the removal of snR190 from the pre-60S particles. When Dbp7 is absent, due to its disruption in the *dbp7Δ* strain, snR190 is stuck on the pre-60S particles and cannot be removed, causing the sick phenotype of the *dbp7Δ* cells. This slow growing phenotype is then relieved when snR190 is also absent in the *snR190Δ dbp7Δ* strain. Analysis of Urb2-Noc1 particles from the *snR190Δ* strain also revealed reduction of other RNA helicases such as Dbp9 and Mak5, pointing to a potential link between snR190 and these helicases on the primordial pre-60S. Apparently, disruption of snR190 did not affect the association of the C/D box snoRNA cofactors such as Nop1, Nop58 and Nop56 with Urb2-Noc1 primordial pre-60S due to the co-enrichment of several other C/D box snoRNAs with the particle. By contrast, disruption of the H/ACA box snR37 has caused a reduction in the H/ACA snoRNA cofactor Cbf5 (a pseudouridine synthase) from the Urb2-Noc1 particle. This is consistent with the finding that only few H/ACA snoRNAs are co-enriched with the primordial pre-60S particle.

On the other hand, double deletion of snR190 and snR37 caused a synergistic reduction of the uncharacterized protein YCR016W from the Urb2-Noc1 primordial pre-60S particle (see Figure 3.9C). YCR016W has a unique domain called DUF2373 (WKF). This domain from C7orf50, the human ortholog of yeast YCR106W, has been identified as an RNA binding domain (Trendel et al., 2019). This suggests YCR016W could be involved in snoRNAs binding on the Urb2-Noc1 particle, which explains why its binding with the particle was reduced upon deletion of snR190 and snR37. In yeast genome-wide genetic interaction network study, YCR016W was linked with negative genetic interactions with the assembly factors Dbp6, Rsa3, Mak11 and Rlp24 and positive genetic interactions with Drs1, Cbf5 and Tif6 (Costanzo et al., 2016). All these evidences indicate that YCR016W plays a potential role at the earliest step of the large subunit assembly, involving RNA binding, presumably to snR190 and snR37.

4.3 Upa1 and Upa2 connection to H/ACA snoRNPs

Upa1 and Upa2 are suitable single baits to enrich the primordial pre-60S particle, yielding a pattern of co-enriched assembly factors highly similar to the one observed with Urb2-Noc1 split affinity purification. Reasons for this stems from the finding that Upa1 and Upa2 are exclusively enriched at the earliest stage of pre-60S assembly. Also, as single baits the overall yield of purified primordial pre-60S particles is significantly higher when compared to the split affinity-purified Urb2-Noc1. We tried to do EM structural analysis with the primordial pre-60S purified with Urb2-Noc1, but it was always difficult due to aggregation of the sample and the fact that this pre-ribosome has many flexible substructures. However, when we isolated the primordial pre-60S particle via Upa1, we managed to identify the overall shape by negative stain EM. Using Upa1 as a bait for isolation of the primordial pre-60S could facilitate further high-resolution structural analysis of this interesting particle using cryo-EM.

The paralogs Upa1 and Upa2 in *Saccharomyces cerevisiae* have resulted from an ancient genome duplication and there is only one in other organisms such as *Homo sapiens* (C9orf114). It is not yet clear what the function of Upa1 and Upa2 in the large ribosomal subunit biogenesis is. However, they were found to be functionally linked to the early pre-60S assembly factors Urb2, Nop8, Dbp6 and Dbp9 (Costanzo et al., 2016). There was also a potential yeast two-hybrid (Y2H) interaction between Upa1 and the pre-60S helicase Dbp6 in a screen using *Chaetomium thermophilum* ribosome assembly factors (Baßler et al., 2017), but the meaning of such interaction is not yet clear. It is possible that Upa1 and Upa2 function together as a heterodimer as I found them always co-purifying each other. They contain a SPOUT domain and it seems that it is a general theme of the SPOUT domain-containing proteins to dimerize. The crystal structure of C9orf114 (SPOUT1), human ortholog of Upa1 and Upa2, shows a homodimer (PDB: 4RG1). The SPOUT domain-containing methyltransferase yeast Emg1 has been shown in the cryo-EM structure of 90S particles as a homodimer (Chaker-Margot et al., 2017; Cheng et al., 2020; Kornprobst et al., 2016).

Another interesting aspect of Upa1 and Upa2 is their disappearance from the Urb2-Noc1 primordial pre-60S upon deletion of the H/ACA snR37. My data also showed that both Upa1 and Upa2 strongly enrich the H/ACA snoRNA-associated pseudouridine synthase Cbf5. This connection to the H/ACA snoRNPs is intriguing. The question here is, what is the relationship between H/ACA snoRNPs, normally

guiding pseudouridylation, and methyltransferases? Interestingly, it was reported that some SPOUT class methyltransferases methylate only pseudouridines. For example, Emg1 methylates U1191 in yeast 18S rRNA only after its pseudouridylation (ψ1191) by snR35 (Meyer et al., 2011). Also, bacterial RlmH methylates a pseudouridine ψ1915 in *E. coli* 23S rRNA (Ero et al., 2008; Purta et al., 2008). Accordingly, Upa1 and Upa2 may be able to methylate a pseudouridine in the primordial pre-60S particle, which was generated earlier by one of the H/ACA snoRNPs.

4.4 The 90-pre-60S super particle

One of the major experimental observation during my work was that disrupting ribosome assembly, either by mutation of assembly factors such as *nop1-4*, deletion of snoRNAs or overexpression of Mak5 D333A, caused significant enrichment of 90S factors on the early pre-60S particles. Possibly, this is the result of delayed pre-rRNA processing, delayed cleavage at ITS1 and the tendency of the mutant cells to undergo a post-transcriptional cleavage (switching from co-transcriptional A_2 to post-transcriptional A_3 cleavage). These results are consistent with earlier findings that depletion of the pre-60S helicase Drs1 has blocked co-transcriptional pre-rRNA processing, which caused accumulation of 90S factors on the isolated pre-60S particles (Talkish et al., 2016). Similarly, my data suggests that the dominant-negative Mak5 D333A caused the accumulation of 90S factors on the primordial pre-60S particle because the 90S and the primordial pre-60S particles could not efficiently detach. This has allowed us for the first time to visualize the long-sought 90S–pre-60S super-particle, revealing the connection between the 90S and pre-60S moieties in the UTP-C–Rrp5 region (see Figure 3.15). This particle is the largest ribosome assembly intermediate in eukaryotic ribosome biogenesis with a size of approximately 70 nm, getting close to the size of the 90 nm nuclear pore complex (NPC) (Figure 4.2).

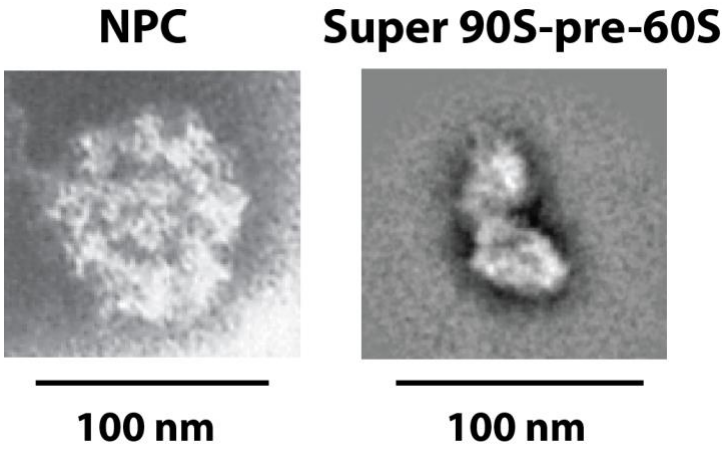

Figure 4.2 Comparison between the size of the NPC and the super 90S-pre-60S particle The figure shows negatively stained NPC from yeast (modified from Rout and Blobel, 1993) and one of super 90S-pre-60S particles obtained by negative stain EM.

The 90S part of this large particle is well developed and many structural features could be distinguished by cryo-EM. By contrast, the pre-60S moiety was substantially in a rudimentary state and flexible, awaiting the compaction of the rRNA subdomains and stable incorporation of bound modules. Similar flexibility is further seen in some of the succeeding and structurally characterized nucleolar pre-60S particles e.g. state A and B pre-60S particles in (Kater et al., 2017); state 1, 2 and 3 pre-60S particles in (Sanghai et al., 2018), which still include a few flexible modules and/or subdomains such as 5S RNP, Ssf1 module, 25S rRNA domains III, IV, V and VI. Interestingly, it is expected that the large 90S–pre-60S super-particles are also present in higher eukaryotes including humans since ribosome assembly in higher eukaryotes follows the post-transcriptional pathway (Gamalinda et al., 2014). This work has revealed the overall architecture and dimensions of the bipartite 90S-pre-60S super particle, which paves the way for future studies on understanding this intermediate and its relevance in human ribosome assembly.

In conclusion, these data revealed insights into the earliest steps of pre-60S ribosome assembly, including the associated network of pre-60S assembly factors and snoRNAs, and its coupling to the upstream 90S pathway. Understanding the molecular details of this earliest phase of large subunit assembly in yeast is important to also promote the comprehensive understanding of ribosome biogenesis in humans. This will help in understanding the link between defects in ribosome assembly and the associated diseases such as cancers and ribosomopathies.

5 Materials and Methods

5.1 Materials

5.1.1 Culture Media and plates

Lysogeny Broth (LB)
0.5 % (w/v) yeast extract
1 % (w/v) tryptone
0.5 % (w/v) NaCl
pH 7.2
100 µg/mL Ampicillin or 30 µg/mL Kanamycin
(1.5% Agar were added for plates)

Yeast extract-Peptone-Dextrose (YPD)
1% (w/v) yeast extract
2% (w/v) Bacto™ peptone
2% (w/v) glucose
pH 5.5
(2% Agar were added for plates)

Yeast extract-Peptone-Galactose (YPG)
1% (w/v) yeast extract
2% (w/v) Bacto™ peptone
2% (w/v) Galactose
pH 5.5

Synthetic Dextrose Complete (SDC-X)
2% (w/v) glucose
0.7% (w/v) yeast nitrogen base without amino acids, complemented with amino acids drop-out mix lacking amino acid X required for selection
pH 5.5
(2% Agar were added for plates)

Synthetic Galactose Complete (SGC-X)
2% (w/v) Galactose
0.7% (w/v) yeast nitrogen base without amino acids, complemented with amino acids drop-out mix lacking amino acid X required for selection
pH 5.5
(2% Agar were added for plates)

5.1.2 Buffers

TAP purification buffer
100 mM NaCl
5 mM $MgCl_2$
50 mM Tris-HCl
5% (v/v) Glycerol
0.1% (v/v) IGEPAL CA-630
1mM dithiothreitol (DTT)
Filtered

Phosphate-buffered saline (PBS)
137 mM NaCl
2.7 mM KCl
10 mM Na_2HPO_4
1.8 mM KH_2PO_4
pH 7.4

50X TAE (for agarose gel electrophoresis)
2M Tris
5.71% Acetic acid
50 mM EDTA

Semi-dry western blotting transfer buffer
48 mM Tris
39 mM Glycine
0.037% SDS
10% Methanol

10X TBE buffer
500 mM Tris
485 mM Borate
20 mM EDTA
Filtered

RNA sample loading dye (for polyacrylamide/Urea gels)
98% Formamide
1 mM EDTA
Pinch of Xylene Cyanol and Bromophenol blue
Hybridization mix (for northern blots)
6X SSPE
5X Denhardt's reagent
0.5% SDS
H_2O up to 50 ml

Filtered

20X SSPE buffer
3,0 M NaCl
0,2 M NaH_2PO_4
0,02 M EDTA
pH 7.4
Filtered

50x Denhardt's
1% (w/v) Ficoll 400
1% (w/v) Polyvinylpyrrolidone
1% (w/v) BSA
in H_2O
Filtered

4 x Protein sample (loading) buffer
250 mM Tris-HCL (pH 7)
9 % (w/v) SDS
40 % (v/v) glycerol
0.2 % (w/v) Bromophenol blue
100 mM DTT

5.1.3 Yeast strains

Table 5.1 List of yeast strains used in this study

Name	Genotype	Source
W303	*Saccharomyces cerevisiae)* MATalpha *ade2-1, trp1-1, leu2-3,112, his3-11,15, ura3-1, can1-100*	(Thomas and Rothstein, 1989)
NOP1+	TF38 Null (haploid), *NOP1*, *ura3*, *his3*	(Tollervey et al., 1993)
nop1-4	TF38 Null (haploid), *nop1::URA3*, *his3*, LEU2, pSB32-*nop1-4*	(Tollervey et al., 1993)
NOP1+, Nsa3-FTpA	TF38 Null (haploid), *NOP1*, *ura3*, *his3*, *NSA3-FTpA*::*natNT2*	This study
nop1-4, Nsa3-FTpA	TF38 Null (haploid), *nop1::URA3*, *his3*, LEU2, pSB32-*nop1-4, NSA3-FTpA*::*natNT2*	This study
Urb1-FTpA	W303*, URB1-FTpA*::*natNT2*	This study
Urb2-FTpA	W303*, URB2-FTpA*::*natNT2*	This study
Urb2-TAP	W303, *URB2-TAP* (Calmodulin-TEV-prot.A)::*HIS3*	This study

Urb2-TAP Noc1-Flag	W303, *URB2-TAP*::*HIS3*, *NOC1-Flag*::*natNT2*	This study
Urb2-TAP Nop58-Flag	W303, *URB2-TAP*::*HIS3*, *NOP58-Flag*::*natNT2*	This study
Urb2-TAP Nsa3-Flag	W303, *URB2-TAP*::*HIS3*, *NSA3-Flag*::*natNT2*	This study
Nsa1-TAP Flag-Ytm1	W303, *NSA1-TAP*::*klURA3*, *Flag-YTM1*::*natNT2*	(Kater et al., 2017)
Noc4-TAP Dhr1-Flag	W303, *NOC4-TAP*::*HIS3*, *DHR1-Flag*::*natNT2*	(Cheng et al., 2020)
Nop4-FTpA	W303, *NOP4-FTpA*::*natNT2*	This study
Nop8-FTpA	W303, *NOP8-FTpA*::*natNT2*	This study
Mak5-FTpA	W303, *MAK5-FTpA*::*natNT2*	This study
Nop56-FTpA	W303, *NOP56-FTpA*::*natNT2*	This study
Nop58-FTpA	W303, *NOP58-FTpA*::*natNT2*	This study
Arx1-FTpA	W303, *ARX1-FTpA*::*natNT2*	(Thoms et al., 2018)
Kre33-FTpA	W303, *Kre33-FTpA*::*HIS3*	(Cheng et al., 2019)
snR190Δ	W303, *snr190*:: *klTRP1*	This study
snR37Δ	W303, *snr37*::*hphNT1*	This study
snR190Δ snR37Δ	W303, *snr190*:: *klTRP1*, *snr37*::*hphNT1*	This study
Urb2-TAP Noc1-Flag snR190Δ	W303, *URB2-TAP*::*HIS3*, *NOC1-Flag*::*natNT2*, *snr190*:: *klTRP1*	This study
Urb2-TAP Noc1-Flag snR37Δ	W303, *URB2-TAP*::*HIS3*, *NOC1-Flag*::*natNT2*, *snr37*::*hphNT1*	This study
Urb2-TAP Noc1-Flag snR190Δ snR37Δ	W303, *URB2-TAP*::*HIS3*, *NOC1-Flag*::*natNT2*, *snr190*:: *klTRP1*, *snr37*::*hphNT1*	This study
Nop4 shuffle	W303, *nop4*::*KanMX6*, pRS316-*NOP4*	This study
Nop4 shuffle snR190Δ	W303, *nop4*::*KanMX6*, pRS316-*NOP4, snr190*:: *klTRP1*	This study
dbp7Δ	W303, *dbp7*:: *natNT2*	This study
snR190Δ dbp7Δ	W303, *snr190*:: *klTRP1*, *dbp7*:: *natNT2*	This study
Rsa3Δ	W303, *rsa3*::*natNT2*	This study
snR190Δ Rsa3Δ	W303, *snr190*:: *klTRP1, rsa3*::*natNT2*	This study
Nsa3-FTpA	W303, *NSA3-FTpA*::*natNT2*	This study
Nsa3-FTpA snR190Δ	W303, *NSA3-FTpA*::*natNT2*, *snr190*:: *klTRP1*	This study

Nsa3-FTpA Rsa3Δ	W303*, NSA3-FTpA*::*HIS3*, *rsa3*::*natNT2*	This study
Nsa3-FTpA snR190Δ Rsa3Δ	W303*, NSA3-FTpA*::*HIS3*, *snr190*:: *klTRP1*, *rsa3*::*natNT2*	This study
Upa1-FTpA	W303*, UPA1-FTpA*::*natNT2*	This study
Upa2-FTpA	W303*, UPA2-FTpA*::*natNT2*	This study

5.1.4 Plasmids

Table 5.2 List of plasmids used in this study

Name	Description	Source
pFA6A-FTpA	For C-terminal tagging	Dieter Kressler
pFA6A-TAP	For C-terminal tagging	Dieter Kressler
pFA6A-FLAG	For C-terminal tagging	Dieter Kressler
pFA6A-natNT2	For genomic disruption	(Janke et al., 2004)
pFA6A-hphNT1	For genomic disruption	(Janke et al., 2004)
pFA6A-TAP-klTRP1	Used for construction of *snR190Δ-U14-klTRP*	Dieter Kressler
pFA6A-KanMX6	For genomic disruption	(Longtine et al., 1998)
pRS316-*snR190-U14*	$P_{snR190\text{-}U14}$, *snR190*, *U14*, *URA3*, ARS/CEN, *AmpR*	This study
pRS316-*NOP4*	P_{NOP4}, *NOP4*, *URA3*, ARS/CEN, *AmpR*	This study
pRS315-*NOP4*	P_{NOP4}, *NOP4*, *LEU2*, ARS/CEN, *AmpR*	This study
pRS315-*nop4*-19	P_{NOP4}, *nop4* F335L, *LEU2*, ARS/CEN, *AmpR*	This study
pRS315-*nop4*-3	P_{NOP4}, *nop4* F557L, *LEU2*, ARS/CEN, *AmpR*	This study
YCplac111	*LEU2*, ARS/ CEN, *AmpR*	(Gietz and Akio, 1988)
YCplac111-GAL-*MAK5*	P_{GAL}, *MAK5*, *LEU2*, ARS/ CEN, *AmpR*	This study
YCplac111-GAL-*mak5 D333A*	P_{GAL}, *mak5 D333A*, *LEU2*, ARS/ CEN, *AmpR*	This study

5.1.5 Oligos

Table 5.3 List of oligos used in this study

Name	Sequence
Nsa3 (F2)	TTAACAATGCAAAAAAGAGATCTTCTAGCGAGCTTGAAAAAGAATCTAGCGA GTCAGAAGCTGTCAAGAAGGCTAAAAGTCGGATCCCCGGGTTAATTAA
Nsa3 (S2)	CACCGCACTCTATGAAATTCAAATTTTTTTCTTCACAAGAAAAAAATGAGAGA AAAGATAGATAAGGAGGAAACAAATTAATCGATGAATTCGAGCTCG

Urb1 (F2)	ACGAGCTTGTCAAATCACAAAAAAGGCTAATATTATGGACAGAAGGTGAT AGCGACAACGTTGTTAAGAGGCTACGTAAACGGATCCCCGGGTTAATTAA
Urb1 (S2)	ATACATTTCGCACATTATATAGAAAAGTGGACATTTAATTCTTCAAATCT TATTTAAAATATCTATCACAAGACAGCTCAATCGATGAATTCGAGCTCG
Urb2 (F2)	CTTTCCTTGACACACCTGGGAAACAATATTTCAAAGCACTTTACCTCCAA TACAAAAAGGTTGGTAAATGGCGCGAAGATCGGATCCCCGGGTTAATTAA
Urb2 (S2)	ACTTGTTTAAGCTCCGTCACCCTGTTATTAAACGTGAGCAGAGAAATGCC TTTTGAAAACACACTAAAACACATAAGTTAATCGATGAATTCGAGCTCG
Noc1 (F2)	AGAGAAAGAATATGCTCAAAAGTCTACCGGTATTTGCATCTGCCGACGATTA TGCTCAATATTTAGATCAAGATTCAGACCGGATCCCCGGGTTAATTAA
Noc1 (S2)	GGACCGTTTTTTATTGTACAAAATTCTGTTTTCCTTATTTAATTTACAACACCG AAGTGTTTAGTTAATGTATTATTATTTTCTAATCGATGAATTCGAGCTCG
Nop58 (F2)	GGAAAAGAAGGAAAAGAAGGAGAAGAAAGAGAAGAAAGAGAAGAAGGAAAA GAAGTCCAAGAAAGAGAAGAAAGAGAAGAAACGGATCCCCGGGTTAATTAA
Nop58 (S2)	GGATAATTATAGAAAATTTTCTAAATCCAAATAAAAGGGAACGCGAGGGGTC ACTAATTATTAAAATGTAAAATGCATCCTTAATCGATGAATTCGAGCTCG
Nop56 (F2)	GAAAGAAAAGAAGGAAAAGAAGGACAAAAAGGAAAAGAAAGATAAAAAGGA AAAGAAGGATAAAAAGAAGAAAAGTAAGGATCGGATCCCCGGGTTAATTAA
Nop56 (S2)	GAAAAACTTTAAAGGGAAGAAAAGTACACAAAAAGATGGGATATACTTTATTT CGATTCATTGTTCCTTTTAATCGATGAATTCGAGCTCG
Nop4 (F2)	CCAATCCCGATGACAAAAAGATGGGCGATGATATAAAGAGAATAATCGGGTT CAAGCGTAAGAGAAAGCACGCAAAAAAACGGATCCCCGGGTTAATTAA
Nop4 (S2)	CATCTATCTACTCTTTGAAAAATAATGTACATACGTAAAGAGAATACAAATCG AAATTCCTATAAATATGGTTCTACCTCTAATCGATGAATTCGAGCTCG
Nop4 (S1)	CTTTTTATTAGTAAAATAGTGAGATTTCTTCGTGAACTAGTGAAAAGCTATCAA TATTACCAATCTACCAAAGTGAGATGCGTACGCTGCAGGTCGAC
Nop8 (F2)	GGACCCGTGATATGAGGCGCAAAATGAAAGATGCATTGAAGCACCGTAAGA GGAAACAATCAAAGAGCGGGCTTCTTCTACGGATCCCCGGGTTAATTAA
Nop8 (S2)	GGAAATGGCTGTTAAGTTCGGTAAAAATGCTTTTTGAATAAGCGCAGAGAAA TCTATACTATATATGTATATATACTCACTAATCGATGAATTCGAGCTCG
Mak5 (F2)	AAAGAGGTCATAATTCTATCATTGGTCATGAAAAGACAAACGCCTTAGAAACT TTGAAGAAAAAGAAAAAGAGAAATAATCGGATCCCCGGGTTAATTAA
Mak5 (S2)	CATAGTGGGTTTAGAGGACCGTGTATATTACGTAGAAAATACAGTGAAAGGA GAGTTTCTCTTCAAAAGCCTCGAGATTAATCGATGAATTCGAGCTCG
Upa1 (F2)	CTGCTTCCGTACCCCAGGGAAATATACCCATTCAAGATAGCCTACCCATAGC TCTTACCATGTTTCAGCGTTGGGCAAGTCGGATCCCCGGGTTAATTAA
Upa1 (S2)	CTAAAAATAGAACTGCATATCCGTAGAAAACGATGATTATATAACATAAATAG TAATATCAGTTATTAATTGCTATTTATTTCAATCGATGAATTCGAGCTCG
Upa2 (F2)	CTCAGCTACCATGCCCCGTATCCAATTCGGACGTTGCAGATGCAATCCCCAT GACACTGACCACTCTTTCAACTGTATTTCGGATCCCCGGGTTAATTAA
Upa2 (S2)	GAGGAAAGTGACAGTAATAATAATGATTGCGTCTCTAATATATACGTACTTAT CCATTGCATGAAGGTAATTTGGGATTAATCGATGAATTCGAGCTCG
snR190 (Northern)	CGTCATGGTCGAATCGG
snR37 (Northern)	AAGCTCCTCATCACTCACAC
U3 (Northern)	GGTTATGGGACTCATCA
Rsa3 (S1)	TATTGTAGTAATATATACAAGAATTTAAACTGCCCACTTGAAATAGCACGGAA AGAACTAGCCATAATATATTATACAGGATGCGTACGCTGCAGGTCGAC
Rsa3 (S2)	CTAAATAATTAATGTGCACGTCAATATATTCTCCGCGGAAACATGACAAACTT TTAGAAAAAGATTTAAAGCAATATTTTTCAATCGATGAATTCGAGCTCG
Dbp7 (S1)	GTACGATTGTTTATATTCTTTTTCCTTTGGGATTATTCATATTCCAAATAAGCA TACTTATTCAGCAATTTAACACCAAGATGCGTACGCTGCAGGTCGAC
Dbp7 (S2)	CTGTAGATTTTATCATTTTCTTTGTCTTCATAGTATACAATTTTTTTTATATGAA TTAATGCTTGTTCTTGTCTATTTAATCGATGAATTCGAGCTCG

snR37 (S1)	AACTTCTTCCCTTTGTTACTTCTTCTTTAAAATTCAAATTTTTCTTTTGATTTTTTTTCAAAAGGCTAACCGTACGCTGCAGGTCGAC
snR37 (S2)	GGTACCAAGACAAGTCCATCCCCGTAGGCACTACAAATTATGGGAATGAGAAAGTATACAAAATATAAACATCGATGAATTCGAGCTCG

5.1.6 Reagents and kits

Table 5.4 List of Reagents, enzymes and kits used in this study

Name	Source	Identifier
Flag peptide (DYKDDDDK)	CASLO	N/A
TEV protease	(Parks et al., 1994)	N/A
SIGMA*FAST*	Sigma–Aldrich	S8830
ANTI-FlagM2 Affinity Gel	Sigma–Aldrich	A2220
IgG–Sepharose 6 Fast Flow	GE Healthcare	17096902
SYBR Green II RNA gel stain	Sigma–Aldrich	S9305
RiboLock RNase inhibitor	Thermo Fisher Scientific	EO0381
T4 PNK	NEB	M0201
T4 DNA ligase	NEB	M0202
Phusion high-Fidelity DNA Polymerase	Thermo Fisher Scientific	F530L
Restriction enzymes	Thermo Fisher Scientific and NEB	N/A
DNase I (RNase-free)	NEB	M0303S
GenElute HP Plasmid Miniprep Kit	Sigma–Aldrich	NA0160
GenElute PCR Clean-up Kit	Sigma–Aldrich	NA1020
GenElute Gel Extraction Kit	Sigma–Aldrich	NA1111
mirVana miRNA Isolation Kit, with phenol	Invitrogen	AM1560
NEBNext Multiplex Small RNA Library Prep Set for Illumina (Set 1)	NEB	E7300S
Bioanalyzer High Sensitivity DNA Analysis	Agilent	5067-4626
Qubit RNA HS Assay Kit	Invitrogen	Q32855
Qubit dsDNA HS Assay Kit	Invitrogen	Q32854
MiniSeq High Output Reagent Kit	Illumina	FC-420-1003

(Kits for Illumina sequencing were used by Dr. JV Gomes-Filho)

5.1.7 Software

Table 5.5 List of software used in this study

Name	Source	Website
MaxQuant	(Cox and Mann, 2008)	https://www.maxquant.org
UCSF Chimera	(Pettersen et al., 2004)	http://www.cgl.ucsf.edu/chimera
ChimeraX	(Goddard et al., 2018)	https://www.rbvi.ucsf.edu/chimerax
Fastqc	Andrews, S. (2010). FastQC: A Quality Control Tool for High Throughput Sequence Data [Online]	https://www.bioinformatics.babraham.ac.uk/projects/fastqc/
Cutadapt	(Martin, 2011)	https://cutadapt.readthedocs.io/en/stable/installation.html
Hisat2	(Kim et al., 2019)	http://daehwankimlab.github.io/hisat2/
Samtools	(Danecek et al., 2021)	http://www.htslib.org/
R-studio	RStudio Team (2020). RStudio: Integrated Development for R. RStudio, PBC, Boston, MA	https://www.rstudio.com/
ggplot2 (R package)	Wickham H (2016). ggplot2: Elegant Graphics for Data Analysis. Springer-Verlag New York. ISBN 978-3-319-24277-4	https://ggplot2.tidyverse.org
IGV	(Robinson et al., 2011)	https://software.broadinstitute.org/software/igv/
CrYOLO	(Wagner et al., 2019)	http://sphire.mpg.de
RELION 3.1.2	(Zivanov et al., 2018) (Zivanov et al., 2020)	https://github.com/3dem/relion
CryoSPARC v3.2.0	(Punjani et al., 2017)	http://www.cryosparc.com/
Gctf	(Zhang, 2016)	https://www2.mrc-lmb.cam.ac.uk/research/locally-developed-software/zhang-software/

Software programs in this table are the collection of software used by myself, Dirk (EM), Matthias (EM) or Vicente (sequencing).

5.2 Methods

5.2.1 Cloning and plasmid construction

Standard molecular biology protocols for cloning and plasmid construction were followed. Phusion high-Fidelity DNA Polymerase was used in the PCR reactions. The oligos used in the PCR reactions were ordered from Sigma-Aldrich and are listed in (Table 5.3 in Materials). The PCR products were run on 1% agarose gel electrophoresis, then the bands were excised from the gel and purified with the GenElute Gel Extraction Kit according to the manufacturer's instruction. The purified PCR products and template plasmids were digested with restriction enzymes from Thermo Fisher Scientific or NEB. Ligation of the digested PCR product into the template plasmid was carried out using T4 DNA ligase. Chemically competent *E. coli* DH5a strain was used to amplify the plasmids. Subsequently, the plasmids were extracted from *E. coli* using GenElute HP Plasmid Miniprep Kit according to the manufacturer's instruction. The plasmids were then confirmed by test digest with restriction enzymes and/or DNA sequencing (Eurofins Genomics, Ebersberg, Germany). The plasmids used in this work are listed in (Table 5.2 in Materials)

5.2.2 Construction of yeast strains

All yeast strains generated and used in this study are listed (Table 5.1) in the Materials section. Genomic integration of tags and gene disruptions were performed using PCR constructs for homologous recombination as described in (Janke et al., 2004; Longtine et al., 1998). F2 and S2 oligos were designed for each ORF in order to amplify PCR constructs for C-terminal tagging, while S1 and S2 oligos were designed for gene disruption (see Table 5.3 in the Materials section). Positive transformants were confirmed for integration events by colony PCR and/or western blot analysis with antibodies against the expressed tagged protein (e.g. anti-protA or anti-Flag).

To create snR190 disruption strain (*snR190Δ* strain), I took into consideration that snR190 is transcribed together with U14 as a bicistronic precursor transcript i.e. promoter-snR190-U14-terminator (Chanfreau et al., 1998). Therefore, I created a construct with 80 nucleotides deletion in snR190 followed by U14 (*snR190Δ*-U14-native terminator). This construct was subsequently inserted into pFA6A-TAP-klTRP1 plasmid upstream of the klTRP1 marker. Using PCR, I amplified the following construct (*snR190Δ*-U14-native terminator- klTRP1). Then, W303 wild-type yeast strain was

transformed with the latter construct to replace the genomic snR190-U14 by homologous recombination. The strain was confirmed by colony PCR and sequencing.

5.2.3 Western blotting

Western blot analysis was performed to check the expression of tagged proteins. Cells were lysed with glass beads in Eppendorf tubes, followed by TCA precipitation of proteins and running the samples on SDS gels. After separation of proteins by SDS-PAGE, they were transferred to a nitrocellulose membrane (GE Healthcare) using semi-dry transfer at 11 V for 1 h. The membrane was stained by Ponceau S to check whether the transfer was successful. The membrane was then blocked with 3% milk in 1X PBS for 1 h or overnight at 4°C. Subsequently, the membrane was incubated with the primary antibody (anti-protA from Sigma-Aldrich 1:300 dilution) at room temperature for 1 hr. Washing of the membrane was performed three times 5 min each in 1X PBS with 0.1% Tween 20. Detection of the HRP conjugated-antibodies was done using detection solution Immobilon Western HRP Substrate (Millipore) and the Image Quant LAS 4000 (GE Healthcare).

5.2.4 Yeast transformation

Yeast cells were harvested at an $OD_{600\ nm}$ value of 0.5-0.7, washed with sterile water and resuspended in solution I (10 mM Tris-HCl pH 7.5, 1 mM EDTA, 100 mM LiAc). In a new Eppendorf tube, the following mix was added: an aliquot of the cell suspension, herring sperm carrier DNA, plasmid or PCR product to be transformed and solution II (10 mM Tris-HCl pH 7.5, 1 mM EDTA, 100 mM LiAc and 40% PEG). Then, the mixture was incubated at 30°C for 30 min rotating on a turning wheel, followed by heat shock for 10-15 min at 42°C and chilling on ice for 3 min. The cells were washed with sterile water and either directly plated on the appropriate selection plates (in case of transformation with plasmid) or let to recover in YPD medium for couple of hours before plating (in case of transformation with PCR construct expressing antibiotic selection marker).

5.2.5 Tandem affinity purification

Yeast strains expressing single-bait proteins C-terminally tagged with FTpA or strains expressing split tags—one protein with TAP and another with Flag—were grown in YPD media at 30°C and harvested at an $OD_{600\ nm}$ value of 2.0–3.0. Cell lysis was

performed in the purification buffer (100 mM NaCl, 5 mM $MgCl_2$, 50 mM Tris-HCl, pH 7.5, 5% (v/v) glycerol, 0.1% (v/v) IGEPAL CA-630, and 1 mM dithiothreitol) supplemented with protease inhibitor cocktail (SIGMA*FAST*) and RiboLock RNase inhibitor. Cells were lysed mechanically either in a bead beater (Fritsch) using glass beads or in a cryogenic mill (Retsch MM400). A pre-clearing step was carried out by centrifugation at 4°C for 10 min at 5000 rpm. Another centrifugation was performed at 4°C with 17,000 rpm for 20 min using Beckman Coulter centrifuges, rotor JA-25.50. The supernatants were used for the first affinity step by incubation with pre-equilibrated IgG Sepharose 6 Fast Flow affinity resin for at least 2.5 h at 4°C. The IgG resin was then washed two times with the purification buffer, collected in smaller mobicol columns (MoBiTec) and bound proteins were eluted by TEV protease (self-made) for 1.5 h on a rotating wheel at 16°C. TEV eluates were transferred to new mobicol columns. The collected TEV eluates were incubated with pre-equilibrated Anti-Flag M2 Affinity Gel for 1.5 h at 4°C in a second affinity step. Anti-Flag beads were then washed with the purification buffer and bound proteins were eluted from the beads with the purification buffer supplemented with Flag peptide (final concentration 300 µg/mL). Flag elution was done at 4°C on a rotating wheel for 1h. Flag eluates were analyzed on 4–12% polyacrylamide gels (NuPAGE, Invitrogen) with colloidal Coomassie staining (Roti Blue, Roth) or used for other analyses e.g. RNA extraction, northern blotting, Illumina sequencing, mass spectrometry or electron microscopy.

In order to induce *mak5* D333A mutant overexpression, the *Urb2–TAP Noc1-Flag* YCplac111-GAL-*mak5* D333A strain was cultured at 30°C in SDC-Leu (glucose) medium to early logarithmic phase then shifted to YPG (galactose) medium and grown for 8 h. Affinity purification of Urb2-TAP Noc1-Flag particles from this mutant strain was performed as described above with final elution from the anti-flag beads using Flag peptide (final concentration 300 µg/mL) in the following buffer: 100 mM NaCl, 5 mM $MgCl_2$, 50 mM Tris-HCl, pH 7.5 and 5% (v/v) glycerol for negative-stain EM analysis. For cryo-EM analysis, the final elution was done using Flag peptide (final concentration 300 µg/mL) in the following buffer: 100 mM NaCl, 5 mM $MgCl_2$, 50 mM Tris-HCl, pH 7.5 and 0.05% Nikkol.

5.2.6 Sucrose gradient analysis

The final eluate of Urb2-TAP Nop58-Flag split affinity purification was loaded on a linear 10%–40% (w/v) sucrose gradient (prepared in buffer containing 100 mM NaCl, 5 mM $MgCl_2$, 50 mM Tris-HCl, pH 7.5) and centrifuged at 129,300 xg for 16 h at 4°C using Beckman Coulter centrifuges, rotor SW40. The sucrose gradient was prepared using a gradient master device from Biocomp Instruments. Subsequently, fractions from the gradient were collected and an equal volume from each was used for RNA extraction and northern blotting. The remainder of each fraction was precipitated with 10% TCA, washed with acetone, resuspended in SDS sample buffer and finally analyzed on 4–12% polyacrylamide gels (NuPAGE, Invitrogen) with colloidal Coomassie staining.

5.2.7 RNA Extraction, SYBR Green staining and northern blot analysis

RNA extraction from the final eluates of affinity-purified pre-ribosomal particles was done using phenol–chloroform extraction. Phenol-chloroform-isoamyl alcohol solution (25:24:1) was added in equal volume to the flag eluates, mixed and centrifuged for 10 min. The aqueous phase was then collected in new Eppendorf tube and equal volume of chloroform was added, then mixed and centrifuged for 5 min. The aqueous phase was collected and three volumes of 100% ethanol, 1/10 volume 3M NaAc pH 5.2 and 1µl glycogen were added. The mix was incubated in ice for at least 1 h or at -20°C overnight to precipitate the RNA. Then, the sample was centrifuged for 20 min at 14000 rpm and the pellet was washed with ice cold 70% Ethanol**.** After washing, the pellet was left to air dry and finally resuspended in sterile water. For detection of snoRNAs, extracted RNA samples were resolved on 8% polyacrylamide/8 M urea gels. For RNA staining, the gels were incubated for 30 min with SYBR Green II RNA gel stain (Sigma–Aldrich) using a 1:5000 dilution in 1X TBE.

For northern blot analysis, the RNA was transferred to a Hybond-N+ nylon membrane (GE Healthcare) and UV-crosslinked in stratalinker. Next, the membrane was incubated in the hybridization mix (see Materials, section 5.1.2 Buffers) for at least 30 min at 37°C. During the incubation, the probes for detection were labeled by mixing: 1xPNK buffer, 10mM DTT, 10 pmol oligo, [γ-^{32}P] ATP and 10U PNK. The mix was incubated 30 min at 37°C and then purified with G25 column (GE healthcare). The

purified labeled probe was added to the membrane with the hybridization mix and incubated overnight. Afterwards, the membrane was washed three times with 6X SSPE at least 20 min each. The signals were finally detected using a Phosphor imager. The membrane was stripped with boiling 0.5% SDS and re-probed again.

5.2.8 Mass Spectrometry

After SDS-PAGE and Coomassie staining and de-staining of the gels, major bands were individually excised, trypsin digested and identified by MALDI-TOF mass spectrometry at the in-house BZH mass spectrometry facility, Heidelberg. To identify the entire set of proteins in the samples, semiquantitative mass spectrometry analysis was performed. To prepare the samples for the analysis, the flag eluates were run only 2 cm for about 5 min on 4–12% NuPAGE gels (Invitrogen) and stained with Coomassie. The 2 cm area of the samples were excised from the gel and sent to the FingerPrints Proteomics Facility (University of Dundee, UK), where the proteins were identified by 1D nLC–ESI-MS/MS. Raw data was analyzed using MaxQuant software (Cox and Mann, 2008).

5.2.9 Illumina Sequencing of RNA

I affinity-purified the particles and sent the flag eluates to Dr. Jose Vincente Gomes-Filho from the Randau lab, Marburg. Vicente performed the Illumina sequencing and wrote this following method paragraph (Illumina Sequencing of RNA).

“RNA was extracted from the selected particles (Urb2–Nop58, Urb2–Noc1) using a mirVana miRNA isolation kit, following the manufacturer’s protocol for enriching of small RNAs. After extraction, RNA was quantified using a Qubit RNA HS assay kit and used as input for library preparation with the NEBNext Small RNA Library Prep Set for Illumina, following the manufacturer’s instructions. Libraries were loaded on a MiniSeq and sequenced in single-end mode with reads of 150 nts length. To generate the final Log2 fold-change values, raw reads were quality checked and processed using in-house scripts.”

5.2.10 Electron Microscopy and Image Processing

I prepared the samples for EM analysis by performing the affinity purification of the particles. Dr. Dirk Flemming (head of the electron microscopy facility at the

Biochemistry Center, Heidelberg) performed all negative stain electron microscopy and 2D classification of the samples. Dr. Dirk Flemming prepared the cryo-EM grids of the Urb2-Noc1 particles isolated from the dominant mak5 mutant as well as collected data using the Glacios cryo-transmission electron microscope. Matthias Thoms, from Beckmann lab at LMU Munich, has processed and analyzed this data. Dirk and Matthias wrote together this following method section (Electron Microscopy and Image Processing).

“Negative-stain EM of isolated pre-ribosomal particles was performed essentially as described by (Lau et al., 2021). For cryo-EM, the Urb2–Noc1 mak5 D333A sample was snap-cooled in buffer containing 50 mM Tris-HCl pH 7.5, 100 mM NaCl, 5 mM $MgCl_2$ and 0.05% Nikkol. Three microliters of the sample were pipetted onto Quantifoil R 2/1 holey carbon grids, which were glow-discharged for 45 s using the PELCO easiGlow system. The grids were blotted for 5 s using a blot force of 10 at 100% humidity using a Vitrobot Mark IV (Thermo Fisher Scientific) operated at 4°C, and immediately plunge-frozen in liquid ethane cooled with liquid nitrogen. Grids were mounted onto auto-grids and imaged using a Thermo Scientific Glacios cryo-transmission electron microscope equipped with a Falcon IIIEC detector and operated at an acceleration voltage of 200 kV. One thousand and one movies were recorded in nanoprobe mode with parallel illumination at a nominal magnification of 45,000 and a spot size of 4 in linear mode. The calibrated object pixel size was 3.17 Å. Micrographs were acquired using dose fractionation to record 119 frames per exposure with a dose rate of 1 e per $Å^2$ per frame. Particles were picked with CrYOLO (Wagner et al., 2019) and images were processed with the RELION 3.1.2 (Zivanov et al., 2018, 2020) and CryoSPARC v3.2.0 (Punjani et al., 2017) software packages. In brief, movie stacks were motion-corrected using MotionCor2 with 5 × 5 as the number of patches, and estimation of contrast transfer function was performed on the motion-corrected micrographs with Gctf (Zhang, 2016). For particle picking, particles from 14 micrographs were manually picked with the CrYOLO box manager and used to refine the general model. A total number of 310,374 particles were picked, extracted using a box size of 180 × 180 pixels, and subjected to 2D classification in CryoSPARC. Good 2D classes were selected and the corresponding 69,486 particles were used for subsequent ab initio reconstruction with three classes. The resulting volumes were used as references for heterogeneous refinement with all picked particles.

Homogeneous refinement was performed for the resulting pre-60S and 90S classes following re-extraction (box size 200 × 200) and 3D classification in RELION 3.1.2. Three-dimensional classification was performed on the pre-60S class, with image alignment and an angular sampling interval of 7.5°; no alignment was performed for the 90S class. The good pre-60S class was further refined, post-processed and local-filtered in RELION. The 90S class was refined and local-filtered with CryoSPARC. Furthermore, the 90S particles were re-extracted with a box size of 450 × 450 pixels and 3D refinement was performed with a mask of 1200 Å, which led to the reconstituted 90S connected to a large and flexible extra density. The particles were iteratively re-extracted, centered, and refined, allowing large shifts, and the final homogeneous refinement and local filtering was performed with CryoSPARC. ChimeraX was used to display cryo-EM structures and models (Goddard et al., 2018).”

6 Appendix

6.1 List of abbreviations

°C	degree Celsius
2D	two-dimensional
3D	three-dimensional
AFs	assembly factors
ATP	Adenosine triphosphate
CP	central protuberance
CRAC	crosslinking and analysis of cDNA
Cryo-EM	cryogenic electron microscopy
EM	electron microscopy
ETS	external transcribed spacer
FTpA	Flag-TEV-protA
GAL	galactose
h	hour
ITS	Internal transcribed spacer
kDa	kilodaltons
LFQ	label-free quantification
min	minutes
mRNA	messenger RNA
NPC	nuclear pore complex
PCR	polymerase chain reaction
PDB	protein data bank
PET	polypeptide exit tunnel
protA	protein A
PTC	peptidyl-transferase center
r-proteins	ribosomal proteins
rDNA	ribosomal DNA
RNA	ribonucleic acid
rRNA	ribosomal RNA
snoRNA	small nucleolar RNA
snoRNPs	small nucleolar ribonucleoproteins
std	standard
TAP	tandem affinity purification
tRNA	transfer RNA
ts	temperature sensitive

6.2 List of figures

6.3 List of Tables

6.4 Own publications

Baßler, J., Ahmed, Y.L., Kallas, M., Kornprobst, M., Calviño, F.R., Gnädig, M., Thoms, M., Stier, G., **Ismail, S**., Kharde, S., et al. (2017). Interaction network of the ribosome assembly machinery from a eukaryotic thermophile. Protein Sci. *26*, 327–342.

Kater, L., Thoms, M., Barrio-Garcia, C., Cheng, J., **Ismail, S**., Ahmed, Y.L., Bange, G., Kressler, D., Berninghausen, O., Sinning, I., et al. (2017). Visualizing the Assembly Pathway of Nucleolar Pre-60S Ribosomes. Cell *171*, 1599-1610.e13.

Ismail, S., Flemming, D., Thoms, M., Gomes-Filho, JV., Randau, L., Beckmann, R., and Hurt, E. (2021). Emergence of the primordial pre-60S from the 90S pre-ribosome. (submitted)

7 References

Anantharam, V., Koonin, E. V., and Aravind, L. (2002). SPOUT: A class of methyltransferases that includes spoU and trmD RNA methylase superfamilies, and novel superfamilies of predicted prokaryotic RNA methylases. J. Mol. Microbiol. Biotechnol. *4*, 71–75.

Anger, A.M., Armache, J.P., Berninghausen, O., Habeck, M., Subklewe, M., Wilson, D.N., and Beckmann, R. (2013). Structures of the human and Drosophila 80S ribosome. Nature *497*, 80–85.

Armache, J.-P., Jarasch, A., Anger, A.M., Villa, E., Becker, T., Bhushan, S., Jossinet, F., Habeck, M., Dindar, G., Franckenberg, S., et al. (2010). Cryo-EM structure and rRNA model of a translating eukaryotic 80S ribosome at 5.5-Å resolution. Proc. Natl. Acad. Sci. *107*, 19748–19753.

Armistead, J., and Triggs-Raine, B. (2014). Diverse diseases from a ubiquitous process: The ribosomopathy paradox. FEBS Lett. *588*, 1491–1500.

Armistead, J., Khatkar, S., Meyer, B., Mark, B.L., Patel, N., Coghlan, G., Lamont, R.E., Liu, S., Wiechert, J., Cattini, P.A., et al. (2009). Mutation of a Gene Essential for Ribosome Biogenesis, EMG1, Causes Bowen-Conradi Syndrome. Am. J. Hum. Genet. *84*, 728–739.

Asano, N., Kato, K., Nakamura, A., Komoda, K., Tanaka, I., and Yao, M. (2015). Structural and functional analysis of the Rpf2-Rrs1 complex in ribosome biogenesis. Nucleic Acids Res. *43*, 4746–4757.

Axt, K., French, S.L., Beyer, A.L., and Tollervey, D. (2014). Kinetic Analysis Demonstrates a Requirement for the Rat1 Exonuclease in Cotranscriptional Pre-rRNA Cleavage. PLoS One *9*, e85703.

Balakin, A.G., Smith, L., and Fournier, M.J. (1996). The RNA world of the nucleolus: Two major families of small RNAs defined by different box elements with related functions. Cell *86*, 823–834.

Barandun, J., Hunziker, M., and Klinge, S. (2018). Assembly and structure of the SSU processome — a nucleolar precursor of the small ribosomal subunit. Curr. Opin. Struct. Biol. *49*, 85–93.

Barrio-Garcia, C., Thoms, M., Flemming, D., Kater, L., Berninghausen, O., Baßler, J., Beckmann, R., and Hurt, E. (2016). Architecture of the Rix1-Rea1 checkpoint machinery during pre-60S-ribosome remodeling. Nat. Struct. Mol. Biol. *23*, 37–44.

Baßler, J., and Hurt, E. (2019). Eukaryotic Ribosome Assembly. Annu. Rev. Biochem. *88*, 281–306.

Baßler, J., Grandi, P., Gadal, O., Leßmann, T., Petfalski, E., Tollervey, D., Lechner, J., and Hurt, E. (2001). Identification of a 60S preribosomal particle that is closely linked to nuclear export. Mol. Cell *8*, 517–529.

Baßler, J., Kallas, M., Pertschy, B., Ulbrich, C., Thoms, M., and Hurt, E. (2010). The AAA-ATPase Rea1 Drives Removal of Biogenesis Factors during Multiple Stages of 60S Ribosome Assembly. Mol. Cell *38*, 712–721.

Baßler, J., Ahmed, Y.L., Kallas, M., Kornprobst, M., Calviño, F.R., Gnädig, M., Thoms, M., Stier, G., Ismail, S., Kharde, S., et al. (2017). Interaction network of the ribosome assembly machinery from a eukaryotic thermophile. Protein Sci. *26*, 327–342.

Baudin-baillieu, A., Fabret, C., Liang, X.H., Piekna-Przybylska, D., Fournier, M.J., and Rousset, J.P. (2009). Nucleotide modifications in three functionally important regions of the Saccharomyces cerevisiae ribosome affect translation accuracy. Nucleic Acids Res. *37*, 7665–7677.

Bécam, A.M., Nasr, F., Racki, W., Zagulski, M., and Herbert, C. (2001). Ria1p (Ynl163c), a protein similar to elongation factors 2, is involved in the biogenesis of the 60S subunit of the ribosome in Saccharomyces cerevisiae. Mol. Genet. Genomics *266*, 454–462.

Beltrame, M., and Tollervey, D. (1995). Base pairing between U3 and the pre-ribosomal RNA is required for 18S rRNA synthesis. EMBO J. *14*, 4350–4356.

Ben-Shem, A., Loubresse, N.G. de, Melnikov, S., Jenner, L., Yusupova, G., and Yusupov, M. (2011). The Structure of the Eukaryotic Ribosome at 3.0 Å Resolution. Science (80-.). *334*, 1524–1529.

Bergès, T., Petfalski, E., Tollervey, D., and Hurt, E.C. (1994). Synthetic lethality with fibrillarin identifies NOP77p, a nucleolar protein required for pre-rRNA processing and modification. EMBO J. *13*, 3136–3148.

Bernstein, K.A., Granneman, S., Lee, A. V., Manickam, S., and Baserga, S.J. (2006). Comprehensive Mutational Analysis of Yeast DEXD/H Box RNA Helicases Involved in Large Ribosomal Subunit Biogenesis. Mol. Cell. Biol. *26*, 1195–1208.

Bogengruber, E., Briza, P., Doppler, E., Wimmer, H., Koller, L., Fasiolo, F., Senger, B., Hegemann, J.H., and Breitenbach, M. (2003). Functional analysis in yeast of the Brix protein superfamily involved in the biogenesis of ribosomes. FEMS Yeast Res. *3*, 35–43.

Boocock, G.R.B., Morrison, J.A., Popovic, M., Richards, N., Ellis, L., Durie, P.R., and Rommens, J.M. (2003). Mutations in SBDS are associated with Shwachman-Diamond syndrome. Nat. Genet. *33*, 97–101.

Bradatsch, B., Katahira, J., Kowalinski, E., Bange, G., Yao, W., Sekimoto, T., Baumgärtel, V., Boese, G., Bassler, J., Wild, K., et al. (2007). Arx1 Functions as an Unorthodox Nuclear Export Receptor for the 60S Preribosomal Subunit. Mol. Cell *27*, 767–779.

Bradatsch, B., Leidig, C., Granneman, S., Gnädig, M., Tollervey, D., Böttcher, B., Beckmann, R., and Hurt, E. (2012). Structure of the pre-60S ribosomal subunit with nuclear export factor Arx1 bound at the exit tunnel. Nat. Struct. Mol. Biol. 2012 1912 *19*, 1234–1241.

Brüning, L., Hackert, P., Martin, R., Sloan, K.E., and Markus, T. (2018). RNA helicases mediate structural transitions and compositional changes in pre-ribosomal complexes. Nat. Commun. *9*, 5383.

Chagnon, P., Michaud, J., Mitchell, G., Mercier, J., Marion, J.F., Drouin, E., Rasquin-Weber, A., Hudson, T.J., and Richter, A. (2002). A missense mutation (R565W) in Cirhin (FLJ14728) in North American Indian childhood cirrhosis. Am. J. Hum. Genet. *71*, 1443–1449.

Chaker-Margot, M., Hunziker, M., Barandun, J., Dill, B.D., and Klinge, S. (2015). Stage-specific assembly events of the 6-MDa small-subunit processome initiate eukaryotic ribosome biogenesis. Nat. Struct. Mol. Biol. 2015 2211 *22*, 920–923.

Chaker-Margot, M., Barandun, J., Hunziker, M., and Klinge, S. (2017). Architecture of the yeast small subunit processome. Science (80-.). *355*.

Chanfreau, G., Rotondo, G., Legrain, P., and Jacquier, A. (1998). Processing of a dicistronic small nucleolar RNA precursor by the RNA endonuclease Rnt1. EMBO J. *17*, 3726–3737.

Cheng, J., Baßler, J., Fischer, P., Lau, B., Kellner, N., Kunze, R., Griesel, S., Kallas, M., Berninghausen, O., Strauss, D., et al. (2019). Thermophile 90S Pre-ribosome Structures Reveal the Reverse Order of Co-transcriptional 18S rRNA Subdomain Integration. Mol. Cell *75*, 1256-1269.e7.

Cheng, J., Lau, B., La Venuta, G., Ameismeier, M., Berninghausen, O., Hurt, E., and Beckmann, R. (2020). 90S pre-ribosome transformation into the primordial 40S subunit. Science (80-.). *369*, 1470–1476.

Choesmel, V., Bacqueville, D., Rouquette, J., Noaillac-Depeyre, J., Fribourg, S., Crétien, A., Leblanc, T., Tchernia, G., Da Costa, L., and Gleizes, P.E. (2007). Impaired ribosome biogenesis in Diamond-Blackfan anemia. Blood *109*, 1275–1283.

Chu, S., Archer, R.H., Zengel, J.M., and Lindahl, L. (1994). The RNA of RNase MRP is required for normal processing of ribosomal RNA. Proc. Natl. Acad. Sci. U. S. A. *91*, 659–663.

Costanzo, M., VanderSluis, B., Koch, E.N., Baryshnikova, A., Pons, C., Tan, G., Wang, W., Usaj, M., Hanchard, J., Lee, S.D., et al. (2016). A global genetic interaction network maps a wiring diagram of cellular function. Science (80-.). *353*.

Cox, J., and Mann, M. (2008). MaxQuant enables high peptide identification rates, individualized p.p.b.-range mass accuracies and proteome-wide protein quantification. Nat. Biotechnol. 2008 2612 *26*, 1367–1372.

Danecek, P., Bonfield, J.K., Liddle, J., Marshall, J., Ohan, V., Pollard, M.O., Whitwham, A., Keane, T., McCarthy, S.A., Davies, R.M., et al. (2021). Twelve years of SAMtools and BCFtools. Gigascience *10*, 1–4.

Daugeron, M.C., and Linder, P. (1998). Dbp7p, a putative ATP-dependent RNA helicase from Saccharomyces cerevisiae, is required for 60S ribosomal subunit assembly. Rna *4*, 566–581.

Decatur, W.A., and Fournier, M.J. (2002). rRNA modifications and ribosome function. Trends Biochem. Sci. *27*, 344–351.

Demoinet, E., Jacquier, A., Lutfalla, G., and Fromont-Racine, M. (2007). The Hsp40 chaperone Jjj1 is required for the nucleo-cytoplasmic recycling of preribosomal factors in Saccharomyces cerevisiae. RNA *13*, 1570–1581.

Devos, D., Dokudovskaya, S., Alber, F., Williams, R., Chait, B.T., Sali, A., and Rout, M.P. (2004). Components of coated vesicles and nuclear pore complexes share a common molecular architecture. PLoS Biol. *2*, e380.

Dez, C., Froment, C., Noaillac-Depeyre, J., Monsarrat, B., Caizergues-Ferrer, M., and Henry, Y. (2004). Npa1p, a component of very early pre-60S ribosomal particles, associates with a subset of small nucleolar RNPs required for peptidyl transferase center modification. Mol. Cell. Biol. *24*, 6324–6337.

Dichtl, B., and Tollervey, D. (1997). Pop3p is essential for the activity of the RNase MRP and RNase P ribonucleoproteins in vivo. EMBO J. *16*, 417–429.

Dong, X.Y., Rodriguez, C., Guo, P., Sun, X., Talbot, J.T., Zhou, W., Petros, J., Li, Q.,

Vessella, R.L., Kibel, A.S., et al. (2008). SnoRNA U50 is a candidate tumor-suppressor gene at 6q14.3 with a mutation associated with clinically significant prostate cancer. Hum. Mol. Genet. *17*, 1031–1042.

Dong, X.Y., Guo, P., Boyd, J., Sun, X., Li, Q., Zhou, W., and Dong, J.T. (2009). Implication of snoRNA U50 in human breast cancer. J. Genet. Genomics *36*, 447–454.

Dragon, F., Gallagher, J.E.G., Compagnone-Post, P.A., Mitchell, B.M., Porwancher, K.A., Wehner, K.A., Wormsley, S., Settlage, R.E., Shabanowitz, J., Osheim, Y., et al. (2002). A large nucleolar U3 ribonucleoprotein required for 18S ribosomal RNA biogenesis. Nat. 2002 4176892 *417*, 967–970.

Draptchinskaia, N., Gustavsson, P., Andersson, B., Pettersson, M., Willig, T.N., Dianzani, I., Ball, S., Tchernia, G., Klar, J., Matsson, H., et al. (1999). The gene encoding ribosomal protein S19 is mutated in Diamond-Blackfan anaemia. Nat. Genet. *21*, 169–175.

Ebert, B.L., Pretz, J., Bosco, J., Chang, C.Y., Tamayo, P., Galili, N., Raza, A., Root, D.E., Attar, E., Ellis, S.R., et al. (2008). Identification of RPS14 as a 5q- syndrome gene by RNA interference screen. Nature *451*, 335–339.

Ero, R., Peil, L., Liiv, A., and Remme, J. (2008). Identification of pseudouridine methyltransferase in Escherichia coli. Rna *14*, 2223–2233.

Farley, K.I., and Baserga, S.J. (2016). Probing the mechanisms underlying human diseases in making ribosomes. Biochem. Soc. Trans. *44*, 1035–1044.

Farrar, J.E., Nater, M., Caywood, E., Mcdevitt, M.A., Kowalski, J., Takemoto, C.M., Talbot, C.C., Meltzer, P., Esposito, D., Beggs, A.H., et al. (2008). Abnormalities of the large ribosomal subunit protein, rpl35a, in diamond-blaekfan anemia. Blood *112*, 1582–1592.

Fatica, A., Cronshaw, A.D., Dlaki, M., and Tollervey, D. (2002). Ssf1p prevents premature processing of an early pre-60S ribosomal particle. Mol. Cell *9*, 341–351.

Finch, A.J., Hilcenko, C., Basse, N., Drynan, L.F., Goyenechea, B., Menne, T.F., Fernández, Á.G., Simpson, P., D'Santos, C.S., Arends, M.J., et al. (2011). Uncoupling of GTP hydrolysis from eIF6 release on the ribosome causes shwachman-diamond syndrome. Genes Dev. *25*, 917–929.

Fournier, D., Palidwor, G.A., Shcherbinin, S., Szengel, A., Schaefer, M.H., Perez-Iratxeta, C., and Andrade-Navarro, M.A. (2013). Functional and genomic analyses of alpha-solenoid proteins. PLoS One *8*, e79894.

Gadal, O., Strauß, D., Kessl, J., Trumpower, B., Tollervey, D., and Hurt, E. (2001). Nuclear Export of 60S Ribosomal Subunits Depends on Xpo1p and Requires a Nuclear Export Sequence-Containing Factor, Nmd3p, That Associates with the Large Subunit Protein Rpl10p. Mol. Cell. Biol. *21*, 3405–3415.

Gallagher, J.E.G., Dunbar, D.A., Granneman, S., Mitchell, B.M., Osheim, Y., Beyer, A.L., and Baserga, S.J. (2004). RNA polymerase I transcription and pre-rRNA processing are linked by specific SSU processome components. Genes Dev. *18*, 2506–2517.

Gamalinda, M., Ohmayer, U., Jakovljevic, J., Kumcuoglu, B., Woolford, J., Mbom, B., Lin, L., and Woolford, J.L. (2014). A hierarchical model for assembly of eukaryotic 60S ribosomal subunit domains. Genes Dev. *28*, 198–210.

Ganot, P., Bortolin, M.L., and Kiss, T. (1997). Site-specific pseudouridine formation in preribosomal RNA is guided by small nucleolar RNAs. Cell *89*, 799–809.

Gasse, L., Flemming, D., and Hurt, E. (2015). Coordinated Ribosomal ITS2 RNA Processing by the Las1 Complex Integrating Endonuclease, Polynucleotide Kinase, and Exonuclease Activities. Mol. Cell *60*, 808–815.

Gazda, H.T., Preti, M., Sheen, M.R., O'Donohue, M.F., Vlachos, A., Davies, S.M., Kattamis, A., Doherty, L., Landowski, M., Buros, C., et al. (2012). Frameshift mutation in p53 regulator RPL26 is associated with multiple physical abnormalities and a specific pre-ribosomal RNA processing defect in diamond-blackfan anemia. Hum. Mutat. *33*, 1037–1044.

Ghalei, H., Schaub, F.X., Doherty, J.R., Noguchi, Y., Roush, W.R., Cleveland, J.L., Elizabeth Stroupe, M., and Karbstein, K. (2015). Hrr25/CK1δ-directed release of Ltv1 from pre-40S ribosomes is necessary for ribosome assembly and cell growth. J. Cell Biol. *208*, 745–759.

Giaever, G., Chu, A.M., Ni, L., Connelly, C., Riles, L., Véronneau, S., Dow, S., Lucau-Danila, A., Anderson, K., André, B., et al. (2002). Functional profiling of the Saccharomyces cerevisiae genome. Nature *418*, 387–391.

Gietz, R.D., and Akio, S. (1988). New yeast-Escherichia coli shuttle vectors constructed with in vitro mutagenized yeast genes lacking six-base pair restriction sites. Gene *74*, 527–534.

Goddard, T.D., Huang, C.C., Meng, E.C., Pettersen, E.F., Couch, G.S., Morris, J.H., and Ferrin, T.E. (2018). UCSF ChimeraX: Meeting modern challenges in visualization and analysis. Protein Sci. *27*, 14–25.

Grandi, P., Rybin, V., Baßler, J., Petfalski, E., Strauß, D., Marzioch, M., Schäfer, T., Kuster, B., Tschochner, H., Tollervey, D., et al. (2002). 90S pre-ribosomes include the 35S pre-rRNA, the U3 snoRNP, and 40S subunit processing factors but predominantly lack 60S synthesis factors. Mol. Cell *10*, 105–115.

Greber, B.J. (2016). Mechanistic insight into eukaryotic 60S ribosomal subunit biogenesis by cryo-electron microscopy. RNA *22*, 1643–1662.

Harnpicharnchai, P., Jakovljevic, J., Horsey, E., Miles, T., Roman, J., Rout, M., Meagher, D., Imai, B., Guo, Y., Brame, C.J., et al. (2001). Composition and functional characterization of yeast 66S ribosome assembly intermediates. Mol. Cell *8*, 505–515.

Hedges, J., West, M., and Johnson, A.W. (2005). Release of the export adapter, Nmd3p, from the 60S ribosomal subunit requires Rpl10p and the cytoplasmic GTPase Lsg1p. EMBO J. *24*, 567–579.

Heiss, N.S., Knight, S.W., Vulliamy, T.J., Klauck, S.M., Wiemann, S., Mason, P.J., Poustka, A., and Dokal, I. (1998). X-linked dyskeratosis congenita is caused by mutations in a highly conserved gene with putative nucleolar functions. Nat. Genet. *19*, 32–38.

Held, W.A., Mizushima, S., and Nomura, M. (1973). Reconstitution of Escherichia coli 30 S Ribosomal Subunits from Purified Molecular Components. J. Biol. Chem. *248*, 5720–5730.

Helm, M. (2006). Post-transcriptional nucleotide modification and alternative folding of RNA. Nucleic Acids Res. *34*, 721–733.

Henras, A.K., Soudet, J., Gérus, M., Lebaron, S., Caizergues-Ferrer, M., Mougin, A., and Henry, Y. (2008). The post-transcriptional steps of eukaryotic ribosome biogenesis. Cell. Mol. Life Sci. *65*, 2334–2359.

Henras, A.K., Plisson-Chastang, C., O'Donohue, M.F., Chakraborty, A., and Gleizes, P.E. (2015). An overview of pre-ribosomal RNA processing in eukaryotes. Wiley Interdiscip. Rev. RNA *6*, 225–242.

Henry, Y., Wood, H., Morrissey, J.P., Petfalski, E., Kearsey, S., and Tollervey, D. (1994). The 5' end of yeast 5.8S rRNA is generated by exonucleases from an upstream cleavage site. EMBO J. *13*, 2452–2463.

Hernandez-Verdun, D., Roussel, P., Thiry, M., Sirri, V., and Lafontaine, D.L.J. (2010). The nucleolus: Structure/function relationship in RNA metabolism. Wiley Interdiscip. Rev. RNA *1*, 415–431.

Hierlmeier, T., Merl, J., Sauert, M., Perez-Fernandez, J., Schultz, P., Bruckmann, A., Hamperl, S., Ohmayer, U., Rachel, R., Jacob, A., et al. (2013). Rrp5p, Noc1p and Noc2p form a protein module which is part of early large ribosomal subunit precursors in S. cerevisiae. Nucleic Acids Res. *41*, 1191–1210.

Higa-Nakamine, S., Suzuki, T., Uechi, T., Chakraborty, A., Nakajima, Y., Nakamura, M., Hirano, N., Suzuki, T., and Kenmochi, N. (2012). Loss of ribosomal RNA modification causes developmental defects in zebrafish. Nucleic Acids Res. *40*, 391–398.

Ho, J.H.N., Kallstrom, G., and Johnson, A.W. (2000). Nmd3p is a Crm1p-dependent adapter protein for nuclear export of the large ribosomal subunit. J. Cell Biol. *151*, 1057–1066.

Horos, R., IJspeert, H., Pospisilova, D., Sendtner, R., Andrieu-Soler, C., Taskesen, E., Nieradka, A., Cmejla, R., Sendtner, M., Touw, I.P., et al. (2012). Ribosomal deficiencies in Diamond-Blackfan anemia impair translation of transcripts essential for differentiation of murine and human erythroblasts. Blood *119*, 262–272.

Hughes, J.M.X. (1996). Functional base-pairing interaction between highly conserved elements of U3 small nucleolar RNA and the small ribosomal subunit RNA. J. Mol. Biol. *259*, 645–654.

Hughes, J.M.X., and Ares, M. (1991). Depletion of U3 small nucleolar RNA inhibits cleavage in the 5' external transcribed spacer of yeast pre-ribosomal RNA and impairs formation of 18S ribosomal RNA. EMBO J. *10*, 4231–4239.

Hung, N.-J., and Johnson, A.W. (2006). Nuclear Recycling of the Pre-60S Ribosomal Subunit-Associated Factor Arx1 Depends on Rei1 in Saccharomyces cerevisiae. Mol. Cell. Biol. *26*, 3718–3727.

Janke, C., Magiera, M.M., Rathfelder, N., Taxis, C., Reber, S., Maekawa, H., Moreno-Borchart, A., Doenges, G., Schwob, E., Schiebel, E., et al. (2004). A versatile toolbox for PCR-based tagging of yeast genes: New fluorescent proteins, more markers and promoter substitution cassettes. Yeast *21*, 947–962.

Jenner, L., Melnikov, S., de Loubresse, N.G., Ben-Shem, A., Iskakova, M., Urzhumtsev, A., Meskauskas, A., Dinman, J., Yusupova, G., and Yusupov, M. (2012). Crystal structure of the 80S yeast ribosome. Curr. Opin. Struct. Biol. *22*, 759–767.

Joret, C., Capeyrou, R., Belhabich-Baumas, K., Plisson-Chastang, C., Ghandour, R., Humbert, O., Fribourg, S., Leulliot, N., Lebaron, S., Henras, A.K., et al. (2018). The npa1p complex chaperones the assembly of the earliest eukaryotic large ribosomal subunit precursor. PLoS Genet. *14*, e1007597.

Jumper, J., Evans, R., Pritzel, A., Green, T., Figurnov, M., Ronneberger, O., Tunyasuvunakool, K., Bates, R., Žídek, A., Potapenko, A., et al. (2021). Highly accurate protein structure prediction with AlphaFold. Nature *596*, 583–589.

Kakihara, Y., and Houry, W.A. (2012). The R2TP complex: Discovery and functions. Biochim. Biophys. Acta - Mol. Cell Res. *1823*, 101–107.

Kampen, K.R., Sulima, S.O., Vereecke, S., and De Keersmaecker, K. (2020). Hallmarks of ribosomopathies. Nucleic Acids Res. *48*, 1013–1028.

Kappel, L., Loibl, M., Zisser, G., Klein, I., Fruhmann, G., Gruber, C., Unterweger, S., Rechberger, G., Pertschy, B., and Bergler, H. (2012). Rlp24 activates the AAA-ATPase Drg1 to initiate cytoplasmic pre-60S maturation. J. Cell Biol. *199*, 771–782.

Karbstein, K. (2013). Quality control mechanisms during ribosome maturation. Trends Cell Biol. *23*, 242–250.

Kaser, A., Bogengruber, E., Hallegger, M., Doppler, E., Lepperdinger, G., Jantsch, M., Breitenbach, M., and Kreil, G. (2001). Brix from Xenopus laevis and Brx1p from yeast define a new family of proteins involved in the biogenesis of large ribosomal subunits. Biol. Chem. *382*, 1637–1647.

Kater, L., Thoms, M., Barrio-Garcia, C., Cheng, J., Ismail, S., Ahmed, Y.L., Bange, G., Kressler, D., Berninghausen, O., Sinning, I., et al. (2017). Visualizing the Assembly Pathway of Nucleolar Pre-60S Ribosomes. Cell *171*, 1599-1610.e13.

De Keersmaecker, K., Sulima, S.O., and Dinman, J.D. (2015). Ribosomopathies and the paradox of cellular hypo- to hyperproliferation. Blood *125*, 1377–1382.

Kemmler, S., Occhipinti, L., Veisu, M., and Panse, V.G. (2009). Yvh1 is required for a late maturation step in the 60S biogenesis pathway. J. Cell Biol. *186*, 863–880.

Kharde, S., Calviño, F.R., Gumiero, A., Wild, K., and Sinning, I. (2015). The structure of Rpf2-Rrs1 explains its role in ribosome biogenesis. Nucleic Acids Res. *43*, 7083–7095.

Khatter, H., Myasnikov, A.G., Natchiar, S.K., and Klaholz, B.P. (2015). Structure of the human 80S ribosome. Nature *520*, 640–645.

Khoshnevis, S., Liu, X., Dattolo, M.D., and Karbstein, K. (2019). Rrp5 establishes a checkpoint for 60S assembly during 40S maturation. Rna *25*, 1164–1176.

Kim, D., Paggi, J.M., Park, C., Bennett, C., and Salzberg, S.L. (2019). Graph-based

genome alignment and genotyping with HISAT2 and HISAT-genotype. Nat. Biotechnol. *37*, 907–915.

King, T.H., Liu, B., McCully, R.R., and Fournier, M.J. (2003). Ribosome structure and activity are altered in cells lacking snoRNPs that form pseudouridines in the peptidyl transferase center. Mol. Cell *11*, 425–435.

Kiss-László, Z., Henry, Y., Bachellerie, J.P., Caizergues-Ferrer, M., and Kiss, T. (1996). Site-specific ribose methylation of preribosomal RNA: A novel function for small nucleolar RNAs. Cell *85*, 1077–1088.

Klinge, S., and Woolford, J.L. (2019). Ribosome assembly coming into focus. Nat. Rev. Mol. Cell Biol. *20*, 116–131.

Klinge, S., Voigts-Hoffmann, F., Leibundgut, M., Arpagaus, S., and Ban, N. (2011). Crystal Structure of the Eukaryotic 60S Ribosomal Subunit in Complex with Initiation Factor 6. Science (80-.). *334*, 941–948.

Konikkat, S., and Woolford, J.L. (2017). Principles of 60S ribosomal subunit assembly emerging from recent studies in yeast. Biochem. J. *474*, 195–214.

Kornprobst, M., Turk, M., Kellner, N., Cheng, J., Flemming, D., Koš-Braun, I., Koš, M., Thoms, M., Berninghausen, O., Beckmann, R., et al. (2016). Architecture of the 90S Pre-ribosome: A Structural View on the Birth of the Eukaryotic Ribosome. Cell *166*, 380–393.

Kos-Braun, I.C., Jung, I., and Koš, M. (2017). Tor1 and CK2 kinases control a switch between alternative ribosome biogenesis pathways in a growth-dependent manner. PLoS Biol. *15*, e2000245.

Koš, M., and Tollervey, D. (2010). Yeast Pre-rRNA Processing and Modification Occur Cotranscriptionally. Mol. Cell *37*, 809–820.

Kressler, D., Hurt, E., and Baßler, J. (2010). Driving ribosome assembly. Biochim. Biophys. Acta - Mol. Cell Res. *1803*, 673–683.

Krogan, N.J., Peng, W.T., Cagney, G., Robinson, M.D., Haw, R., Zhong, G., Guo, X., Zhang, X., Canadien, V., Richards, D.P., et al. (2004). High-Definition Macromolecular Composition of Yeast RNA-Processing Complexes. Mol. Cell *13*, 225–239.

Kumar, A., and Warner, J.R. (1972). Characterization of ribosomal precursor particles from HeLa cell nucleoli. J. Mol. Biol. *63*, 233–246.

De La Cruz, J., Lacombe, T., Deloche, O., Linder, P., and Kressler, D. (2004). The

Putative RNA Helicase Dbp6p Functionally Interacts with Rp13p, Nop8p and the Novel trans-acting Factor Rsa3p during Biogenesis of 60S Ribosomal Subunits in Saccharomyces cerevisiae. Genetics *166*, 1687–1699.

Lamanna, A.C., and Karbstein, K. (2009). Nob1 binds the single-stranded cleavage site D at the 3′-end of 18S rRNA with its PIN domain. Proc. Natl. Acad. Sci. *106*, 14259–14264.

Lapeyre, B., and Purushothaman, S.K. (2004). Spb1p-Directed Formation of Gm2922 in the Ribosome Catalytic Center Occurs at a Late Processing Stage. Mol. Cell *16*, 663–669.

Lau, B., Cheng, J., Flemming, D., La Venuta, G., Berninghausen, O., Beckmann, R., and Hurt, E. (2021). Structure of the Maturing 90S Pre-ribosome in Association with the RNA Exosome. Mol. Cell *81*, 293-303.e4.

Lebaron, S., Segerstolpe, Å., French, S.L., Dudnakova, T., de lima Alves, F., Granneman, S., Rappsilber, J., Beyer, A.L., Wieslander, L., and Tollervey, D. (2013). Rrp5 binding at multiple sites coordinates Pre-rRNA processing and assembly. Mol. Cell *52*, 707–719.

Lebreton, A., Saveanu, C., Decourty, L., Rain, J.C., Jacquier, A., and Fromont-Racine, M. (2006). A functional network involved in the recycling of nucleocytoplasmic pre-60S factors. J. Cell Biol. *173*, 349–360.

Léger-Silvestre, I., Trumtel, S., Noaillac-Depeyre, J., and Gas, N. (1999). Functional compartmentalization of the nucleus in the budding yeast Saccharomyces cerevisiae. Chromosoma *108*, 103–113.

Leidig, C., Thoms, M., Holdermann, I., Bradatsch, B., Berninghausen, O., Bange, G., Sinning, I., Hurt, E., and Beckmann, R. (2014). 60S ribosome biogenesis requires rotation of the 5S ribonucleoprotein particle. Nat. Commun. *5*, 1–8.

Liang, X. hai, Liu, Q., and Fournier, M.J. (2007). rRNA Modifications in an Intersubunit Bridge of the Ribosome Strongly Affect Both Ribosome Biogenesis and Activity. Mol. Cell *28*, 965–977.

Liang, X.H., Liu, Q., and Fournier, M.J. (2009). Loss of rRNA modifications in the decoding center of the ribosome impairs translation and strongly delays pre-rRNA processing. RNA *15*, 1716–1728.

Liao, J., Yu, L., Mei, Y., Guarnera, M., Shen, J., Li, R., Liu, Z., and Jiang, F. (2010). Small nucleolar RNA signatures as biomarkers for non-small-cell lung cancer. Mol. Cancer *9*, 1–10.

Lindahl, L., Archer, R.H., and Zengel, J.M. (1992). A new rRNA processing mutant of Saccharomyces cerevisiae. Nucleic Acids Res. *20*, 295–301.

Lo, K.Y., Li, Z., Wang, F., Marcotte, E.M., and Johnson, A.W. (2009). Ribosome stalk assembly requires the dual-specificity phosphatase Yvh1 for the exchange of Mrt4 with P0. J. Cell Biol. *186*, 849–862.

Longtine, M.S., McKenzie, A., Demarini, D.J., Shah, N.G., Wach, A., Brachat, A., Philippsen, P., and Pringle, J.R. (1998). Additional modules for versatile and economical PCR-based gene deletion and modification in Saccharomyces cerevisiae. Yeast *14*, 953–961.

Lygerou, Z., Allmang, C., Tollervey, D., and Séraphin, B. (1996). Accurate Processing of a Eukaryotic Precursor Ribosomal RNA by Ribonuclease MRP in Vitro. Science (80-.). *272*, 268–270.

Ma, C., Wu, S., Li, N., Chen, Y., Yan, K., Li, Z., Zheng, L., Lei, J., Woolford, J.L., and Gao, N. (2017). Structural snapshot of cytoplasmic pre-60S ribosomal particles bound with Nmd3, Lsg1, Tif6 and Reh1. Nat. Struct. Mol. Biol. *24*, 214–220.

Madru, C., Lebaron, S., Blaud, M., Delbos, L., Pipoli, J., Pasmant, E., Réty, S., and Leulliot, N. (2015). Chaperoning 5S RNA assembly. Genes Dev. *29*, 1432–1446.

Marcel, V., Ghayad, S.E., Belin, S., Therizols, G., Morel, A.P., Solano-Gonzàlez, E., Vendrell, J.A., Hacot, S., Mertani, H.C., Albaret, M.A., et al. (2013). P53 Acts as a Safeguard of Translational Control by Regulating Fibrillarin and rRNA Methylation in Cancer. Cancer Cell *24*, 318–330.

Martin, M. (2011). Cutadapt removes adapter sequences from high-throughput sequencing reads. EMBnet.Journal *17*, 10.

Matsuo, Y., Granneman, S., Thoms, M., Manikas, R.G., Tollervey, D., and Hurt, E. (2014). Coupled GTPase and remodelling ATPase activities form a checkpoint for ribosome export. Nature *505*, 112–116.

McCann, K.L., Charette, J.M., Vincent, N.G., and Baserga, S.J. (2015). A protein interaction map of the LSU processome. Genes Dev. *29*, 862–875.

Mélèse, T., and Xue, Z. (1995). The nucleolus: an organelle formed by the act of building a ribosome. Curr. Opin. Cell Biol. *7*, 319–324.

Melnikov, S., Ben-Shem, A., Garreau De Loubresse, N., Jenner, L., Yusupova, G., and Yusupov, M. (2012). One core, two shells: Bacterial and eukaryotic ribosomes.

Nat. Struct. Mol. Biol. *19*, 560–567.

Menne, T.F., Goyenechea, B., Sánchez-Puig, N., Wong, C.C., Tonkin, L.M., Ancliff, P.J., Brost, R.L., Costanzo, M., Boone, C., and Warren, A.J. (2007). The Shwachman-Bodian-Diamond syndrome protein mediates translational activation of ribosomes in yeast. Nat. Genet. *39*, 486–495.

Meyer, A.E., Hung, N.J., Yang, P., Johnson, A.W., and Craig, E.A. (2007). The specialized cytosolic J-protein, Jjj1, functions in 60S ribosomal subunit biogenesis. Proc. Natl. Acad. Sci. U. S. A. *104*, 1558–1563.

Meyer, B., Wurm, J.P., Kötter, P., Leisegang, M.S., Schilling, V., Buchhaupt, M., Held, M., Bahr, U., Karas, M., Heckel, A., et al. (2011). The Bowen-Conradi syndrome protein Nep1 (Emg1) has a dual role in eukaryotic ribosome biogenesis, as an essential assembly factor and in the methylation of Ψ1191 in yeast 18S rRNA. Nucleic Acids Res. *39*, 1526–1537.

Miller, O.L., and Beatty, B.R. (1969). Visualization of Nucleolar Genes. Science (80-.). *164*, 955–957.

Mitchell, P., Petfalski, E., Shevchenko, A., Mann, M., and Tollervey, D. (1997). The exosome: A conserved eukaryotic RNA processing complex containing multiple 3'→5' exoribonucleases. Cell *91*, 457–466.

Mitterer, V., Murat, G., Réty, S., Blaud, M., Delbos, L., Stanborough, T., Bergler, H., Leulliot, N., Kressler, D., and Pertschy, B. (2016). Sequential domain assembly of ribosomal protein S3 drives 40S subunit maturation. Nat. Commun. *7*, 1–15.

Mnaimneh, S., Davierwala, A.P., Haynes, J., Moffat, J., Peng, W.T., Zhang, W., Yang, X., Pootoolal, J., Chua, G., Lopez, A., et al. (2004). Exploration of essential gene functions via titratable promoter alleles. Cell *118*, 31–44.

Mougey, E.B., O'Reilly, M., Osheim, Y., Miller, O.L., Beyer, A., and Sollner-Webb, B. (1993). The terminal balls characteristic of eukaryotic rRNA transcription units in chromatin spreads are rRNA processing complexes. Genes Dev. *7*, 1609–1619.

Narla, A., and Ebert, B.L. (2010). Ribosomopathies: Human disorders of ribosome dysfunction. Blood *115*, 3196–3205.

Nierhaus, K.H., and Dohme, F. (1974). Total Reconstitution of Functionally Active 50S Ribosomal Subunits from Escherichia coli. Proc. Natl. Acad. Sci. U. S. A. *71*, 4713.

Nissan, T.A., Baßler, J., Petfalski, E., Tollervey, D., and Hurt, E. (2002). 60S pre-ribosome formation viewed from assembly in the nucleolus until export to the

cytoplasm. EMBO J. *21*, 5539–5547.

Nousbeck, J., Spiegel, R., Ishida-Yamamoto, A., Indelman, M., Shani-Adir, A., Adir, N., Lipkin, E., Bercovici, S., Geiger, D., van Steensel, M.A., et al. (2008). Alopecia, Neurological Defects, and Endocrinopathy Syndrome Caused by Decreased Expression of RBM28, a Nucleolar Protein Associated with Ribosome Biogenesis. Am. J. Hum. Genet. *82*, 1114–1121.

Oeffinger, M., Zenklusen, D., Ferguson, A., Wei, K.E., El Hage, A., Tollervey, D., Chait, B.T., Singer, R.H., and Rout, M.P. (2009). Rrp17p Is a Eukaryotic Exonuclease Required for 5′ End Processing of Pre-60S Ribosomal RNA. Mol. Cell *36*, 768–781.

Osheim, Y.N., French, S.L., Keck, K.M., Champion, E.A., Spasov, K., Dragon, F., Baserga, S.J., and Beyer, A.L. (2004). Pre-18S ribosomal RNA is structurally compacted into the SSU processome prior to being cleaved from nascent transcripts in Saccharomyces cerevisiae. Mol. Cell *16*, 943–954.

Palade, G.E. (1955). A SMALL PARTICULATE COMPONENT OF THE CYTOPLASM. J. Biophys. Biochem. Cytol. *1*, 59–68.

Panse, V.G., and Johnson, A.W. (2010). Maturation of eukaryotic ribosomes: acquisition of functionality. Trends Biochem. Sci. *35*, 260–266.

Parks, T.D., Leuther, K.K., Howard, E.D., Johnston, S.A., and Dougherty, W.G. (1994). Release of proteins and peptides from fusion proteins using a recombinant plant virus proteinase. Anal. Biochem. *216*, 413–417.

Peña, C., Hurt, E., and Panse, V.G. (2017). Eukaryotic ribosome assembly, transport and quality control. Nat. Struct. Mol. Biol. *24*, 689–699.

Pérez-Fernández, J., Román, Á., De Las Rivas, J., Bustelo, X.R., and Dosil, M. (2007). The 90S Preribosome Is a Multimodular Structure That Is Assembled through a Hierarchical Mechanism. Mol. Cell. Biol. *27*, 5414–5429.

Pertschy, B., Saveanu, C., Zisser, G., Lebreton, A., Tengg, M., Jacquier, A., Liebminger, E., Nobis, B., Kappel, L., van der Klei, I., et al. (2007). Cytoplasmic Recycling of 60S Preribosomal Factors Depends on the AAA Protein Drg1. Mol. Cell. Biol. *27*, 6581–6592.

Pertschy, B., Schneider, C., Gnädig, M., Schäfer, T., Tollervey, D., and Hurt, E. (2009). RNA helicase Prp43 and its co-factor Pfa1 promote 20 to 18 S rRNA processing catalyzed by the endonuclease Nob1. J. Biol. Chem. *284*, 35079–35091.

Pettersen, E.F., Goddard, T.D., Huang, C.C., Couch, G.S., Greenblatt, D.M., Meng,

E.C., and Ferrin, T.E. (2004). UCSF Chimera - A visualization system for exploratory research and analysis. J. Comput. Chem. *25*, 1605–1612.

Piekna-Przybylska, D., Decatur, W.A., and Fournier, M.J. (2007). New bioinformatic tools for analysis of nucleotide modifications in eukaryotic rRNA. RNA *13*, 305–312.

Pöll, G., Li, S., Ohmayer, U., Hierlmeier, T., Milkereit, P., and Perez-Fernandez, J. (2014). In Vitro Reconstitution of Yeast tUTP/UTP A and UTP B Subcomplexes Provides New Insights into Their Modular Architecture. PLoS One *9*, e114898.

Pratte, D., Singh, U., Murat, G., and Kressler, D. (2013). Mak5 and Ebp2 act together on early pre-60S particles and their reduced functionality bypasses the requirement for the essential pre-60S factor Nsa1. PLoS One *8*, 1–23.

Punjani, A., Rubinstein, J.L., Fleet, D.J., and Brubaker, M.A. (2017). CryoSPARC: Algorithms for rapid unsupervised cryo-EM structure determination. Nat. Methods *14*, 290–296.

Purta, E., Kaminska, K.H., Kasprzak, J.M., Bujnicki, J.M., and Douthwaite, S. (2008). YbeA is the m3ψ methyltransferase RlmH that targets nucleotide 1915 in 23S rRNA. Rna *14*, 2234–2244.

Rabl, J., Leibundgut, M., Ataide, S.F., Haag, A., and Ban, N. (2011). Crystal Structure of the Eukaryotic 40S Ribosomal Subunit in Complex with Initiation Factor 1. Science (80-.). *331*, 730–736.

Reichow, S.L., Hamma, T., Ferré-D'Amaré, A.R., and Varani, G. (2007). The structure and function of small nucleolar ribonucleoproteins. Nucleic Acids Res. *35*, 1452–1464.

Ridanpää, M., Van Eenennaam, H., Pelin, K., Chadwick, R., Johnson, C., Yuan, B., VanVenrooij, W., Pruijn, G., Salmela, R., Rockas, S., et al. (2001). Mutations in the RNA component of RNase MRP cause a pleiotropic human disease, cartilage-hair hypoplasia. Cell *104*, 195–203.

Robinson, J.T., Thorvaldsdóttir, H., Winckler, W., Guttman, M., Lander, E.S., Getz, G., and Mesirov, J.P. (2011). Integrative genomics viewer. Nat. Biotechnol. *29*, 24–26.

Rosado, I. V, and De La Cruz, J. (2004). Npa1p is an essential trans-acting factor required for an early step in the assembly of 60S ribosomal subunits in Saccharomyces cerevisiae. RNA *10*, 1073–1083.

Rosado, I. V, Dez, C., Lebaron, S., Caizergues-Ferrer, M., Henry, Y., and de la Cruz, J. (2007). Characterization of Saccharomyces cerevisiae Npa2p (Urb2p) reveals a low-molecular-mass complex containing Dbp6p, Npa1p (Urb1p), Nop8p, and Rsa3p

involved in early steps of 60S ribosomal subunit biogenesis. Mol. Cell. Biol. *27*, 1207–1221.

Rout, M.P., and Blobel, G. (1993). Isolation of the yeast nuclear pore complex. J. Cell Biol. *123*, 771–783.

Sahoo, T., Del Gaudio, D., German, J.R., Shinawi, M., Peters, S.U., Person, R.E., Garnica, A., Cheung, S.W., and Beaudet, A.L. (2008). Prader-Willi phenotype caused by paternal deficiency for the HBII-85 C/D box small nucleolar RNA cluster. Nat. Genet. *40*, 719–721.

Sanghai, Z.A., Miller, L., Molloy, K.R., Barandun, J., Hunziker, M., Chaker-Margot, M., Wang, J., Chait, B.T., and Klinge, S. (2018). Modular assembly of the nucleolar pre-60S ribosomal subunit. Nature *556*, 126–129.

Sarkar, A., Pech, M., Thoms, M., Beckmann, R., and Hurt, E. (2016). Ribosome-stalk biogenesis is coupled with recruitment of nuclear-export factor to the nascent 60S subunit. Nat. Struct. Mol. Biol. *23*, 1074–1082.

Saveanu, C., Bienvenu, D., Namane, A., Gleizes, P.E., Gas, N., Jacquier, A., and Fromont-Racine, M. (2001). Nog2p, a putative GTPase associated with pre-60S subunits and required for late 60S maturation steps. EMBO J. *20*, 6475–6484.

Schäfer, T., Strauß, D., Petfalski, E., Tollervey, D., and Hurt, E. (2003). The path from nucleolar 90S to cytoplasmic 40S pre-ribosomes. EMBO J. *22*, 1370–1380.

Schäfer, T., Maco, B., Petfalski, E., Tollervey, D., Böttcher, B., Aebi, U., and Hurt, E. (2006). Hrr25-dependent phosphorylation state regulates organization of the pre-40S subunit. Nature *441*, 651–655.

Schattner, P., Decatur, W.A., Davis, C.A., Ares, M., Fournier, M.J., and Lowe, T.M. (2004). Genome-wide searching for pseudouridylation guide snoRNAs: analysis of the Saccharomyces cerevisiae genome. Nucleic Acids Res. *32*, 4281–4296.

Scherrer, K., and Darnell, J.E. (1962). Sedimentation characteristics of rapidly labelled RNA from HeLa cells. Biochem. Biophys. Res. Commun. *7*, 486–490.

Scherrer, K., Latham, H., and Darnell, J.E. (1963). DEMONSTRATION OF AN UNSTABLE RNA AND OF A PRECURSOR TO RIBOSOMAL RNA IN HELA CELLS. Proc. Natl. Acad. Sci. U. S. A. *49*, 240.

Schmitt, M.E., and Clayton, D.A. (1993). Nuclear RNase MRP is required for correct processing of pre-5.8S rRNA in Saccharomyces cerevisiae. Mol. Cell. Biol. *13*, 7935–7941.

Schosserer, M., Minois, N., Angerer, T.B., Amring, M., Dellago, H., Harreither, E., Calle-Perez, A., Pircher, A., Gerstl, M.P., Pfeifenberger, S., et al. (2015). Methylation of ribosomal RNA by NSUN5 is a conserved mechanism modulating organismal lifespan. Nat. Commun. *6*, 6158.

Schuller, J.M., Falk, S., Fromm, L., Hurt, E., and Conti, E. (2018). Structure of the nuclear exosome captured on a maturing preribosome. Science (80-.). *360*, 219–222.

Senger, B., Lafontaine, D.L.J., Graindorge, J.S., Gadal, O., Camasses, A., Sanni, A., Garnier, J.M., Breitenbach, M., Hurt, E., and Fasiolo, F. (2001). The nucle(ol)ar Tif6p and Efl1p are required for a late cytoplasmic step of ribosome synthesis. Mol. Cell *8*, 1363–1373.

Sharma, K., and Tollervey, D. (1999). Base Pairing between U3 Small Nucleolar RNA and the 5′ End of 18S rRNA Is Required for Pre-rRNA Processing. Mol. Cell. Biol. *19*, 6012–6019.

Sharma, S., and Lafontaine, D.L.J. (2015). "View From A Bridge": A New Perspective on Eukaryotic rRNA Base Modification. Trends Biochem. Sci. *40*, 560–575.

Sharma, S., Yang, J., Watzinger, P., Kötter, P., and Entian, K.-D. (2013). Yeast Nop2 and Rcm1 methylate C2870 and C2278 of the 25S rRNA, respectively. Nucleic Acids Res. *41*, 9062–9076.

Sloan, K.E., Warda, A.S., Sharma, S., Entian, K.D., Lafontaine, D.L.J., and Bohnsack, M.T. (2017). Tuning the ribosome: The influence of rRNA modification on eukaryotic ribosome biogenesis and function. RNA Biol. *14*, 1138–1152.

Strunk, B.S., Novak, M.N., Young, C.L., and Karbstein, K. (2012). A translation-like cycle is a quality control checkpoint for maturing 40S ribosome subunits. Cell *150*, 111–121.

Su, H., Xu, T., Ganapathy, S., Shadfan, M., Long, M., Huang, T.H.M., Thompson, I., and Yuan, Z.M. (2014). Elevated snoRNA biogenesis is essential in breast cancer. Oncogene *33*, 1348–1358.

Sulima, S., Kampen, K., and De Keersmaecker, K. (2019). Cancer Biogenesis in Ribosomopathies. Cells *8*, 229.

Sun, C., and Woolford, J.L. (1994). The yeast NOP4 gene product is an essential nucleolar protein required for pre-rRNA processing and accumulation of 60S ribosomal subunits. EMBO J. *13*, 3127–3135.

Sun, C., and Woolford, J.L. (1997). The yeast nucleolar protein Nop4p contains four RNA recognition motifs necessary for ribosome biogenesis. J. Biol. Chem. *272*, 25345–25352.

Sun, Q., Zhu, X., Qi, J., An, W., Lan, P., Tan, D., Chen, R., Wang, B., Zheng, S., Zhang, C., et al. (2017). Molecular architecture of the 90S small subunit pre-ribosome. Elife *6*.

Szczepińska, T., Kutner, J., Kopczyński, M., Pawłowski, K., Dziembowski, A., Kudlicki, A., Ginalski, K., and Rowicka, M. (2014). Probabilistic Approach to Predicting Substrate Specificity of Methyltransferases. PLoS Comput. Biol. *10*.

Talkish, J., Campbell, I.W., Sahasranaman, A., Jakovljevic, J., and Woolford, J.L. (2014). Ribosome assembly factors Pwp1 and Nop12 are important for folding of 5.8S rRNA during ribosome biogenesis in Saccharomyces cerevisiae. Mol. Cell. Biol. *34*, 1863–1877.

Talkish, J., Biedka, S., Jakovljevic, J., Zhang, J., Tang, L., Strahler, J.R., Andrews, P.C., Maddock, J.R., and Woolford, J.L. (2016). Disruption of ribosome assembly in yeast blocks cotranscriptional pre-rRNA processing and affects the global hierarchy of ribosome biogenesis. RNA *22*, 852–866.

Tamaoki, T. (1966). The particulate fraction containing 45 s RNA in L cell nuclei. J. Mol. Biol. *15*, 624–639.

Tan, R.Z., and Van Oudenaarden, A. (2010). Transcript counting in single cells reveals dynamics of rDNA transcription. Mol. Syst. Biol. *6*, 358.

Tanaka, R., Satoh, H., Moriyama, M., Satoh, K., Morishita, Y., Yoshida, S., Watanabe, T., Nakamura, Y., and Mori, S. (2000). Intronic U50 small-nucleolar-RNA (snoRNA) host gene of no protein-coding potential is mapped at the chromosome breakpoint t(3;6)(q27;q15) of human B- cell lymphoma. Genes to Cells *5*, 277–287.

Taoka, M., Nobe, Y., Yamaki, Y., Yamauchi, Y., Ishikawa, H., Takahashi, N., Nakayama, H., and Isobe, T. (2016). The complete chemical structure of Saccharomyces cerevisiae rRNA: Partial pseudouridylation of U2345 in 25S rRNA by snoRNA snR9. Nucleic Acids Res. *44*, 8951–8961.

Thiry, M., and Lafontaine, D.L.J. (2005). Birth of a nucleolus: The evolution of nucleolar compartments. Trends Cell Biol. *15*, 194–199.

Thiry, M., Cheutin, T., O'Donohue, M.F., Kaplan, H., and Ploton, D. (2000). Dynamics and three-dimensional localization of ribosomal RNA within the nucleolus. RNA *6*, 1750–1761.

Thomas, B.J., and Rothstein, R. (1989). Elevated recombination rates in transcriptionally active DNA. Cell *56*, 619–630.

Thoms, M., Thomson, E., Baßler, J., Gnädig, M., Griesel, S., and Hurt, E. (2015). The Exosome Is Recruited to RNA Substrates through Specific Adaptor Proteins. Cell *162*, 1029–1038.

Thoms, M., Mitterer, V., Kater, L., Falquet, L., Beckmann, R., Kressler, D., and Hurt, E. (2018). Suppressor mutations in Rpf2–Rrs1 or Rpl5 bypass the Cgr1 function for pre-ribosomal 5S RNP-rotation. Nat. Commun. *9*, 1–13.

Thomson, E., and Tollervey, D. (2010). The Final Step in 5.8S rRNA Processing Is Cytoplasmic in Saccharomyces cerevisiae. Mol. Cell. Biol. *30*, 976–984.

Tkaczuk, K.L., Dunin-Horkawicz, S., Purta, E., and Bujnicki, J.M. (2007). Structural and evolutionary bioinformatics of the SPOUT superfamily of methyltransferases. BMC Bioinformatics *8*.

Tollervey, D., Lehtonen, H., Jansen, R., Kern, H., and Hurt, E.C. (1993). Temperature-sensitive mutations demonstrate roles for yeast fibrillarin in pre-rRNA processing, pre-rRNA methylation, and ribosome assembly. Cell *72*, 443–457.

Toussaint, M., Levasseur, G., Tremblay, M., Paquette, M., and Conconi, A. (2011). Psoralen photocrosslinking, a tool to study the chromatin structure of RNA polymerase I - transcribed ribosomal genes. Https://Doi.Org/10.1139/O05-141 *83*, 449–459.

Trainor, P.A., Dixon, J., and Dixon, M.J. (2009). Treacher Collins syndrome: Etiology, pathogenesis and prevention. Eur. J. Hum. Genet. *17*, 275–283.

Trapman, J., Retèl, J., and Planta, R.J. (1975). Ribosomal precursor particles from yeast. Exp. Cell Res. *90*, 95–104.

Traub, P., and Nomura, M. (1968). Structure and function of E. coli ribosomes. V. Reconstitution of functionally active 30S ribosomal particles from RNA and proteins. Proc. Natl. Acad. Sci. U. S. A. *59*, 777.

Trendel, J., Schwarzl, T., Horos, R., Prakash, A., Bateman, A., Hentze, M.W., and Krijgsveld, J. (2019). The Human RNA-Binding Proteome and Its Dynamics during Translational Arrest. Cell *176*, 391-403.e19.

Tschochner, H., and Hurt, E. (2003). Pre-ribosomes on the road from the nucleolus to the cytoplasm. Trends Cell Biol. *13*, 255–263.

Udem, S.A., and Warner, J.R. (1972). Ribosomal RNA synthesis in Saccharomyces cerevisiae. J. Mol. Biol. *65*, 227–242.

Ulbrich, C., Diepholz, M., Baßler, J., Kressler, D., Pertschy, B., Galani, K., Böttcher, B., and Hurt, E. (2009). Mechanochemical Removal of Ribosome Biogenesis Factors from Nascent 60S Ribosomal Subunits. Cell *138*, 911–922.

Velculescu, V.E., Zhang, L., Zhou, W., Vogelstein, J., Basrai, M.A., Bassett, D.E., Hieter, P., Vogelstein, B., and Kinzler, K.W. (1997). Characterization of the Yeast Transcriptome. Cell *88*, 243–251.

Venema, J., and Tollervey, D. (1996). RRP5 is required for formation of both 18S and 5.8S rRNA in yeast. EMBO J. *15*, 5701–5714.

Wagner, T., Merino, F., Stabrin, M., Moriya, T., Antoni, C., Apelbaum, A., Hagel, P., Sitsel, O., Raisch, T., Prumbaum, D., et al. (2019). SPHIRE-crYOLO is a fast and accurate fully automated particle picker for cryo-EM. Commun. Biol. *2*, 1–13.

Warner, J.R. (1990). The nucleolus and ribosome formation. Curr. Opin. Cell Biol. *2*, 521–527.

Warner, J.R. (1999). The economics of ribosome biosynthesis in yeast. Trends Biochem. Sci. *24*, 437–440.

Warner, J.R., and Soeiro, R. (1967). Nascent ribosomes from HeLa cells. Proc. Natl. Acad. Sci. U. S. A. *58*, 1984.

Warner, J.R., Knopf, P.M., and Rich, A. (1963). A MULTIPLE RIBOSOMAL STRUCTURE IN PROTEIN SYNTHESIS. Proc. Natl. Acad. Sci. U. S. A. *49*, 122.

Watkins, N.J., and Bohnsack, M.T. (2012). The box C/D and H/ACA snoRNPs: Key players in the modification, processing and the dynamic folding of ribosomal RNA. Wiley Interdiscip. Rev. RNA *3*, 397–414.

West, M., Hedges, J.B., Chen, A., and Johnson, A.W. (2005). Defining the Order in Which Nmd3p and Rpl10p Load onto Nascent 60S Ribosomal Subunits. Mol. Cell. Biol. *25*, 3802–3813.

Woloszynek, J.R., Rothbaum, R.J., Rawls, A.S., Minx, P.J., Wilson, R.K., Mason, P.J., Bessler, M., and Link, D.C. (2004). Mutations of the SBDS gene are present in most patients with Shwachman-Diamond syndrome. Blood *104*, 3588–3590.

Woolford, J.L., and Baserga, S.J. (2013). Ribosome biogenesis in the yeast Saccharomyces cerevisiae. Genetics *195*, 643–681.

Wu, S., Tutuncuoglu, B., Yan, K., Brown, H., Zhang, Y., Tan, D., Gamalinda, M., Yuan, Y., Li, Z., Jakovljevic, J., et al. (2016). Diverse roles of assembly factors revealed by structures of late nuclear pre-60S ribosomes. Nat. 2016 5347605 *534*, 133–137.

Yang, J., Sharma, S., Watzinger, P., Hartmann, J.D., Kötter, P., and Entian, K.D. (2016). Mapping of complete set of ribose and base modifications of yeast rRNA by RP-HPLC and mung bean nuclease assay. PLoS One *11*, 1–18.

Yao, W., Roser, D., Köhler, A., Bradatsch, B., Baßler, J., and Hurt, E. (2007). Nuclear Export of Ribosomal 60S Subunits by the General mRNA Export Receptor Mex67-Mtr2. Mol. Cell *26*, 51–62.

Yelick, P.C., and Trainor, P.A. (2015). Ribosomopathies: Global process, tissue specific defects. Rare Dis. *3*, e1025185.

Yusupov, M.M., Yusupova, G.Z., Baucom, A., Lieberman, K., Earnest, T.N., Cate, J.H.D., and Noller, H.F. (2001). Crystal Structure of the Ribosome at 5.5 Å Resolution. Science (80-.). *292*, 883–896.

Yusupova, G., and Yusupov, M. (2014). High-Resolution Structure of the Eukaryotic 80S Ribosome.

Zagorski, J., Tollervey, D., and Fournier, M.J. (1988). Characterization of an SNR gene locus in Saccharomyces cerevisiae that specifies both dispensible and essential small nuclear RNAs. Mol. Cell. Biol. *8*, 3282–3290.

Zhang, K. (2016). Gctf: Real-time CTF determination and correction. J. Struct. Biol. *193*, 1–12.

Zhang, J., Harnpicharnchai, P., Jakovljevic, J., Tang, L., Guo, Y., Oeffinger, M., Rout, M.P., Hiley, S.L., Hughes, T., and Woolford, J.L. (2007). Assembly factors Rpf2 and Rrs1 recruit 5S rRNA and ribosomal proteins rpL5 and rpL11 into nascent ribosomes. Genes Dev. *21*, 2580–2592.

Zhang, L., Wu, C., Cai, G., Chen, S., and Ye, K. (2016). Stepwise and dynamic assembly of the earliest precursors of small ribosomal subunits in yeast. Genes Dev. *30*, 718–732.

Zhao, R., Kakihara, Y., Gribun, A., Huen, J., Yang, G., Khanna, M., Costanzo, M., Brost, R.L., Boone, C., Hughes, T.R., et al. (2008). Molecular chaperone Hsp90 stabilizes Pih1/Nop17 to maintain R2TP complex activity that regulates snoRNA accumulation. J. Cell Biol. *180*, 563–578.

Zhou, D., Zhu, X., Zheng, S., Tan, D., Dong, M.-Q., and Ye, K. (2018). Cryo-EM structure of an early precursor of large ribosomal subunit reveals a half-assembled intermediate. Protein Cell 1–11.

Zivanov, J., Nakane, T., Forsberg, B.O., Kimanius, D., Hagen, W.J.H., Lindahl, E., and Scheres, S.H.W. (2018). New tools for automated high-resolution cryo-EM structure determination in RELION-3. Elife *7*.

Zivanov, J., Nakane, T., and Scheres, S.H.W. (2020). Estimation of high-order aberrations and anisotropic magnification from cryo-EM data sets in RELION-3.1. IUCrJ *7*, 253–267.